



Aristotle University of Thessaloniki
Faculty of Engineering
Department of Civil Engineering



Boğaziçi University
The Kandilli Observatory
and Earthquake Research Institute
Department of Earthquake
Engineering

Theodoros, Perilis, Civil Engineer

**RAPID SEISMIC RISK ASSESSMENT AT URBAN SCALE:
APPLICATION IN ISTANBUL & THESSALONIKI
BUILDING STOCK**

[Master Thesis]

Supervisors:

Kyriazis Pitilakis, Professor, Aristotle University of Thessaloniki
Can Zulfikar, Associate Professor, Boğaziçi University
Anastasios Anastasiadis, Assistant Professor, Aristotle University of Thessaloniki

Thessaloniki, November 2012

Executive Summary

Earthquakes in the Mediterranean Region are the main natural disasters for the people and urban systems in the area. After the 1978 Volvi and the 1999 Kocaeli catastrophic seismic events near Thessaloniki and Istanbul respectively, civil protection authorities and researchers have focused on the reduction of potential impact on urban societies, given that it is impossible to predict accurately when the next earthquake will occur. As a result, different methodologies and tools have been developed in terms of earthquake rapid response system to estimate ground motion parameters, building damages, human and social losses.

One of the newly developed software is E.L.E.R (**E**arthquake **L**oss **E**stimation **R**outine). ELER is as a powerful tool, which can essentially calculate at near real-time consequences (building damage, consequential human casualties), resulting from the ground motion generated by a specific earthquake, or obtained from a hazard study. The ultimate goal is the rapid estimation of losses for effective emergency response and public information after potential damaging earthquakes.

Two case studies are considered in this thesis. In the first one, the 1999 Kocaeli earthquake is studied. Then, using building and population data from Zeytinburnu district in Istanbul, as well as appropriate fragility and capacity curves, building damages and casualties are calculated and compared with the observed damages from the actual event. Similar to that, losses are also calculated from a deterministic scenario using data from the Main Marmara Fault.

In the second case study, the city of Thessaloniki is investigated for two scenarios; the first one referring to the 1978 Volvi earthquake and the second one based on a potential seismic event caused by Anthemountas Fault. The scenarios are studied in ELER in order to examine the vulnerability of the building stock in Thessaloniki. Both analysis results and observed damages are compared in order to examine the reliability of the ELER software.

Περίληψη

Οι σεισμοί στην περιοχή γύρω από τη Μεσόγειο αποτελούν την κυριότερη φυσική καταστροφή για τους ανθρώπους και το δομημένο περιβάλλον. Έπειτα από τους καταστροφικούς σεισμούς της Βόλβης το 1978 και του Κοτζαέλι το 1999, κοντά στη Θεσσαλονίκη και την Κωνσταντινούπολη αντίστοιχα, η πολιτική προστασία και οι επιστήμονες έχουν πλέον επικεντρωθεί στη μείωση του πιθανού αντίκτυπου σε αστικές περιοχές, δεδομένου ότι είναι αδύνατο να προβλεφθεί ακριβώς πότε θα συμβεί το επόμενο σεισμικό γεγονός. Αποτέλεσμα αυτού, διάφορες μεθοδολογίες και εργαλεία έχουν αναπτυχθεί στα πλαίσια του μηχανισμού της άμεσης σεισμικής απόκρισης για τον υπολογισμό των παραμέτρων της εδαφικής κίνησης, των ζημιών-βλαβών σε κτήρια και ανθρωπίνων και κοινωνικών απωλειών.

Ένα από τα εργαλεία-λογισμικά για τον παραπάνω υπολογισμό είναι το E.L.E.R. Το ELER αποτελεί ένα δυνατό εργαλείο, το οποίο ουσιαστικά μπορεί να υπολογίσει σε σχεδόν πραγματικό χρόνο κτηριακές ζημιές και ανθρώπινες απώλειες, χρησιμοποιώντας την εδαφική κίνηση, η οποία προκύπτει από έναν ορισμένο σεισμό ή από μελέτη σεισμικής επικινδυνότητας. Βασικός στόχος είναι η άμεση εκτίμηση απωλειών για την έγκαιρη αντίδραση-κινητοποίηση και την πληροφόρηση των κατοίκων μιας περιοχής μετά από ένα πιθανό καταστροφικό σεισμό.

Δύο περιπτώσεις εξετάζονται στη συγκεκριμένη διπλωματική. Η πρώτη αναφέρεται στο σεισμό του 1999 με επίκεντρο το Κοτζαέλι. Έχοντας δεδομένα για τα κτήρια και τη δημογραφική κατανομή στη περιοχή Ζεϊτίνμπουρνου της Κωνσταντινούπολης, όπως επίσης και κατάλληλες καμπύλες τρωτότητας και αντίστασης, υπολογίζονται οι ζημιές στα κτήρια και απώλειες στον αστικό πληθυσμό και συγκρίνονται με τις παρατηρηθείσες ζημιές από το πραγματικό σεισμικό γεγονός. Παρομοίως, απώλειες υπολογίζονται λαμβάνοντας υπόψη και ένα αιτιοκρατικό σενάριο, χρησιμοποιώντας στοιχεία από το κύριο ρήγμα στη θάλασσα του Μαρμαρά που χωροθετείται πλησίον της Κωνσταντινούπολης.

Η δεύτερη περίπτωση εστιάζει στη Θεσσαλονίκη, όπου διερευνώνται δύο σενάρια. Το πρώτο βασίζεται στο σεισμό του 1978 με επίκεντρο τη Βόλβη και το δεύτερο σε ένα πιθανό σεισμό προερχόμενος από το ρήγμα του Ανθεμούντα. Η μελέτη τους γίνεται στο πρόγραμμα ELER με σκοπό να εξεταστεί η τρωτότητα του κτηριακού αποθέματος της Θεσσαλονίκης. Βλάβες που προκύπτουν ως αποτέλεσμα της ανάλυσης και βλάβες από τις πραγματικές καταγραφές του '78 συγκρίνονται για να εξεταστεί η αξιοπιστία του λογισμικού.

Acknowledgement

This study was sponsored by the NERA TA activities, supported by KOERI (Kandilli Observatory & Earthquake Research Institute) and taken place in Istanbul. During the three months of my staying in Istanbul, many people contributed and provided the preparation and completion of this study with their valuable assistance.

First and foremost, I would like to express my utmost gratitude to Professor Kyriazis Pitilakis, who believed in me from the very beginning of my attempt. Collaborating with him has been a real pleasure to me.

Furthermore, I am very grateful to my supervisor Associate Professor, Can Zulfikar, for insightful comments both on my work and on this thesis, for his support, and for many motivating discussions.

Since the beginning of my master thesis, I had the pleasure to collaborate with Sotiris Argyroudis, Post-Doctorate researcher and Evi Riga, PhD student, who both have observed my progress. We spent together lots of hours via teleconferences to hurdle all the obstacles upon the completion of this research work.

I am most grateful to GIS Engineer, Nagihan Gok, for providing me with GIS knowledge. Her talent and her patience helped me a lot to use the manipulation of my input data.

In addition, I have been very privileged to get to know and to collaborate with many other respected scientists in KOERI over the last three months. I have greatly enjoyed the opportunity to work with Mine B. Demircioglu, Research Associate and Cunezt Tuzun, Associate Professor. Both of them were always available to provide answers to a number of my questions.

I would like to thank, my friends, Cem Yenidogan, Zeynep Coşkun, Yasin Toksoy, Ozge Zulfikar, Okan Ilhan and Barbaros Cetiner for the moral support and their useful advice.

Last but not least, I am so grateful to my family, to Pepi Dimitriadou, Civil Engineer and Apostolia Dagloudi, ELT, for giving me strength to overcome all the difficulties I experienced.

List of Contents

EXECUTIVE SUMMARY	2
ΠΕΡΙΛΗΨΗ	3
ACKNOWLEDGEMENT	4
LIST OF CONTENTS	5
LIST OF TABLES	7
LIST OF FIGURES	9
1. INTRODUCTION	12
1.1 ISTANBUL EARTHQUAKE RAPID RESPONSE SYSTEM.....	12
1.2 SHORT DESCRIPTION OF THE E.L.E.R. METHODOLOGY AND SOFTWARE.....	14
1.3 MAIN OBJECTIVES OF THE THESIS	16
1.4 OVERVIEW OF THE THESIS.....	16
2. ELER METHODOLOGY AND SOFTWARE	17
2.1 HAZARD MODULE.....	17
2.1.1 <i>Introduction</i>	17
2.1.2 <i>Terminology</i>	18
2.1.3 <i>Input specification</i>	21
2.2 URBAN EARTHQUAKE LOSS ASSESSMENT MODULE (LEVEL 2)	26
2.2.1 <i>Introduction</i>	26
2.2.2 <i>Spectral Capacity-Based Vulnerability Assessment</i>	27
2.2.3 <i>Representation of the Seismic Demand</i>	28
2.2.4 <i>Representation of the Building Capacity</i>	30
2.2.5 <i>Demand Spectrum and the Performance Point</i>	31
2.2.6 <i>Fragility Curves</i>	38
2.2.7 <i>Casualty Model</i>	42
3. APPLICATION TO ISTANBUL	43
3.1 BUILDINGS AND POPULATION DATA FOR ZEYTINBURNU DISTRICT OF ISTANBUL	43
3.1.1 <i>Classification of buildings in Istanbul (Zeytinburnu)</i>	43
3.2 FRAGILITY AND CAPACITY CURVES FOR ISTANBUL BUILDING STOCK.....	46
3.2.1 <i>Structural Damage Levels</i>	46
3.2.2 <i>Fragility curves</i>	46
3.2.3 <i>Capacity curves</i>	47
3.3 HAZARD SCENARIOS FOR ISTANBUL; THE 1999 KOCAELI EARTHQUAKE (SCENARIO A)	48
3.3.1 <i>Introduction</i>	48
3.3.2 <i>Regional seismicity and tectonic setting</i>	48
3.3.3 <i>Input data for ELER</i>	51
3.3.4 <i>Output results</i>	56
3.4 HAZARD SCENARIOS FOR ISTANBUL; THE “CREDIBLE WORST CASE” SCENARIO EARTHQUAKE FOR ISTANBUL (SCENARIO B)	58
3.4.1 <i>Introduction</i>	58
3.4.2 <i>Input data for ELER</i>	58
3.4.3 <i>Output results</i>	60
3.5 BUILDING DAMAGES & CASUALTIES FOR SCENARIO A	62
3.5.1 <i>Building damages (analysis results)</i>	62

3.5.2	<i>Comparison with observed damages from the 1999 Kocaeli Earthquake</i>	65
3.5.3	<i>Casualties</i>	65
3.6	BUILDING DAMAGES & CASUALTIES FOR SCENARIO B	66
3.6.1	<i>Building damages (analysis results)</i>	66
3.6.2	<i>Casualties</i>	68
4.	APPLICATION TO THESSALONIKI	69
4.1	MANIPULATION OF VS30 DATA IN GEOGRAPHICAL INFORMATION SYSTEMS	69
4.1.1	<i>The Thessaloniki Vs30 map from point to polygon</i>	69
4.1.2	<i>The Central Macedonia Vs30 map generated by USGS</i>	73
4.1.3	<i>Interpolation of USGS Vs30 map</i>	74
4.1.4	<i>Joining to a single map</i>	76
4.2	BUILDINGS AND POPULATION DATA FOR THESSALONIKI	78
4.2.1	<i>Division into grids; from blocks to grid-cells</i>	78
4.2.2	<i>Classification of buildings in Thessaloniki</i>	80
4.3	FRAGILITY AND CAPACITY CURVES FOR THESSALONIKI BUILDING STOCK	83
4.3.1	<i>Structural Damage Levels</i>	83
4.3.2	<i>Generate in ELER Software</i>	83
4.4	HAZARD SCENARIOS FOR THESSALONIKI; THE 1978 VOLVI EARTHQUAKE (SCENARIO C)	87
4.4.1	<i>Introduction</i>	87
4.4.2	<i>Regional seismicity and tectonic setting around Thessaloniki</i>	87
4.4.3	<i>Input data for ELER</i>	87
4.4.4	<i>Output results</i>	90
4.5	HAZARD SCENARIOS FOR THESSALONIKI; THE ANTHEMOUNTAS FAULT; ONE OF THE MOST HAZARDOUS EARTHQUAKE SOURCES FOR THESSALONIKI (SCENARIO D)	95
4.5.1	<i>Introduction</i>	95
4.5.2	<i>Regional seismicity and tectonic setting around Thessaloniki</i>	95
4.5.3	<i>Input data for ELER</i>	96
4.5.4	<i>Output results</i>	98
4.6	BUILDING DAMAGES AND CASUALTIES FROM SCENARIO C	103
4.6.1	<i>Building damages (analysis results)</i>	103
4.6.2	<i>Observed damage from the 1978 Thessaloniki earthquake</i>	110
4.6.3	<i>Comparison between calculated and observed vulnerability</i>	110
4.6.4	<i>Casualties</i>	111
4.7	BUILDING DAMAGES AND CASUALTIES FROM SCENARIO D	112
4.7.1	<i>Building damages (analysis results)</i>	112
4.7.2	<i>Casualties</i>	119
5.	CONCLUSION	120
6.	REFERENCES	121

List of Tables

TABLE 2.1 EC8 TYPE 1 ELASTIC RESPONSE SPECTRA PARAMETERS.....	29
TABLE 2.2 DEGRADATION FACTORS (K) AS A FUNCTION OF SHORT, MODERATE AND LONG EARTHQUAKE DURATION (HAZUS-MH TECHNICAL MANUAL).....	35
TABLE 2.3 MINIMUM ALLOWABLE VALUES FOR THE SPECTRAL REDUCTION FACTORS	35
TABLE 2.4 C ₀ COEFFICIENT (ASCE/SEI 41-06 2007).....	36
TABLE 2.5 DAMAGE PERCENTAGES FOR EACH DAMAGE STATE FOR BUILDING TYPOLOGY RC3.2ML IN GRIDID 348	41
TABLE 2.6 INJURY SEVERITY LEVELS	42
TABLE 3.1 THE LOGIC TREE TO OBTAIN THE NUMBERS FOR EACH OF BUILDING CLASS (TAKEN FROM ELER) ..	43
TABLE 3.2 BUILDING INVENTORY OF ZEYTINBURNU BASED ON RISK-UE BUILDING TAXONOMY	44
TABLE 3.3 THE 1999 KOCAELI EARTHQUAKE FAULT IDENTITY.....	52
TABLE 3.4 INPUT PARAMETERS FOR ISTANBUL- THE 1999 KOCAELI EARTHQUAKE (SCENARIO A)	56
TABLE 3.5 THE MAIN MARMARA FAULT IDENTITY (STUDIED SEGMENTS).....	59
TABLE 3.6 INPUT PARAMETERS FOR SCENARIO B	60
TABLE 3.7 DAMAGE ESTIMATION RESULTS FOR ZEYTINBURNU SCENARIO A, USING THE GMPE BY CAMPBELL & BOZORGNIA (2008).....	63
TABLE 3.8 DAMAGE ESTIMATION RESULTS FOR ZEYTINBURNU SCENARIO B, USING THE GMPE BY CAMPBELL & BOZORGNIA (2008).....	66
TABLE 4.1 SPECIFIC BUILDING TYPES AND DESIGN LEVELS FOR R/C BUILDING ANALYSIS (KAPPOS ET AL., 2006)	81
TABLE 4.2 RISK-UE BUILDING TYPOLOGY MATRIX; CONTAINS ONLY THE BUILDING TYPES USED IN THESSALONIKI	82
TABLE 4.3 DAMAGE STATES AND LOSSES INDICES FOR R/C BUILDINGS (KAPPOS ET AL., 2006).....	83
TABLE 4.4 ESTIMATED S _d FRAGILITY CURVE PARAMETERS FOR THESSALONIKI (MEDIAN VALUES IN M), (KAPPOS ET AL, 2006)	85
TABLE 4.5 ESTIMATED CAPACITY CURVES FOR THESSALONIKI (DISPLACEMENT VALUES IN M, ACCELERATION VALUES IN M/SEC ² , DAMPING VALUES IN %), (KAPPOS ET AL, 2006).....	85
TABLE 4.6 ESTIMATED ADDITIONAL PARAMETERS FOR ANALYTICAL VULNERABILITY ANALYSIS (PERIOD VALUES IN SEC), (KAPPOS ET AL, 2006)	85
TABLE 4.7 THE GERAKAROU FAULT IDENTITY	87
TABLE 4.8 INPUT PARAMETERS FOR THESSALONIKI (SCENARIO C).....	90
TABLE 4.9 INPUT PARAMETERS FOR THESSALONIKI (SCENARIO C).....	92
TABLE 4.10 INPUT PARAMETERS FOR THESSALONIKI (SCENARIO C).....	93
TABLE 4.11 THE ANTHEMOUNTAS FAULT IDENTITY.....	97
TABLE 4.12 INPUT PARAMETERS FOR THESSALONIKI (SCENARIO D).....	98
TABLE 4.13 INPUT PARAMETERS FOR THESSALONIKI (SCENARIO D).....	100
TABLE 4.14 INPUT PARAMETERS FOR THESSALONIKI (SCENARIO D).....	102
TABLE 4.15 DAMAGE ESTIMATION RESULTS FOR THESSALONIKI (SCENARIO C), USING THE GMPE BY BOORE AND ATKINSON (2008)	104
TABLE 4.16 DAMAGE ESTIMATION RESULTS FOR THESSALONIKI (SCENARIO C) USING THE GMPE BY CAMPBELL & BOZORGNIA (2008).....	107
TABLE 4.17 DAMAGE ESTIMATION RESULTS FOR THESSALONIKI (SCENARIO C) USING THE GMPE BY	109
TABLE 4.18 OBSERVED DAMAGES IN THESSALONIKI	110
TABLE 4.19 DAMAGES GENERATED IN ELER VS OBSERVED DAMAGES	110
TABLE 4.20 DAMAGE ESTIMATION RESULTS FOR THESSALONIKI (SCENARIO D) USING THE GMPE BY BOORE AND ATKINSON (2008)	113
TABLE 4.21 DAMAGE ESTIMATION RESULTS FOR THESSALONIKI (SCENARIO D) USING THE GMPE BY CAMPBELL & BOZORGNIA (2008).....	116

TABLE 4.22 DAMAGE ESTIMATION RESULTS FOR THESSALONIKI (SCENARIO D) USING THE GMPE'S BY AKKAR & BOMMER (2007)	118
--	-----

List of Figures

FIGURE 1.1 RAPID RESPONSE STATIONS (ERDIK ET AL., 2003).....	12
FIGURE 1.2 EARLY WARNING STATIONS (ERDIK ET AL., 2003).....	13
FIGURE 1.3 FLOW CHART FOR MULTI-LEVEL ANALYSIS METHODOLOGY OF ELER (ELER, 2010).....	14
FIGURE 2.1 FLOWCHART OF THE HAZARD MODULE GUI (ELER, 2010).....	17
FIGURE 2.2 HAZARD MODULE GUI.....	17
FIGURE 2.3 FAULT TYPES (HTTP://WWW.GLY.UGA.EDU/RAILSBACK/1121SIMPLEFAULTS.JPEG).....	19
FIGURE 2.4 COMPARISON OF EARTHQUAKE MAGNITUDE SCALES (HEATON ET AL., 1986).....	20
FIGURE 2.5 DEFINITION OF BASIC FAULT GEOMETRY INCLUDING HYPOCENTER AND EPICENTER.....	21
FIGURE 2.6 EXAMPLE EARTHQUAKE EVENT IN XML FORMAT.....	21
FIGURE 2.7 MULTI-SEGMENT FAULT DEFINED BY FOUR VERTICES.....	22
FIGURE 2.8 GRID MATRIX, REFERENCE VECTOR AND VS30 MAP IN MATLAB.....	24
FIGURE 2.9 GROUND MOTION ESTIMATION ON THE LEFT AND INSTRUMENTAL INTENSITY ESTIMATION ON THE RIGHT FIGURE.....	25
FIGURE 2.10 SPECTRAL CAPACITY-BASED VULNERABILITY AND DAMAGE ASSESSMENT METHODOLOGY.....	28
FIGURE 2.11 SHAPE OF THE HORIZONTAL ELASTIC RESPONSE SPECTRUM BY EC8.....	28
FIGURE 2.12 SHAPE OF THE HORIZONTAL ELASTIC RESPONSE SPECTRUM BY IBC-2006.....	30
FIGURE 2.13 TYPICAL STRUCTURAL CAPACITY CURVE (LEFT) AND ITS SIMPLIFIED FORM (RIGHT).....	31
FIGURE 2.14 THE NEHRP – IBC 2006 STANDARDIZED SPECTRUM SHAPE PLOTTED IN ADRS S_{AE} -T (LEFT) FORMAT (RIGHT).....	31
FIGURE 2.15 NEHRP SPECTRUM PLOTTED IN ADRS FORMAT (T_A , T_C AND T_D SHOW THE CHARACTERISTIC PERIODS. S_{AES} AND S_{AEI} RESPECTIVELY INDICATE THE SHORT PERIOD AND 1S PERIOD SPECTRAL (ELASTIC) ACCELERATIONS).....	32
FIGURE 2.16 GRAPHICAL REPRESENTATION OF THE IDEALIZED HYSTERETIC DAMPING AND THE REDUCTION OF THE 5%-DAMPED ELASTIC DEMAND SPECTRUM (MODIFIED AFTER ATC-40).....	34
FIGURE 2.17 CAPACITY AND DEMAND SPECTRA, AND THE PERFORMANCE POINT AT THE LAST STEP OF PROCEDURE A (TAKEN FROM ATC).....	36
FIGURE 2.18 GENERAL EXAMPLE FRAGILITY CURVES (HAZUS, 2003).....	38
FIGURE 2.19 EXAMPLE FRAGILITY CURVES FOR FOUR DAMAGE LEVELS (KAPPOS ET AL., 2006).....	39
FIGURE 2.20 EC8 ELASTIC RESPONSE SPECTRUM.....	39
FIGURE 2.21 SPECTRAL CAPACITY - BASED VULNERABILITY. THE PERFORMANCE POINT IS THE INTERSECTION OF THE CAPACITY CURVE AND THE REDUCED ADRS.....	40
FIGURE 2.22 DAMAGE ASSESSMENT METHODOLOGY. FRAGILITY CURVES ARE TAKEN FROM (KAPPOS ET AL., 2006).....	41
FIGURE 2.23 DAMAGE PERCENTAGES FOR EACH DAMAGE STATES FOR BUILDING TYPOLOGY RC3.2 ML IN GRIDID 348.....	41
FIGURE 3.1 LOCATION OF ZEYTINBURNU DISTRICT IN ISTANBUL METROPOLITAN MUNICIPALITY.....	44
FIGURE 3.2 BUILDING DENSITY IN ZEYTINBURNU.....	45
FIGURE 3.3 ARCGIS SHAPE FILE WITH ITS ATTRIBUTE TABLE; DATA REFERS TO CELLS.....	45
FIGURE 3.4 SPECTRAL DISPLACEMENT- BASED FRAGILITY CURVES PARAMETERS.....	47
FIGURE 3.5 EXAMPLE EXCEL DOCUMENT FOR FRAGILITY AND CAPACITY CURVES IN ISTANBUL.....	47
FIGURE 3.6 LOCATIONS OF M 6.0 EARTHQUAKES (A.D. 1509-1999) (NOTE: PARENTHESES IN THE LEGEND DENOTE THE BREAKDOWN OF EARTHQUAKES; CATEGORY-1 FAULTS WERE RECENTLY VISUALIZED USING BATHYMETRIC IMAGES AND SEISMIC REFLECTION SURVEY; CATEGORY-2 FAULTS INDICATE THE PREVIOUSLY KNOWN FAULTS) (KALKAN ET AL., 2008).....	49
FIGURE 3.7 DESTRUCTIVE EARTHQUAKES ALONG THE NORTH ANATOLIAN FAULT BETWEEN ERZINCAN AND ISTANBUL IN THIS CENTURY (ULUTAS & OZER, 2009).....	50
FIGURE 3.8 NORTH ANATOLIAN FAULT SYSTEM IN MARMARA REGION AND THE SURFACE RUPTURES AFTER IZMIT AND DUZCE EARTHQUAKES (ULUTAS & OZER, 2009).....	50

FIGURE 3.9 EVENT LOCATION OF THE 1999 KOCAELI EARTHQUAKE. RED STAR IN THE FIGURE DENOTES THE EPICENTER OF THE EVENT.	51
FIGURE 3.10 SEGMENTATION MODEL OF KOCAELI FAULT	52
FIGURE 3.11 THE SEGMENTS OF THE KOCAELI FAULT CONSIDERED IN THE ANALYSIS.....	53
FIGURE 3.12 DISTRIBUTION OF VS30 IN TURKEY	53
FIGURE 3.13 DISTRIBUTION OF VS30 IN MARMARA REGION. THE MAIN FOCUS OF THE WHITE FRAME IS ON THE METROPOLITAN AREA OF ISTANBUL	54
FIGURE 3.14 GMPE INPUT SCREEN (CAMPBELL & BOZORGNIA, 2008).....	55
FIGURE 3.15 ALTERNATIVE GROUND MOTION PARAMETERS	56
FIGURE 3.16 PGA (%G) AND SPECTRAL ACCELERATIONS (%G) AT T=0.2SEC AND T=1.0SEC OBTAINED FROM THE CAMPBELL AND BOZORGNIA (2008) GMPE FOR SCENARIO A	57
FIGURE 3.17 FAULT SEGMENTATION MODEL PROPOSED FOR THE MARMARA REGION. STUDIED AREA CONSISTS OF THREE SEGMENTS S5, S6 AND S7 (ERDIK ET AL., 2004).....	58
FIGURE 3.18 EVENT EPICENTER FOR SCENARIO B (CLOSE TO ATATURK INTERNATIONAL AIRPORT).....	59
FIGURE 3.19 SEGMENTATION MODEL OF THE FAULT CONSIDERED IN SCENARIO B.....	60
FIGURE 3.20 PGA (%G) AND SPECTRAL ACCELERATIONS (%G) AT T=0.2SEC AND T=1.0SEC OBTAINED FROM THE CAMPBELL AND BOZORGNIA (2008) GMPE FOR SCENARIO B	61
FIGURE 3.21 DISCRETE DAMAGE PROBABILITIES UNDER ANALYSIS 50 (SCENARIO A).....	63
FIGURE 3.22 THE DISTRIBUTION OF DAMAGED BUILDINGS IN ZEYTINBURNU RESULTING FROM ANALYSIS 50, IBC DEMAND SPECTRUM AND CSM AS SELECTED METHOD-LEVEL 2 ANALYSIS (SCENARIO A).....	64
FIGURE 3.23 DISTRIBUTION OF MODERATE DAMAGED BUILDINGS IN ISTANBUL DUE TO AUGUST 17, 1999 KOCAELI EARTHQUAKE (SCENARIO A).....	65
FIGURE 3.24 THE DISTRIBUTION OF CASUALTIES IN ZEYTINBURNU DISTRICT RESULTING FROM THE 1999 KOCAELI EARTHQUAKE SCENARIO.....	65
FIGURE 3.25 DISCRETE DAMAGE PROBABILITIES UNDER ANALYSIS 56 (SCENARIO B).....	67
FIGURE 3.26 THE DISTRIBUTION OF DAMAGED BUILDINGS IN ZEYTINBURNU RESULTING FROM ANALYSIS 56, IBC DEMAND SPECTRUM AND CSM AS SELECTED METHOD-LEVEL 2 ANALYSIS (SCENARIO B).....	67
FIGURE 3.27 THE DISTRIBUTION OF CASUALTIES IN ZEYTINBURNU DISTRICT RESULTING FROM EARTHQUAKE SCENARIO B	68
FIGURE 4.1 DISTRIBUTION OF VS30 IN THE CITY	70
FIGURE 4.2 MUNICIPALITY OF THESSALONIKI; MANIPULATION OF AVAILABLE DATA. EACH CELL HAS ITS UNIQUE GRIDID.	71
FIGURE 4.3 SELECTED VS30 VALUES THAT CORRESPOND TO THE STUDIED REGION	72
FIGURE 4.4 DISTRIBUTION OF VS30 IN THESSALONIKI	72
FIGURE 4.5 EUROCODE 8 SITE CLASSIFICATION OF THESSALONIKI GROUND	73
FIGURE 4.6 DISTRIBUTION OF VS30 IN CENTRAL MACEDONIA (GENERATED BY USGS).....	74
FIGURE 4.7 SELECTED AND DEFAULT BY USGS GRID INTERVAL.....	75
FIGURE 4.8 USGS VS30 GRIDS. THE FOCUS OF THE BLACK FRAME IS ON THE MUNICIPALITY OF THESSALONIKI	75
FIGURE 4.9 THE FINAL VS30 MAP OF CENTRAL MACEDONIA	76
FIGURE 4.10 TEXT2GRID FOR EXTERNAL DATA INTEGRATION	77
FIGURE 4.11 TEXT2GRID GUI, INPUT AND OUTPUT.....	77
FIGURE 4.12 SHAPE FILE WITH ITS ATTRIBUTE TABLE; DATA REFERS TO BLOCKS	78
FIGURE 4.13 PREPARATION OF COMPILED BUILDING DATA.....	79
FIGURE 4.14 SHAPE FILE INPUT WITH ITS ATTRIBUTE TABLE; DATA NOW REFERS TO GRID-CELLS	80
FIGURE 4.15 BUILDING DISTRIBUTION BASED ON STRUCTURAL SYSTEM	83
FIGURE 4.16 BUILDING DISTRIBUTION BASED ON DESIGN LEVEL.....	83
FIGURE 4.17 CAPACITY CURVE FOR RC42LM BUILDING TYPE (KAPPOS ET AL., 2006).....	84
FIGURE 4.18 MAIN MENU OF BUILDING DATABASE CREATOR.....	84
FIGURE 4.19 RC42LM FRAGILITY CURVES (KAPPOS ET AL., 2006).....	86
FIGURE 4.20 RC42HH FRAGILITY CURVES (KAPPOS ET AL., 2006).....	86
FIGURE 4.21 DEFINITION OF RC31HL BUILDING PARAMETERS IN ELER	86
FIGURE 4.22 SEGMENTATION MODEL OF GERAKAROU FAULT	88

FIGURE 4.23 VS30 DISTRIBUTION IN CENTRAL MACEDONIA	88
FIGURE 4.24 PGA (%G) AND SPECTRAL ACCELERATIONS (%G) AT T=0.2SEC AND T=1.0SEC OBTAINED FROM THE BOORE & ATKINSON (2008) GMPE FOR THESSALONIKI (SCENARIO C).....	91
FIGURE 4.25 PGA (%G) OBTAINED FROM THE AKKAR & BOOMER (2007) GMPE FOR THESSALONIKI (SCENARIO C).....	92
FIGURE 4.26 PGA (%G) AND SPECTRAL ACCELERATIONS (%G) AT T=0.2SEC AND T=1.0SEC OBTAINED FROM THE CAMPBELL AND BOZORGNIA (2008) GMPE FOR THESSALONIKI (SCENARIO C).....	94
FIGURE 4.27 THE ANTHEMOUNTAS FAULT WITH RED COLOUR AND ITS SEGMENTS (ZERVOPOULOU ET AL., 2007).....	95
FIGURE 4.28 EVENT DATA FOR THE FORTH SCENARIO	96
FIGURE 4.29 SEGMENTATION MODEL OF ANTHEMOUNTAS FAULT	97
FIGURE 4.30 PGA (%G) AND SPECTRAL ACCELERATIONS (%G) AT T=0.2SEC AND T=1.0SEC OBTAINED FROM THE BOORE & ATKINSON (2008) GMPE FOR THESSALONIKI (SCENARIO D).....	99
FIGURE 4.31 PGA (%G) AND SPECTRAL ACCELERATIONS (%G) AT T=0.2SEC AND T=1.0SEC OBTAINED FROM THE CAMPBELL AND BOZORGNIA (2008) GMPE FOR THESSALONIKI (SCENARIO D)	101
FIGURE 4.32 PGA (%G) OBTAINED FROM THE AKKAR & BOOMER (2007) GMPE FOR THESSALONIKI (SCENARIO D).....	102
FIGURE 4.33 DISCRETE DAMAGE PROBABILITIES UNDER ANALYSIS 59	105
FIGURE 4.34 THE DISTRIBUTION OF DAMAGE BUILDINGS IN THESSALONIKI RESULTING FROM ANALYSIS 59, IBC DEMAND SPECTRUM AND CSM AS SELECTED METHOD-LEVEL 2 ANALYSIS	106
FIGURE 4.35 DISCRETE DAMAGE PROBABILITIES UNDER ANALYSIS 64	108
FIGURE 4.36 COMPARISON OF DAMAGES BETWEEN THE SELECTED GMPE	108
FIGURE 4.37 DAMAGE RESULTS OBTAINED FROM THE GROUND MOTION OF THE THREE SELECTED GMPE'S .	109
FIGURE 4.38 BAR CHART WITH RESULTS OBTAINED FROM OBSERVED DATA AND ANALYSIS 59	111
FIGURE 4.39 HUMAN LOSSES FROM THE STUDIED SCENARIO CALCULATED BY HAZUS METHODOLOGY	111
FIGURE 4.40 THE DISTRIBUTION OF DAMAGE BUILDINGS IN THESSALONIKI RESULTING FROM ANALYSIS 67, IBC DEMAND SPECTRUM AND CSM AS SELECTED METHOD-LEVEL 2 ANALYSIS	114
FIGURE 4.41 DISCRETE DAMAGE PROBABILITIES UNDER ANALYSIS 67 (SCENARIO D).....	115
FIGURE 4.42 DISCRETE DAMAGE PROBABILITIES UNDER ANALYSIS 59 (SCENARIO C) AND 67 (SCENARIO D)	115
FIGURE 4.43 DISCRETE DAMAGE PROBABILITIES UNDER ANALYSIS 69	117
FIGURE 4.44 COMPARISON OF DAMAGES BETWEEN THE SELECTED GMPE	117
FIGURE 4.45 DAMAGE RESULTS OBTAINED FROM THE GROUND MOTION OF THE THREE SELECTED GMPE'S .	118
FIGURE 4.46 HUMAN LOSSES FOR THE ANALYSIS 67 CALCULATED BY HAZUS METHODOLOGY	119

Ten of the strong motion stations are sited at locations as close as possible to the Great Marmara Fault in on-line data transmission mode to enable Earthquake Early Warning (Figure 1.2).

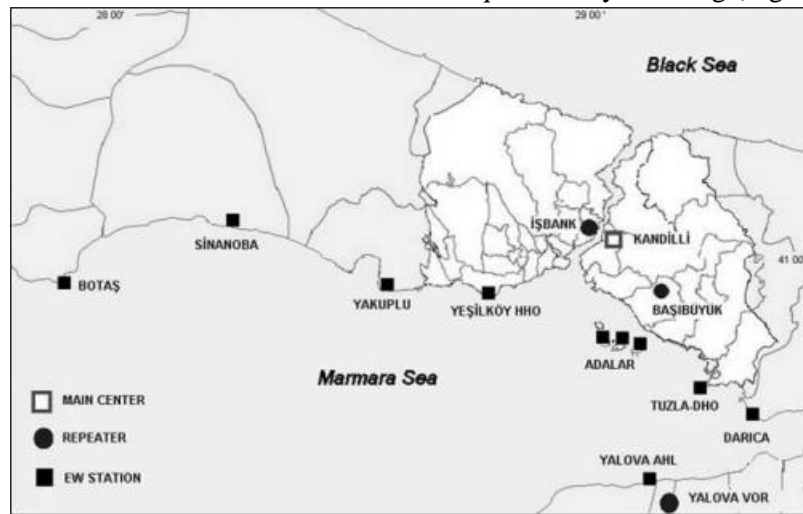


Figure 1.2 Early warning stations (Erdik et al., 2003)

The remaining 40 strong motion recorder units will be placed on critical engineering structures in addition to the already instrumented structures in Istanbul (<http://www.koeri.boun.edu.tr/deprenmmuh/stromotion.htm>). Altogether this network and its functions are called Istanbul Earthquake Rapid Response and Early Warning System (IERREWS). The system is designed and operated by Bogazici University with the logistical support of the Governorate of Istanbul, First Army Headquarters and Istanbul Metropolitan Municipality.

When triggered by an earthquake, each station processes the streaming three-channel strong motion data to yield the spectral accelerations at specific periods, 12 Hz filtered peak ground acceleration and peak ground velocity and sends these parameters in the form of SMS messages at 20 s intervals directly to the main data center through the GSM communication system. The main data processing center is located at the Department of Earthquake Engineering, Kandilli Observatory and Earthquake Research Institute of Bogazici University (KOERI-BU). A secondary center located at the Seismological Laboratory of the same Institute serves as a redundant secondary center that can function in case of failure in the main center. Shake, damage and casualty distribution maps are automatically generated at the data centers after the earthquake and communicated to the end users within 5 minutes. Full-recorded waveforms at each station can be retrieved using GSM and GPRS modems subsequent to an earthquake (Erdik et al., 2003).

The Rapid Response part of the IERREWS has the objective of providing (Erdik et al., 2003):

- Reliable information for accurate, effective characterization of the shaking and damage for rapid response
- Recorded motion for post-earthquake performance analysis of structures
- Empirical basis for long-term improvements in seismic microzonation, seismic provisions of building codes and construction guidelines
- Seismological data to improve the understanding of earthquake generation at the source and seismic wave propagation.

To achieve that, a new methodology and software (**E.L.E.R-Earthquake Loss Estimation Routine**) for the rapid estimation of earthquake shaking and losses in the Euro-Mediterranean region has been developed under the JRA-3 component of the EU FP-6 NERIES Project. This tool is utilized in the present thesis.

1.2 Short description of the E.L.E.R. Methodology and Software

The methodology encompasses the following general steps:

- i. Estimation of the spatial distribution of selected ground motion parameters for a given earthquake (with given magnitude and epicenter) through region specific Ground Motion Prediction Equations (GMPEs) and using distribution of average shear wave velocity at 30m depth from surface (V_{s30}), to describe local site effects.
- ii. Incorporation of actual strong ground motion data for the improvement and bias correction of the theoretical estimations.
- iii. Estimation of the building damages and human casualties at different levels in urban environment.
- iv. Assessment of direct economic losses associated with building damages.
- v. Estimation of damages for urban pipeline systems

Figure 1.3 depicts the general steps of the procedure:

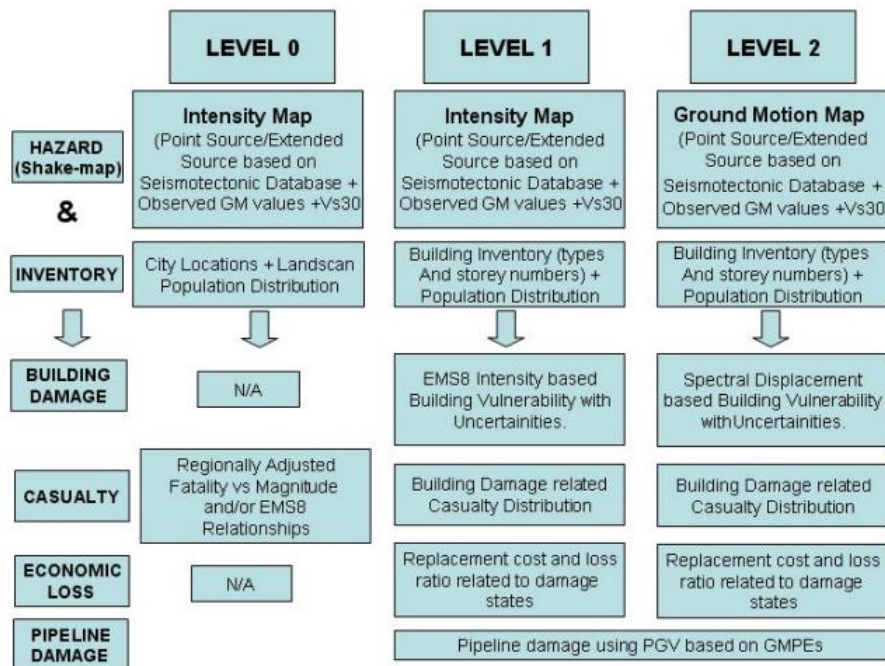


Figure 1.3 Flow chart for multi-level analysis methodology of ELER (ELER, 2010)

The methodology of ELER aims at generating an estimation of the consequences ("loss estimate") to a city under probabilistic earthquake hazard or exposure to a "scenario earthquake", that is, an earthquake with a specified magnitude and location. Although the study is carried out for Istanbul, if it is applied to other cities in Mediterranean region, the study will help guide the allocation of national resources to stimulate risk mitigation efforts and to plan for national earthquake response. For this reason, the case of Thessaloniki is also investigated.

The general steps for using the methodology for a scenario earthquake are the following:

1. Select the city is about to be studied.
2. Define an earthquake scenario with potential focal mechanism.
3. Gather information for local soil conditions.
4. Gather building and population data.
5. Estimate ground motion parameters for specific locations in the city.
6. Provide software with vulnerability data.
7. Estimate damage of buildings to different levels and casualties.

To achieve that, ELER software provides the following modules (ELER, 2010):

- i. Hazard module: For a given earthquake magnitude and epicenter information, spatially distributed intensity and ground motion parameters (i.e. PGA, PGV, S_a , S_d) are estimated through region specific ground motion prediction equations and gridded shear wave velocity information (V_{s30})
- ii. In Level 0 module, the casualty estimation is done utilizing regionally adjusted intensity-casualty or magnitude-casualty correlations based on the Landscan population distribution inventory.
- iii. Level 1 module calculates the number of damaged buildings and associated casualties. The intensity based empirical vulnerability relationship is employed to find the number of damaged buildings. The casualty estimation is done through the number of damaged buildings.
- iv. Level 2 module calculates the number of damaged buildings and associated casualties. The spectral acceleration-displacement-based vulnerability assessment methodology is utilized for the building damage estimation. The casualty estimation is made through the number of damaged buildings using HAZUS99 (FEMA, 1999) and HAZUS-MH (FEMA, 2003) methodologies.

Apart from ELER software, ArcGIS was also used for the data manipulation (building stock, population inventory, V_{s30} map). Details are given in the following chapters.

1.3 Main objectives of the thesis

The main objectives of this thesis are the following:

- Loss estimation of Istanbul and Thessaloniki building stock for different seismic scenarios using ELER software.
- The examination of two seismic scenarios for Istanbul in order to improve the quality of the Shake maps considering local soil conditions.
- Preparation of all necessary input data such as demographic/building inventory and soil parameters in a grid format. Application of ELER routine in Thessaloniki case study for two seismic scenarios.
- Use of different ground motion prediction equations for the estimation of the required ground motion parameters.
- Validation of the results based on observations from past earthquakes.

In the case of Istanbul city, default seismic scenario (scenario A), as well as a new one (scenario B) are examined using existing Vs30 map, attenuation relations and building and population inventory data, which are incorporated in ELER.

In the case of Thessaloniki city, two different seismic scenarios (scenarios C and D) are applied based on regional tectonics. Damages are also calculated based on provided building and population inventory and local soil conditions, which must be firstly prepared to the appropriate format to be used within ELER.

1.4 Overview of the thesis

Besides the present introductory chapter, the thesis comprises 3 more chapters.

Chapter 2 provides an overview of ELER methodology and software package. The theoretical background of the methodologies adopted in ELER is described in detail. The work in Chapter 2 reflects both the diversity of parameters (magnitude, focal mechanism, local soil conditions, Ground Motion Prediction Equations) involved in Hazard Module and the spectral displacement-based vulnerability assessment methodology for the building damage estimation. Together, they provide a comprehensive overview of rapid loss estimation after potential damaging earthquakes.

Chapter 3 focuses on the application of the software in Istanbul. Two different scenarios are applied; the ‘1999 Kocaeli Disastrous Earthquake’ and one possible worst case scenario associated with the Main Marmara Fault. Ground motion distribution and building damage in Zeytinburnu district are the outputs results based on these two scenarios.

Similarly to Chapter 3, **Chapter 4** is referred to the case of Thessaloniki. The ‘1978 Thessaloniki Earthquake’ located in Mygdonia basin and one of the most hazardous earthquake sources, the Anthemountas Fault, are studied to estimate the ground motion parameters and the building vulnerability.

2. ELER Methodology and Software

2.1 Hazard Module

2.1.1 Introduction

The hazard module can be run independently or combined with the loss assessment modules. On the other hand the required ground motion parameters for each level of loss assessment can be calculated using the hazard module or provided externally. All parameters, options and modes of the ground motion computation are specified through the graphical user interface of the Hazard Module. As an example, a flowchart and a snapshot are given in Figure 2.1 and Figure 2.2.

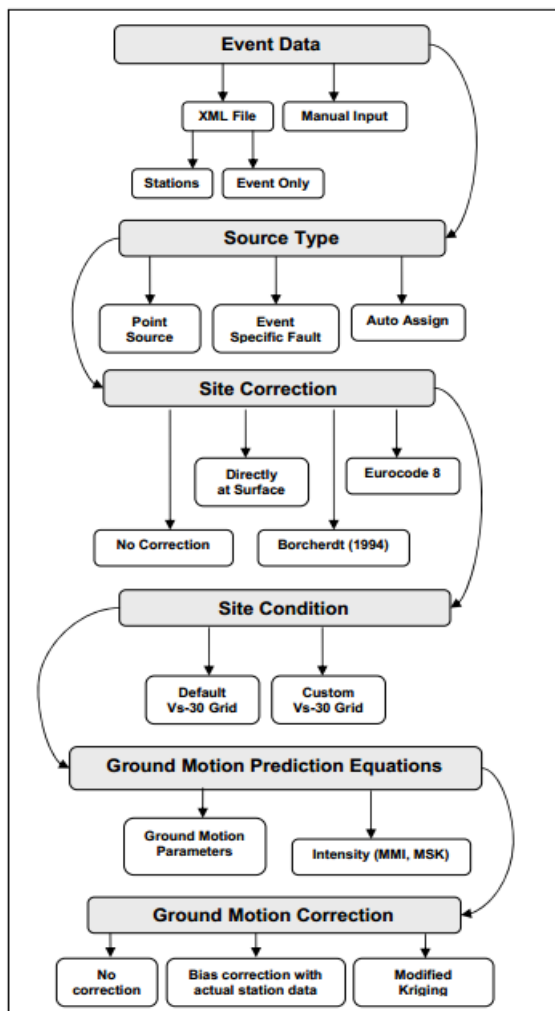


Figure 2.1 Flowchart of the Hazard Module GUI (ELER, 2010)

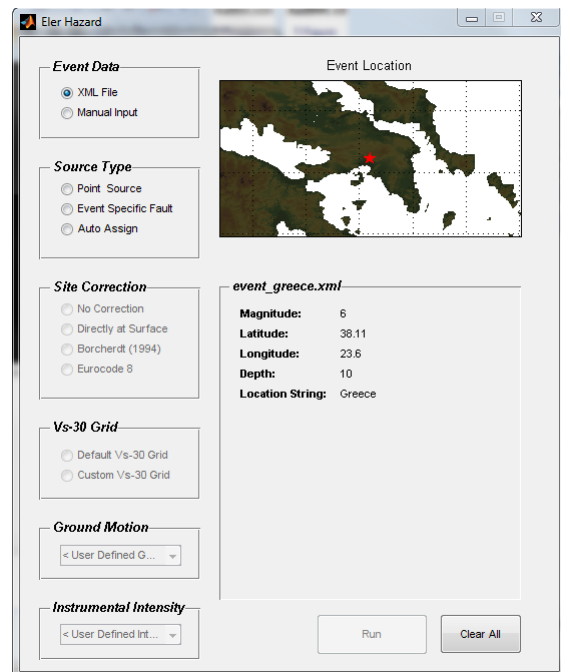


Figure 2.2 Hazard Module GUI

2.1.2 Terminology

In order to be able to use the Hazard Module, the user has to be familiar with the specific terminology. The definition of some specific terms is given below:

Fault Movements: Faults are created when the stresses within geologic materials exceed the ability of those materials to withstand the stresses. Most faults that exist today are the result of tectonic activity that occurred in earlier geological times. These faults are usually non-seismogenic (i.e. incapable of generating earthquakes, or inactive).

However, faults related to past tectonism may be reactivated by present-day tectonism in seismically active areas and can also be activated by anthropogenic (man-made) activities such as impoundment of a reservoir by a dam or injection of fluids (e.g. waste liquids) deep into the subsurface.

The maximum size of an earthquake on an anthropogenically reactivated fault is a subject of some controversy, but earthquakes as large as moment magnitude 6.5 have been attributed to reservoir impoundment.

Not all faults along which relative movement is occurring are a source of earthquakes. Some faults may be surfaces along which relative movement is occurring at a slow, relatively continuous rate, with an insufficient stress drop to cause an earthquake. Such movement is called *fault creep*. Fault creep may occur along a shallow fault, where the low overburden stress on the fault results in a relatively low threshold stress for initiating displacement along the fault. Alternatively, a creeping fault may be at depth in soft and/or ductile materials that deform plastically. Also, there may be a lack of frictional resistance or asperities (non-uniformities) along the fault plane, allowing steady creep and the associated release of the strain energy along the fault. Fault creep may also prevail where phenomena such as magma intrusion or growing salt domes activate small shallow faults in soft sediments. Faults generated by extraction of fluids (e.g., oil or water in southern California), which causes ground settlement and thus activates faults near the surface may also result in fault creep. Faults activated by other non-tectonic mechanisms, e.g. faults generated by gravity slides that take place in thick, unconsolidated sediments, could also produce fault creep.

Type of Faults: Faults may be broadly classified according to their mode, or style of relative movement. The principal modes of relative displacement are depicted in Figure 2.3 and are described subsequently.

Simple faults and why they form

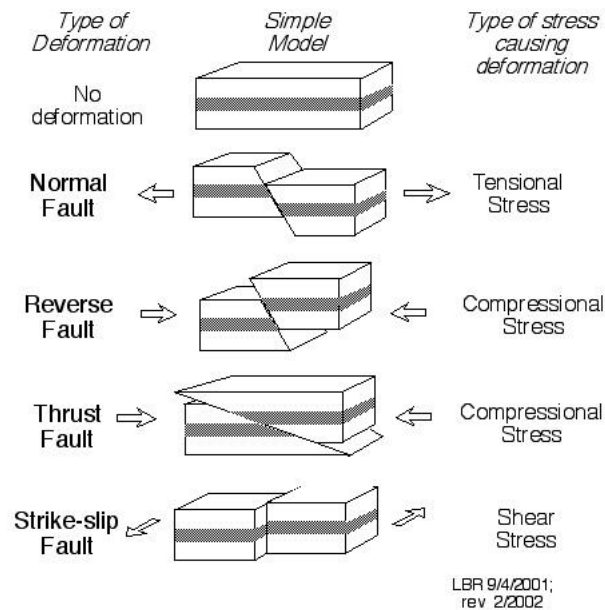


Figure 2.3 Fault types (<http://www.gly.uga.edu/railsback/1121SimpleFaults.jpeg>)

Strike Slip Faults: Faults along which relative movement is essentially horizontal (i.e., the opposite sides of the fault slide past each other laterally), are called strike slip faults. Strike slip faults are often essentially linear (or planar) features.

Dip Slip Faults: Faults in which the deformation is perpendicular to the fault plane may occur due to either *normal* (extensional) or *reverse* (compressional) motion. These faults are referred to as *dip slip* faults. Reverse faults are also referred to as *thrust faults*. Dip slip faults may produce multiple fractures within rather wide and irregular fault zones.

Other Special Cases: Faults that show both strike slip and dip slip displacement may be referred to as *oblique slip faults*.

Earthquake Magnitude: M , is a measure of the energy released by an earthquake. A variety of different earthquake magnitude scales exist. The differences among these scales are attributable to the earthquake characteristic used to quantify the energy content. Characteristics used to quantify earthquake energy content include the local intensity of ground motions, the body waves generated by the earthquake, and the surface waves generated by the earthquake.

Due to limitations in the ability of some recording instruments to measure values above a certain amplitude, some of these magnitude scales tend to reach an asymptotic upper limit. To correct this, the *moment magnitude*, M_w , scale was developed by seismologists (Hanks and Kanamori, 1979). The moment magnitude of an earthquake is a measure of the kinetic

energy released by the earthquake. M_w is proportional to the *seismic moment*, defined as a product of the material rigidity, fault rupture area, and the average dislocation of the rupture surface. Moment magnitude has been proposed as a unifying, consistent magnitude measure of earthquake energy content. Figure 2.4(Heaton et al., 1986) provides a comparison of the various other magnitude scales with the moment magnitude scale.

Hypocenter and Epicenter and Site-to-Source Distance: The *hypocenter* (focus) of an earthquake is the point from which the seismic waves first emanate. Conceptually, it may be considered as the point on a fault plane where the slip responsible for an earthquake was initiated. The *epicenter* is a point on the ground surface directly above the hypocenter. Figure 2.5 shows the relationship between the hypocenter, epicenter, fault plane, and rupture zone of an earthquake.

The horizontal distance between the site of interest to the epicenter is termed epicentral distance, R_E . The distance between the site and the hypocenter is termed hypocentral distance, R_H .

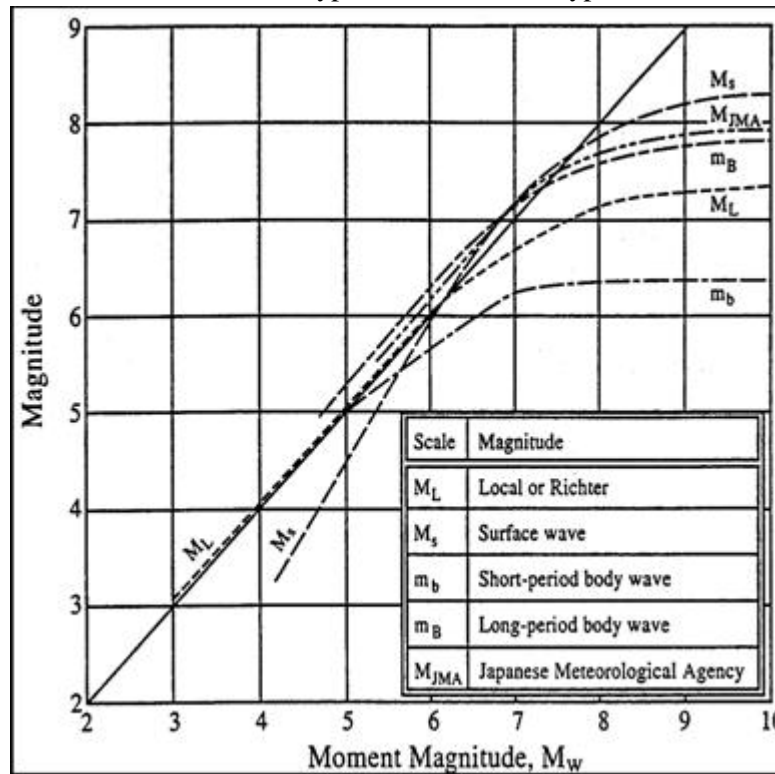


Figure 2.4 Comparison of Earthquake Magnitude Scales (Heaton et al., 1986)

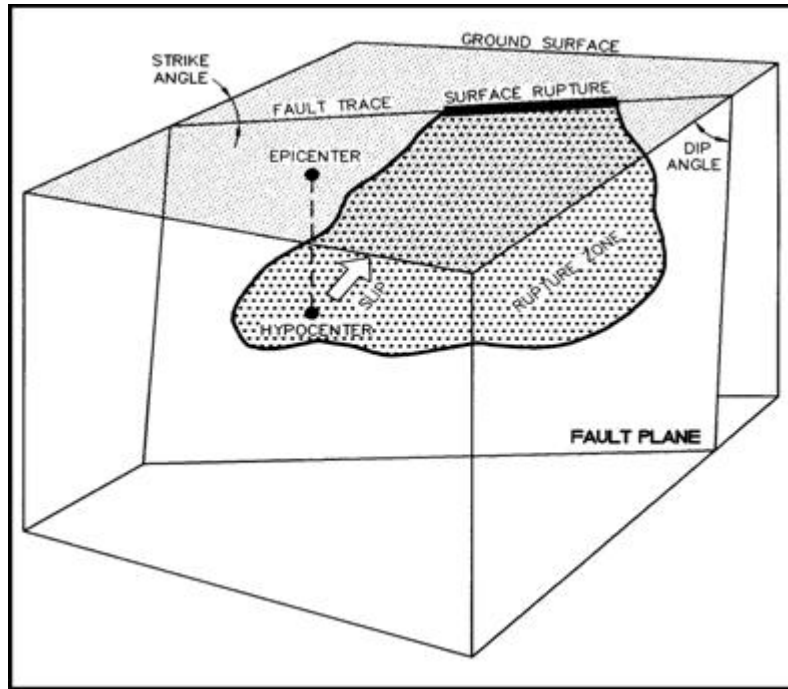


Figure 2.5 Definition of Basic Fault Geometry Including Hypocenter and Epicenter

2.1.3 Input specification

Event data

To begin with, ELER software gives two options to enter the event data. The first one is to use an XML file containing the information of the seismic event. Alternative way is to enter manually the data from the graphical user interface (GUI). An example event XML file is given in Figure 2.6

```

event_greece.xml
1  <shakemap-data>
2  <earthquake id="9583002_se"
3  lat="38.11"
4  lon="23.60"
5  mag="6"
6  year="1992"
7  month="3"
8  day="13"
9  hour="00"
10 minute="00"
11 second="00"
12 timezone="GMT"
13 depth="10"
14 locstring="Greece"
15 created="982348863"/>
16 </shakemap-data>
17

```

Figure 2.6 Example earthquake event in XML format

Source type

The Source Type panel defines the source mechanism associated with the event. For small magnitude events the source can be given as a point (point source mode), while for large magnitude events the user can specify the source type as a finite fault (event specific mode).

Point Source mode:

In this mode a point source will be defined by the epicentral coordinates and the depth of the event. The ground motion distribution will be calculated for this point source.

Event Specific Fault mode:

To define the source as a finite fault, the user should select a text file containing the coordinates of the ruptured fault. Faults are defined by their vertices as a pair of latitude and longitude. Examples of single and multi-segment fault files are given in Figure 2.7.

```
>
40.714594 29.380615
40.695632 30.671500
>
40.689311 30.727665
40.803988 31.028354
>
```

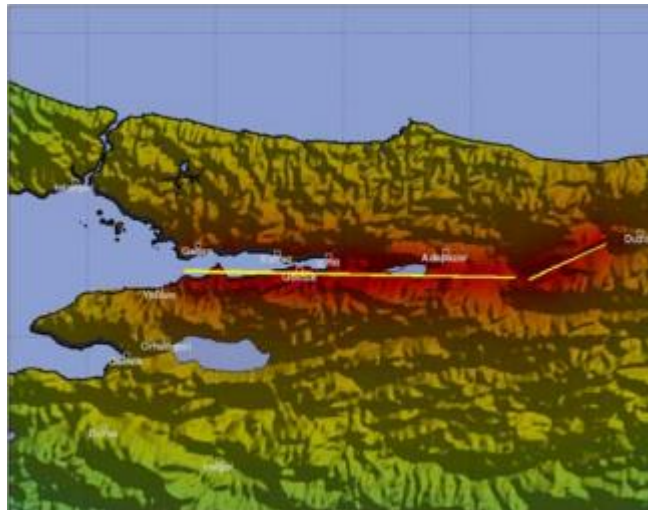


Figure 2.7 Multi-segment fault defined by four vertices

Site correction

The Site Correction panel determines how the effect of the local site conditions will be incorporated into the calculations of ground motion parameters. There are four available options:

No Site Correction:

In this mode all ground motion estimations are calculated at the engineering bedrock. Site condition is not taken into account, thus the site condition selection panel remains disabled. Since site correction requires additional computing No Correction mode is considerably faster than the other site correction modes.

Borcherdt (1994):

In this method all ground motion parameters are calculated at the engineering bedrock. The obtained grid based ground motion is then corrected with the site amplification factors (F_a and F_v) given in Borcherdt (1994) according to the selected Vs30 map. Since this procedure involves element-wise operations on large grids, it is considerably slower.

Eurocode 8:

This mode differs from Borcherdt (1994) in the calculation of the site amplification factors. In Eurocode 8 mode only the peak ground acceleration values are modified according to the site condition. Thus in this mode ELER produces only the site corrected PGA distribution. The same element-wise site correction procedure used in Borcherdt (1994) mode is utilized.

Calculation at Surface:

In this newly developed approach rather than calculating bedrock values and then amplifying these with respect to site conditions, ELER uses ground motion prediction equations (Boore et al., 1997, Campbell and Bozorgnia, 2008, Boore and Atkinson, 2008, Chiou and Youngs, 2008) taking Vs30 as an input parameter to calculate the ground motion values directly at the surface.

Site condition

In order to calculate the effect of the geologic conditions ELER needs the site condition map of the region. Site condition is represented by one parameter: average shear wave velocity at 30m depth (Vs30). The user has the following two options in choosing the site condition.

Default Site Condition Map:

ELER comes with a default site condition map covering the entire Euro-Mediterranean region. The default site condition map has been compiled from the USGS Global Vs30 Map Server.

Custom Site Condition Map:

Custom site condition maps should be in form of Vs30 grids. In MATLAB grids are defined by a matrix containing the values of each cell and a reference vector which is used to map each cell to its corresponding geographical location. An example of a grid matrix, its reference vector and the resulting map is given in Figure 2.8. The first element of the reference vector defines the number of cells per degree while the second and third elements specify the latitude and longitude of the upper left corner of the grid.

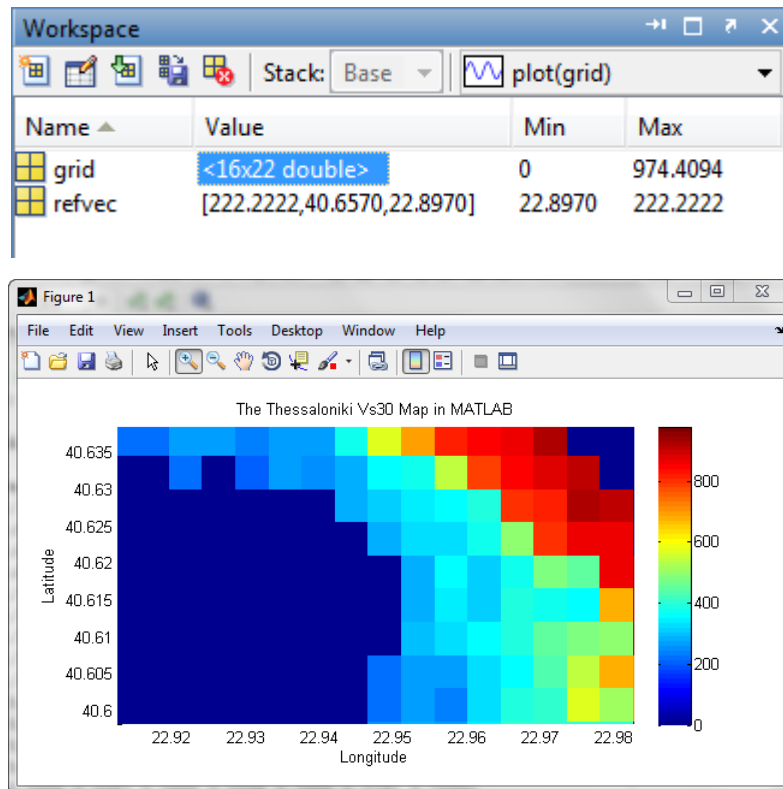


Figure 2.8 Grid Matrix, Reference Vector and Vs30 Map in MATLAB

Ground Motion Prediction Equations (GMPE) and Instrumental Intensity Prediction Equations (IPE)

Ground Motion Prediction Equations (GMPE) are considered a very important parameter for any earthquake hazard analysis and are very significant on the resulting earthquake design loads (Ambraseys and Bommer, 1995). Despite the fact that the number of strong-motion accelerographs has been increasing, for some hazard and risk assessment purposes the intensity scales remain an important measure of strength of ground shaking in earthquakes (Dowrick, 1992).

There are a large number of attenuation relationships available for both PGA and intensity, which allows the selection of the most appropriate or the most convenient equation for each particular situation. One of the main criteria for the selection and application of an attenuation law is that the seismological and strong-motion input data have been completely reconsidered and published and that they are typical of the seismotectonic environment of the area under consideration (Ambraseys and Bommer, 1995).

In ELER, the final stage of the input specification is the selection of GMPE's. Since different prediction equations are derived from different event catalogues the user must select a suitable equation taking into account the regional characteristics, magnitude and ground motion parameter of interest. Three options are available:

Ground Motion Estimation:

The selected GMPE's used to estimate measurable ground motion parameters such as PGA and spectral accelerations. Each prediction equation has its unique set of input parameters resulting from the regression analysis. The common parameters such as event magnitude distance to source and site condition are set automatically. The remaining parameters such as fault type, hanging wall effect etc. should be specified by the user. Figure 2.10 (left figure) illustrates how it can be applied.

Instrumental Intensity Estimation:

The selected method is used to obtain the estimated intensity distribution. Figure 2.9(right figure) illustrates how it can be applied.

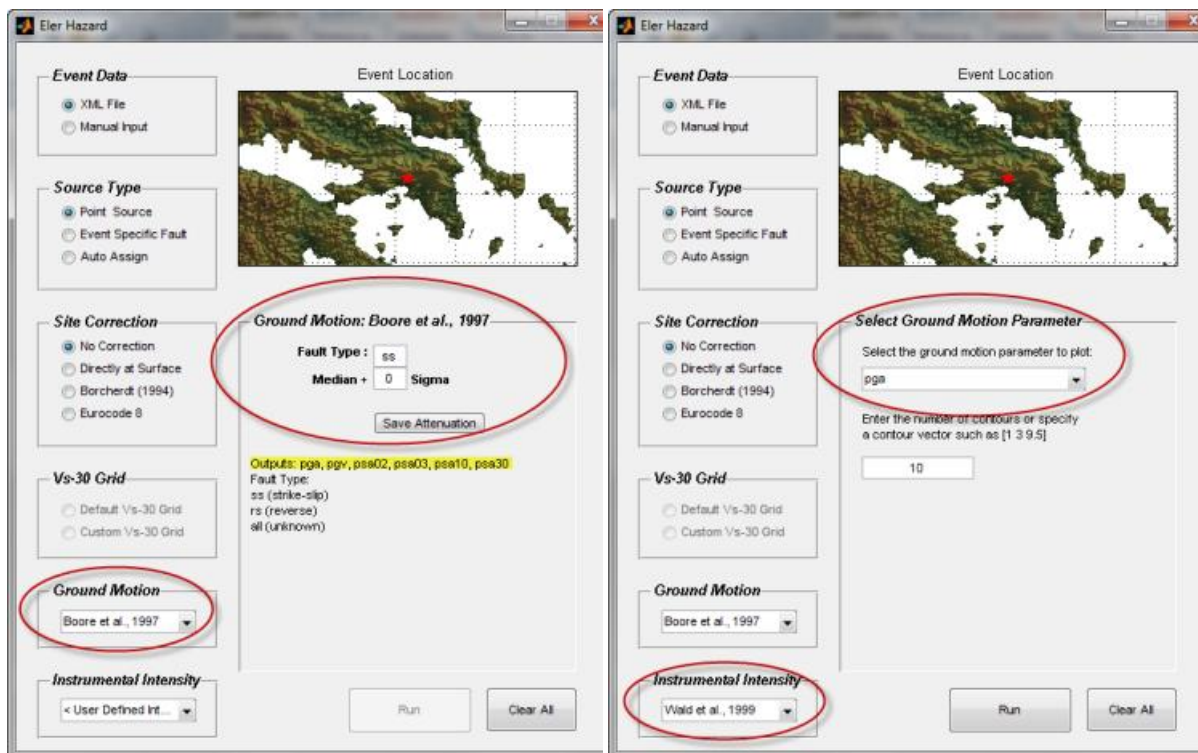


Figure 2.9 Ground Motion Estimation on the left and Instrumental Intensity Estimation on the right figure

Custom Ground Motion Prediction Equations:

ELER Hazard Module also enables the user to define custom ground motion prediction equations (GMPEs). With this feature the user is able to input his/her custom GMPEs in a simple text file format. A user defined equation can also be used for the estimation of intensity values.

Outputs of GMPE's and IPE's can be:

- pga : Peak Ground Acceleration
- pgv : Peak Ground Velocity
- psa02 : PseudoSpectral Acceleration at T=0.2sec
- psa03 : PseudoSpectral Acceleration at T=0.3sec
- psa1.0 : PseudoSpectral Acceleration at T=1.0sec
- psa3.0 : PseudoSpectral Acceleration at T=3.0sec
- intens : Intensity

2.2 Urban Earthquake Loss Assessment module (Level 2)

2.2.1 Introduction

Over the last decade a decent number of earthquake damage or loss scenarios studies were performed, wherein some of the most have been applied to a number of European cities. By scenario it is understood here that the study refers to a given earthquake (having a probability of exceedance higher, equal, or lower than that of the design earthquake specified in the seismic code in force) and provides a comprehensive description of what could happen if such an earthquake occurred; this is different from 'risk analysis' that refers to all the possible earthquakes, estimating the probability of losses over a specified period of time.

Level 2 analysis is essentially intended for earthquake loss assessment (building damage, consequential human casualties and macro-economic loss quantifiers) in urban areas. The basic Shake Mapping is similar to the Level 0 and Level 1 analysis (see Figure 1.3). The spectral acceleration-displacement-based vulnerability assessment methodology is utilized for the building damage estimation. The following methods can be chosen for the analysis:

1. Capacity Spectrum Method (CSM)
2. Coefficient Method (CM)

The building and population data for the Level 2 analysis consist of grid (geo-cell) based urban building and demographic inventories. The user has also the capability to define custom capacity and fragility curves by Building Database Creator- BDC in order to use with any selected method of the Level 2 analysis. Once having calculated the damaged buildings with one of the above methods, casualties in Level 2 analysis are estimated based on the number of buildings in different damage states and the casualty rates for each building type and damage level. Modifications to the casualty rates can be used if necessary.

In the following information of the main items of the spectral capacity-based vulnerability assessment methodology, i.e. representation of the seismic demand, representation of the building capacity and estimation of the performance point. In the next sections the implementation of the analytical methods and the casualty estimation methodology in Istanbul and Thessaloniki are explained in detail.

2.2.2 Spectral Capacity-Based Vulnerability Assessment

The so-called Capacity Spectrum Method (ATC-40, 1996 and HAZUS99) developed for the analytical assessment of the structural vulnerabilities evaluates the seismic performance of structures (represented by equivalent single-degree-of-freedom, SDOF, models) by comparing their structural capacity and the seismic demand curves drawn in spectral acceleration (S_a) versus spectral displacement (S_d) coordinates (hence the terminology: capacity curve and demand spectrum). The key to this method is the reduction of 5%-damped elastic response spectra of the ground motion (in S_a - S_d or the so-called ADRS format) to take into account the inelastic behavior of the structure under consideration. The performance of the building structure to earthquake ground shaking is then identified by the so-called “performance point” located at the intersection of the capacity spectrum of the equivalent non-linear single-degree-of-freedom system and the reduced earthquake demand spectrum. After estimation of the performance point the damage is assessed through the use of fragility curves. Fragility curves calculate the probability of being equal or exceeding a damage state assuming log-normal distribution of damage.

The main ingredients of the capacity spectrum method can be summarized as follow:

- Seismic demand representation : Demand Spectrum
- Structural system representation : Building Capacity Curve
- Structural response assessment : Performance Point
- Representation of the damage probability : Fragility Curves

A schematic description of the methodology is provided in Figure 2.10 where the inelastic acceleration-displacement spectrum for the ground motion (seismic demand spectrum) superimposed with the capacity of a building (capacity curve) and the fragility curves are illustrated. The probability distributions, drawn over both the capacity and demand curves, indicate the associated uncertainty and randomness of performance. The intersection of these spectra gives the expected level of performance (performance point). As it can be seen from Figure 2.10, there is a substantial uncertainty of the location of the performance point and the fragility curves should be able to characterize this probabilistic nature of the problem.

The capacity spectrum method is an approximate method which essentially assumes that a complex non-linear multi-degree-of-freedom system such as a multi-storey building undergoing severe plastic deformations during an earthquake can be modeled as an equivalent single degree of freedom system with an appropriate level of inelasticity. The advantage of the method is its simplicity, as no time history analyses need to be performed.

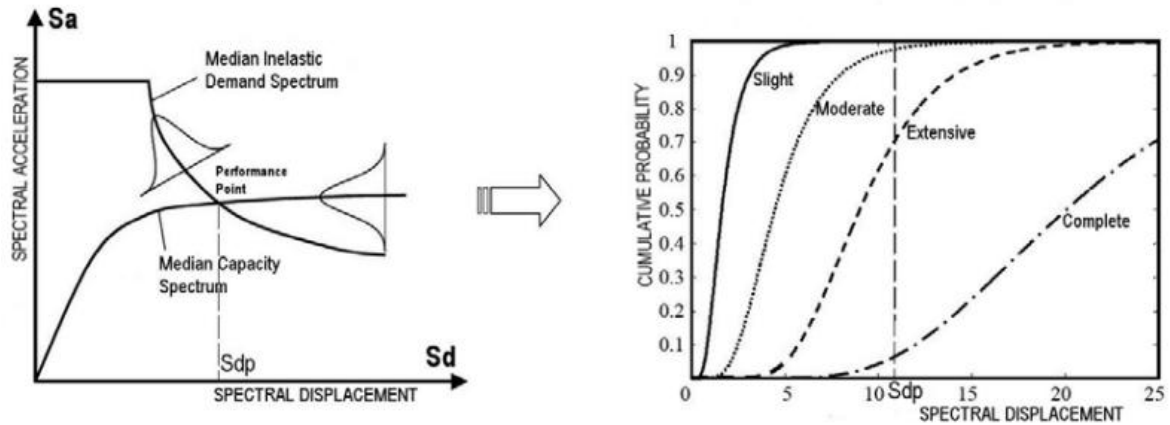


Figure 2.10 Spectral capacity-based vulnerability and damage assessment methodology

2.2.3 Representation of the Seismic Demand

Seismic demand is represented by 5%-damped elastic response spectrum. ELER provides two options for the construction of the response spectral shape:

1. Eurocode 8 Spectrum
2. IBC 2006 Spectrum

In the development process of CSM method NEHRP design spectrum is conducted to obtain the performance point of the buildings.

Eurocode 8-EC8 (European Committee for Standardization CEN, 2003)

EC8 suggests two types of elastic acceleration response spectra for horizontal components of the ground motion: Type 1 and Type 2. The shape of the elastic response spectrum is illustrated in (Figure 2.11).

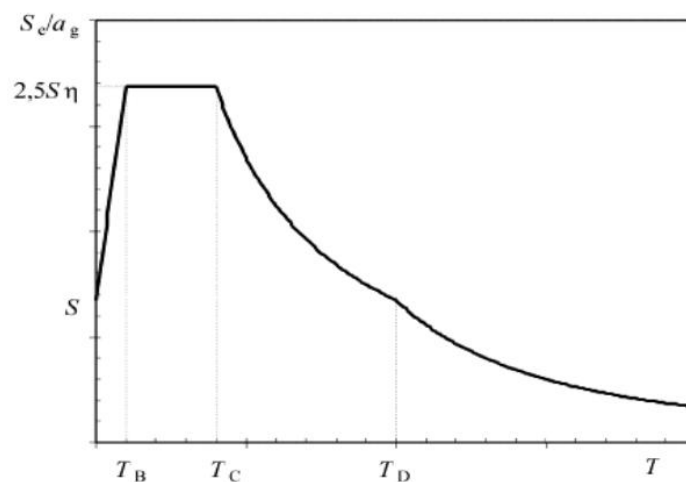


Figure 2.11 Shape of the horizontal elastic response spectrum by EC8

If the earthquakes that contribute most to the seismic hazard defined for the site for the purpose of probabilistic hazard assessment have a surface-wave magnitude, M_s , not greater than 5.5, it is recommended that the Type 2 spectrum is adopted. Type 1 spectrum is used for the earthquakes with magnitude greater than 5.5.

The horizontal elastic response spectrum is defined by:

- a_g : Design ground acceleration on type A ground
- T_B, T_C : The periods that limit the constant spectral acceleration region
- T_D : The period that define the beginning of the constant displacement range of the spectrum
- S : Soil factor
- η : Damping correction factor

The values of T_B, T_C, T_D and S for each ground type and type of spectrum are given in Table 2.1.

Table 2.1 EC8 Type 1 elastic response spectra parameters

Ground type	S	T_B (sec)	T_C (sec)	T_D (sec)
A	1	0.15	0.4	2
B	1.2	0.15	0.5	2
C	1.15	0.2	0.6	2
D	1.35	0.2	0.8	2
E	1.4	0.15	0.5	2

International Building Code-IBC 2006 (International Building Council)

IBC 2006 provides a general horizontal elastic acceleration response spectrum (Figure 2.12). It is defined by:

- S_S, S_1 : Spectral accelerations at short periods and 1-sec period, respectively
- S_{DS}, S_{D1} : Short period and 1-sec period design response spectral accelerations adjusted for the specified site class and damping value
- T_0, T_S : Corner periods of the constant spectral acceleration region given by $T_0=0.2T_S$ and $T_S= S_{D1}/S_{DS}$
- T_L : Long-period transition period. It is a regional-dependent parameter and it is assumed that $T_L=5s$ herein.

The recommended values for the site and damping corrections are given in IBC 2006 and NEHRP 2003 Provisions.

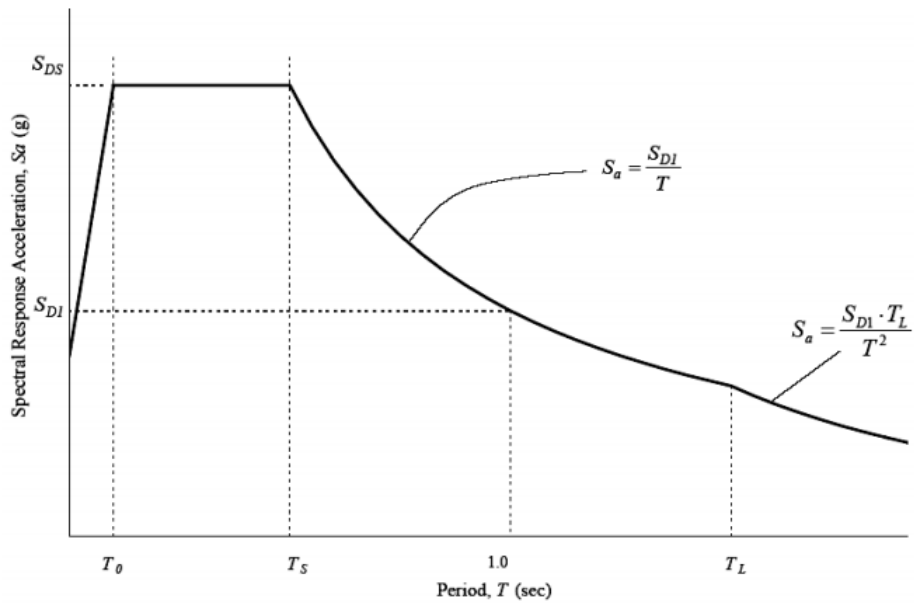


Figure 2.12 Shape of the horizontal elastic response spectrum by IBC-2006

2.2.4 Representation of the Building Capacity

A building capacity curve is the plot of the building's lateral load resistance as a function of a characteristic lateral displacement and quantifies the inelastic structural capacity of the structure. Capacity spectrum can be approximated from a "pushover" analysis in which monotonically increasing lateral loads are applied to the structure and the characteristic deformations (usually roof level displacement) are plotted against the lateral load. The capacity spectrum based vulnerability analysis requires the pushover curve of the MDOF system, quantified by the base shear (V) and the top floor displacement (D), be converted to the capacity spectrum of the equivalent single-degree-of-freedom (SDOF) system quantified by the spectral acceleration (S_a) and spectral displacement (S_d) for direct comparison with the associated demand spectrum.

For each building type the capacity curve has an initial linear section where the slope depends on the typical natural frequency of vibration of the building class, and rises to a plateau level of spectral acceleration at which the maximum attainable resistance to static lateral force has been reached. As an example, a capacity spectrum is shown in Figure 2.13. As it can be seen the capacity curve is controlled by the points of design, yield and ultimate capacities. These points can be correlated with the damage limit states.

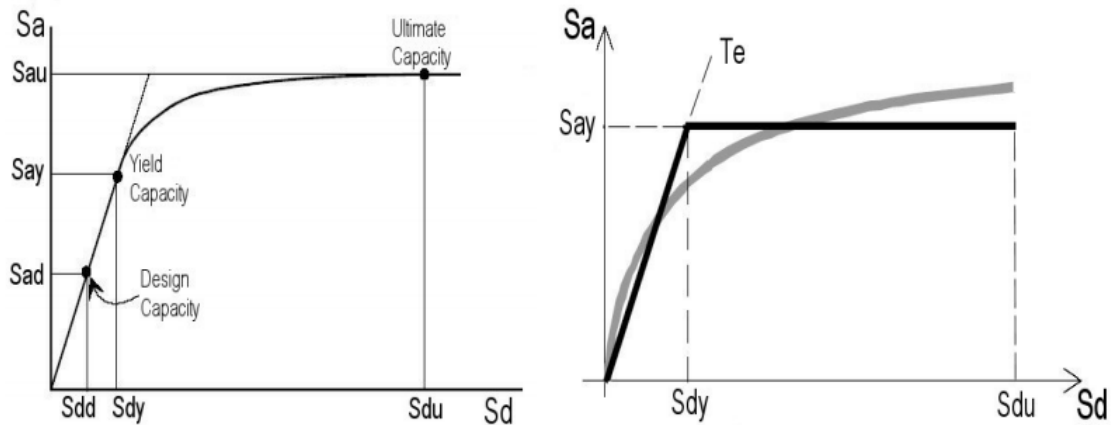


Figure 2.13 Typical structural capacity curve (left) and its simplified form (right)

For the building taxonomies of RISK-UE and HAZUS99, the capacity curve parameters as described above are provided in the ELER database.

2.2.5 Demand Spectrum and the Performance Point

For utilization in capacity spectrum-based vulnerability analysis, the elastic 5% damped response spectra (in spectral acceleration versus period format, S_{ae}, T) is converted into the spectral acceleration (S_{ae}) versus spectral displacement (S_{de}), the so-called ADRS format, through the use of the following transformation (Figure 2.14):

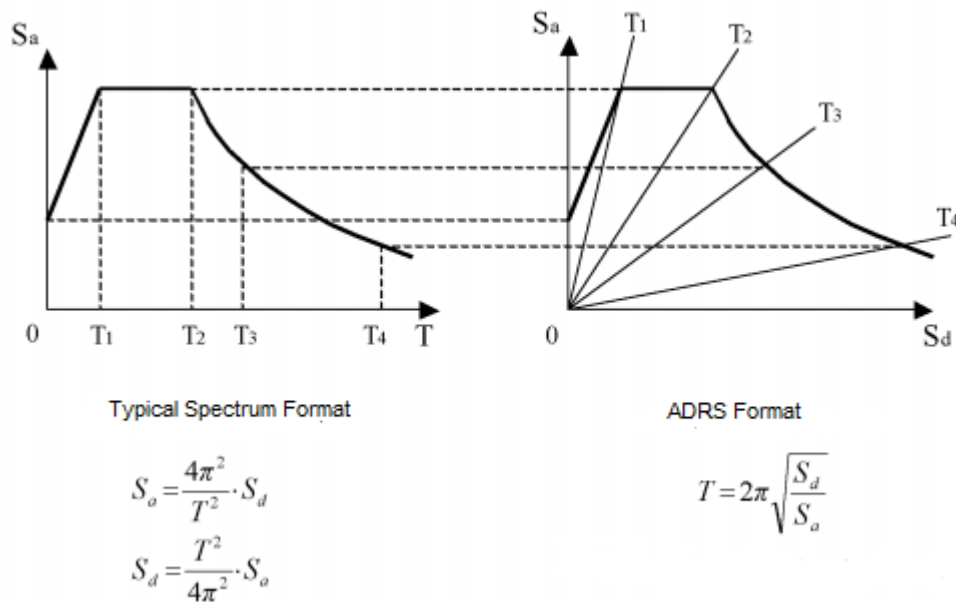


Figure 2.14 The NEHRP – IBC 2006 standardized spectrum shape plotted in ADRS S_{ae} - T (left) format (right).

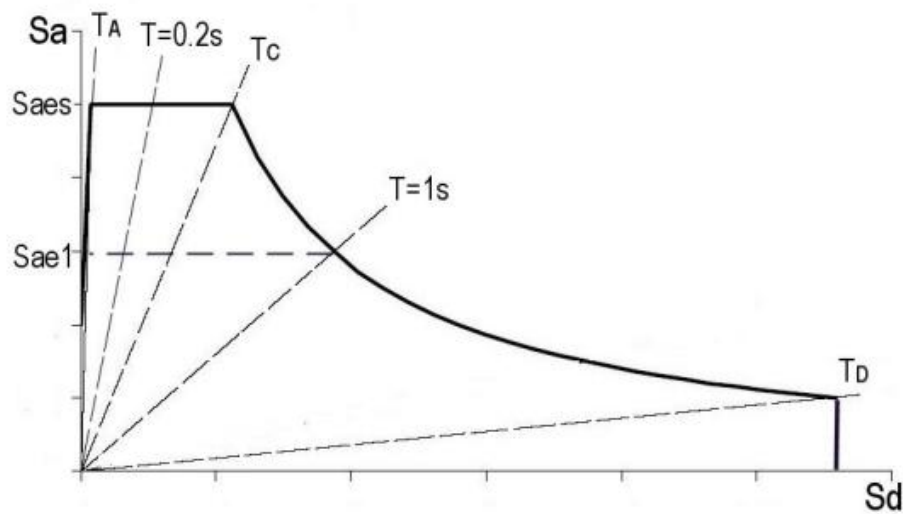


Figure 2.15 NEHRP Spectrum Plotted in ADRS Format (T_A , T_C and T_D show the characteristic periods. S_{aes} and S_{ae1} respectively indicate the short period and 1s period spectral (elastic) accelerations)

Nonlinear Static Procedures are widely used approaches to estimate the performance point (target displacement). The three of commonly used (code-based) procedures are: the Capacity Spectrum Method specified in ATC-40 (1996), its recently modified and improved version Modified Acceleration-Displacement Response Spectrum Method (FEMA-440) and the Coefficient Method originally incorporated in FEMA-356 (2000).

The Capacity Spectrum Method is a form of equivalent linearization that uses empirically derived relationships for the effective period and damping to estimate the response of an equivalent linear SDOF model. The Modified Acceleration-Displacement Response Spectrum Method basically differs from the Capacity Spectrum Method in the reduction of the elastic demand curve. The basic assumption of the equivalent linearization is that the maximum displacement of a nonlinear SDOF system can be estimated from the maximum displacement of a linear elastic SDOF system that has a period and a damping ratio that are larger than those of the initial values for the nonlinear system. The elastic SDOF system that is used to estimate the maximum inelastic displacement of the nonlinear system is usually referred to as the equivalent or substitute system. Similarly, the period of vibration and damping ratio of the elastic system are commonly referred to as equivalent period and equivalent damping ratio, respectively. The equivalent period is computed from the initial period of vibration of the nonlinear system and from the maximum displacement ductility ratio, μ . On the other hand, the equivalent damping ratio is computed as a function of damping ratio in the nonlinear system and the displacement ductility ratio.

The Coefficient Method is essentially a spectral displacement modification procedure in which several empirically derived factors are used to modify the response of a linearly-elastic equivalent SDOF model of the building structure.

Another nonlinear static procedure is the so-called “N2” method (Fajfar, 2000) in which the inelastic demand spectra is obtained from standardized (code-based) elastic design spectra using ductility based reduction factors. The “N2” method (herein called the Reduction Factor Method) has been implemented in the so-called “Mechanical-Based Method” of vulnerability analysis (Lagomarsino and Giovinazzi, 2006) in the RISK-UE (2001-2004) project.

All four of these methodologies require development of a pushover curve (capacity spectrum for the equivalent SDOF system) to provide the relationship between the base shear and lateral displacement of a control node (usually located at roof level). They differ mainly in the computation of the demand spectrum and the performance point. For the *Level 2 Loss Assessment*, computation of the demand spectrum and estimation of the performance point by each method is explained in the forthcoming sections. Following the computation of the performance point, calculation of the damage probabilities by use of fragility curves and the estimation of casualties are described.

Capacity Spectrum Method (CSM)

The Capacity Spectrum Method (CSM) utilizes the equivalent linearization for the estimation of the performance point which is the intersection of the building capacity spectrum with the demand response spectrum reduced for nonlinear effects. The performance point represents the condition for which the seismic capacity of the structure is equal to the seismic demand imposed on the structure by the given level of ground shaking (ATC-40).

To account for the increased hysteretic damping as the building shifts from elastic into inelastic response, the spectral reduction factors in terms of effective damping are introduced. The effective damping (essentially the equivalent damping, β_{eq}) can be calculated as a function of the capacity curve, the estimated displacement demand and the resulting hysteresis loop. Figure 2.16 shows the building capacity spectrum with the idealized hysteresis loop for a ductile building with equivalent viscous damping less than 30% and subjected to relatively short duration of ground shaking. For more realistic approximation of the hysteretic energy dissipated by the structure, the effective viscous damping (β_{eff}) concept is utilized with the consideration of a damping modification factor (κ). By the incorporation of Figure 2.16, the effective damping is defined as:

$$\beta_{eff} = \kappa\beta_o + 5 = \frac{63.7\kappa(a_y d_{pi} - d_y a_{pi})}{a_{pi} d_{pi}} + 5$$

where β_o is the hysteretic damping and “5” stands for the 5% viscous damping inherent in the structure (assumed to be constant).

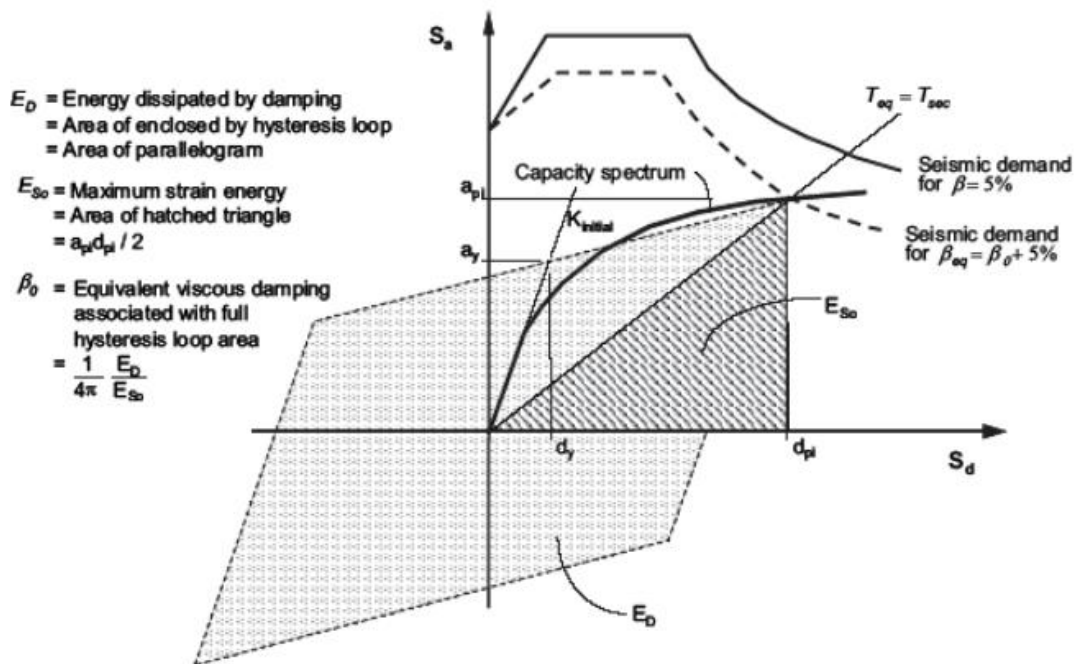


Figure 2.16 Graphical representation of the idealized hysteretic damping and the reduction of the 5%-damped elastic demand spectrum (modified after ATC-40)

The κ -factor is related to the structural behaviour. ATC-40 provides three categories of structural behavior:

- Type A– stable, reasonably full hysteresis loops
- Type B– moderately reduced hysteretic behavior
- Type C– poor hysteretic behavior

The variation of κ values is presented in Table 2.2.

Besides, the methodology recognizes the importance of the duration of ground shaking on building response by reducing effective damping (i.e., κ factors) as a function of shaking duration. Shaking duration is described qualitatively as *short*, *moderate* or *long*, and is assumed to be a function of earthquake magnitude (although proximity to fault rupture also influences the duration of ground shaking).

- For scenario earthquakes of magnitude $M \leq 5.5$, effective damping is based on the assumption of ground shaking of Short duration
- For scenario earthquakes of magnitude $M \geq 7.5$, effective damping is based on the assumption of ground shaking of Long duration
- Effective damping is based on the assumption of Moderate duration for all other earthquake magnitudes (including probabilistic, or other, analyses of unknown magnitude)

Table 2.2 Degradation factors (κ) as a Function of Short, Moderate and Long Earthquake Duration (Hazus-MH Technical Manual)

Degradation factors (κ)			
Behavior type	Duration of Earthquake		
	Short	Moderate	Long
Poor	0.6	0.3	0.1
Average	0.8	0.4	0.2
New	0.9	0.6	0.4

To obtain the reduced demand spectrum ATC-40 applies the following spectral reduction factors:

$$SR_A = \frac{3.21 - 0.68 \ln(\beta_{eff})}{2.12}$$

$$SR_V = \frac{2.31 - 0.41 \ln(\beta_{eff})}{1.65}$$

SR_A and SR_V are, respectively, applied to the constant acceleration and the constant velocity regions of the 5%-damped elastic demand spectrum. SR_A and SR_V are limited by the values given in Table 2.3.

Table 2.3 Minimum allowable values for the spectral reduction factors

Structural Behavior Type	SRA	SRV
Type C	0.56	0.67
Type B	0.44	0.56
Type A	0.33	0.5

For the determination of the performance point two criteria needs to be satisfied:

1. the point must lie on the capacity curve to represent the structure at a given displacement
2. the point must lie on a reduced demand spectrum that represents the nonlinear demand at the same structural displacement

In order to achieve this, three iterative procedures based on trial and error search are suggested in ATC-40. The so-called Procedure A is utilized in the implementation of the CSM herein. In Procedure A, a trial performance point (a_{pi} , d_{pi}), is selected. Then, the bilinear capacity spectrum and the reduced demand spectrum are drawn on the same plot. It is determined whether the demand spectrum intersects the capacity spectrum at the point (a_{pi} , d_{pi}) or if the displacement at which the demand spectrum intersects the capacity spectrum, d_i , is within acceptable tolerance of d_{pi} . Figure 2.17 illustrates the determination of the performance point by Procedure A.

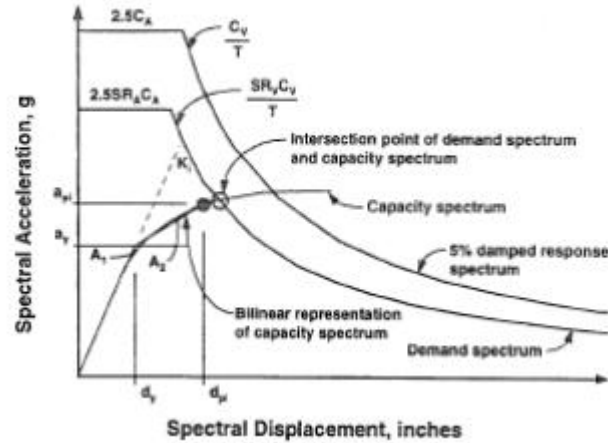


Figure 2.17 Capacity and demand spectra, and the performance point at the last step of Procedure A (taken from ATC)

Coefficient Method (CM)

The Coefficient Method (CM), presented as a nonlinear static analysis procedure in FEMA-356 (2000) and FEMA-273 (1977) essentially modifies the linear elastic response of the equivalent SDOF system by multiplying it by a series coefficients to generate an estimate of the target displacement (performance point). The coefficient method has been critically evaluated in FEMA-440 (2005) and the results reflected in ASCE/SEI 41-06 (2007).

Using this method the inelastic spectral displacement demand (the performance point, S_{dp}) is obtained through multiplying the elastic spectral displacement (S_{de}) by the C_0 , C_1 and C_2 coefficients.

$$S_{dp} = C_0 C_1 C_2 S_{de}$$

The elastic spectral displacement is computed at the fundamental period (T_e) of the equivalent SDOF system.

C_0 is the modification factor that relates the spectral displacement of the equivalent SDOF system to the roof displacement of the building's MDOF structural system. C_0 is equal to the first mode participation factor at the roof level ($C_0 = \Gamma$ if the amplitude of the mode at the roof level is set to unity). Table 2.4 provides tabulated values of C_0 for general building types (ASCE/SEI 41-06 2007). C_0 increases with number of floors and varies between 1 and 1.5.

Table 2.4 C_0 Coefficient (ASCE/SEI 41-06 2007)

Number of Stories	C_0
1	1
2	1.2
3	1.3
5	1.4
10+	1.5

The C_1 coefficient, defined as the modification factor to relate expected maximum inelastic displacements to displacements calculated for linear elastic response, is given by (ASCE/SEI 41-06, 2007):

$$C_1 = 1 + (R_y - 1) / (aT_{eff}^2)$$

$$C_1 \leq C_1(T_{eff} = 0.2 \text{ sec}) \text{ for } T_{eff} \leq 0.2 \text{ sec}$$

$$C_1 = 1.0 \text{ for } T_{eff} \geq 1.0 \text{ sec}$$

where T_{eff} is the effective fundamental period of the building computed by modifying the fundamental mode vibration period (T_e , obtained from linearly elastic dynamic analysis) by:

$$T_{eff} = T_e \sqrt{\frac{K_i}{K_{eff}}}$$

where K_i is the elastic stiffness of the building and K_{eff} is the effective stiffness of the building obtained by idealizing the pushover curve as a bilinear relationship. In the application of Coefficient Method herein, it is assumed that T_{eff} is equal to T_e .

R_y represents the ratio of elastic strength demand to yield strength:

$$R_y = \frac{S_{ae}(T_{eff})}{S_{ay}}$$

where $S_{ae}(T_{eff})$ represents the elastic spectral acceleration at the effective fundamental period of the structure and S_{ay} refers to the yield spectral acceleration.

The factor “a” is called the site class factor and is assigned the following values:

a=130 for NEHRP site class A and B

a=90 for NEHRP site class C

a=60 for NEHRP site class D, E and F

The C_2 coefficient represents the modification factor for the effect of pinched hysteresis shape, cyclic stiffness degradation and strength deterioration (ASCE/SEI 41-06, 2007):

$$C_2 = 1 + \frac{1}{800} \left(\frac{R_y - 1}{T_{eff}} \right)^2$$

$$C_2 = 1.0 \text{ for } T_{eff} \geq 0.7 \text{ sec}$$

When comparing the Coefficient Method with the Capacity Spectrum Method of Level 2 analysis, discrepancies in damage estimations might be expected to some degree. While CSM method relies on more complicated procedures, e.g. equivalent linearization, reduction of the demand spectra and the iterative procedures for estimating the performance point, the Coefficient Method modifies the elastic spectral displacement by multiplying some coefficients to obtain the performance point.

2.2.6 Fragility Curves

To estimate the performance of a group of buildings of a particular class under given ground shaking, the spectral response of the building at the performance point for the standard building of that class, as defined above, is used in conjunction with a set of fragility curves for that class, which estimate the probability of any particular building exceeding each of the damage states after shaking at any given spectral response level.

The fragility curves represent the probability-based relation between the expected response and the performance limits in terms of the cumulative density function of the probability of exceeding of specific damage limit states for a given peak value of a seismic demand. If structural capacity and seismic demand are random variables that roughly conform to either a normal or log-normal distribution then, following the central limit theorem, it can be shown that the composite performance outcome will be log-normally distributed. Therefore, the probabilistic distribution is expressed in the form of a so-called fragility curve given by a log-normal cumulative probability density function (Figure 2.18).

The analytical expression of each fragility curve is based on the assumption that earthquake damage distribution can be represented by the cumulative standard lognormal distribution function, Φ , (HAZUS 1999, Kircher et al. 1997).

$$P[Damage \geq D_k | S_{dp}] = \Phi \left[(1/\beta_k) \ln(S_{dp} / \bar{S}_{d,k}) \right]$$

Here S_{dp} is performance point, $S_{d,k}$ is median spectral displacement value corresponding to the related damage level (i.e. slight, moderate, heavy or very heavy), β_k is standard deviation of spectral displacements natural logarithm for related damage level and Φ is cumulative standard normal distribution function. Median spectral displacements are estimated for each building type depending on the floor displacements.

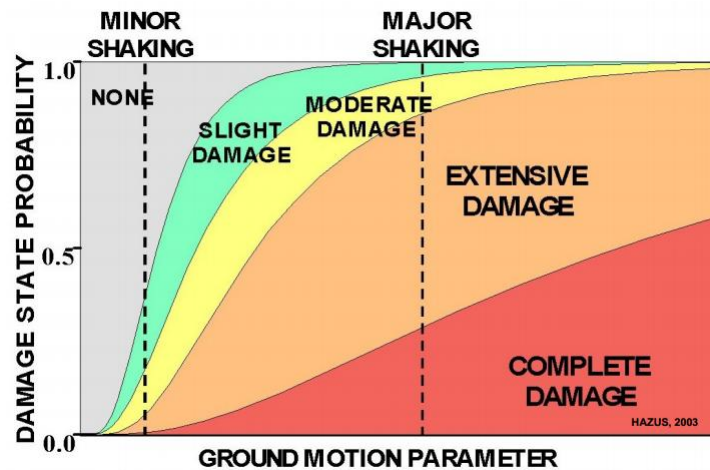


Figure 2.18 General example fragility curves (HAZUS, 2003)

In Figure 2.19 , the horizontal axis represents the spectral displacement demand and the vertical axis refers to the cumulative probability of structural damage reaching or exceeding the threshold of a given damage state.

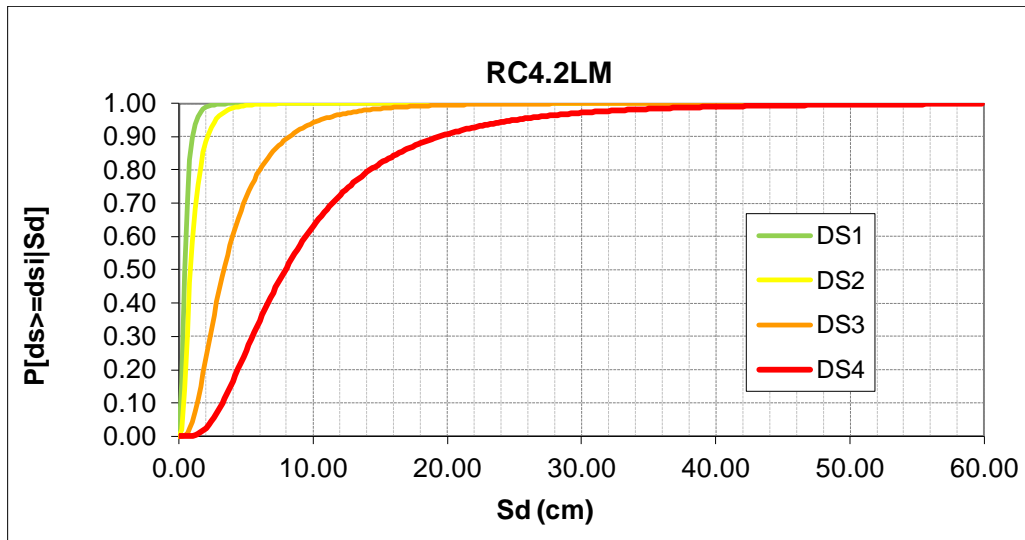


Figure 2.19 Example fragility curves for four damage levels (Kappos et al., 2006)

An example how Capacity Spectrum Method in ELER combines fragility curves, capacity curves and demand spectrum is given below:

To estimate the building damage in each cell, ELER firstly calculates the PGA value at bedrock in each cell in Hazard Module. Taking the Vs30 value in the same cell, the user can create the elastic response spectrum by EC8 (Figure 2.20).

GridID	Vs30 (m/s)	Type	PGA (g)
348	431	B	0.10

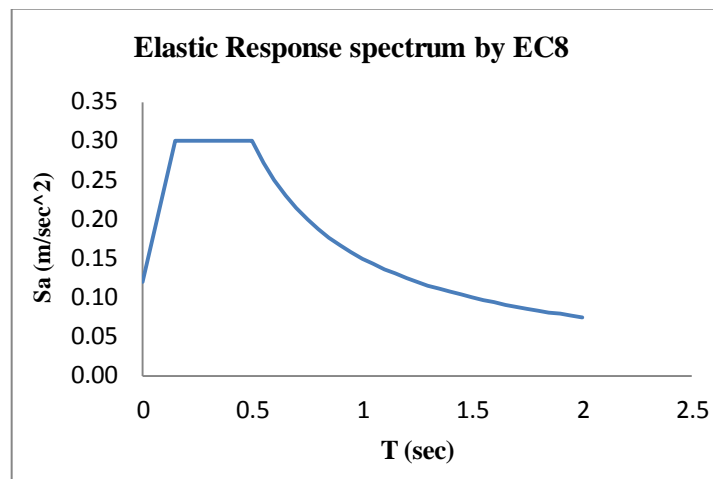


Figure 2.20 EC8 elastic response spectrum

Following this, the elastic response spectrum is converted into the spectral acceleration versus spectral displacement spectrum; the so-called ADRS format (Acceleration-Displacement Response Spectrum).

The demand response spectrum is reduced for nonlinear effects, taking into consideration the equivalent damping β_{eq} (Figure 2.21). In the same plot, the capacity curve is also plotted in order to determine the performance point. For the specific example, the performance point is equal to 2.42 cm.

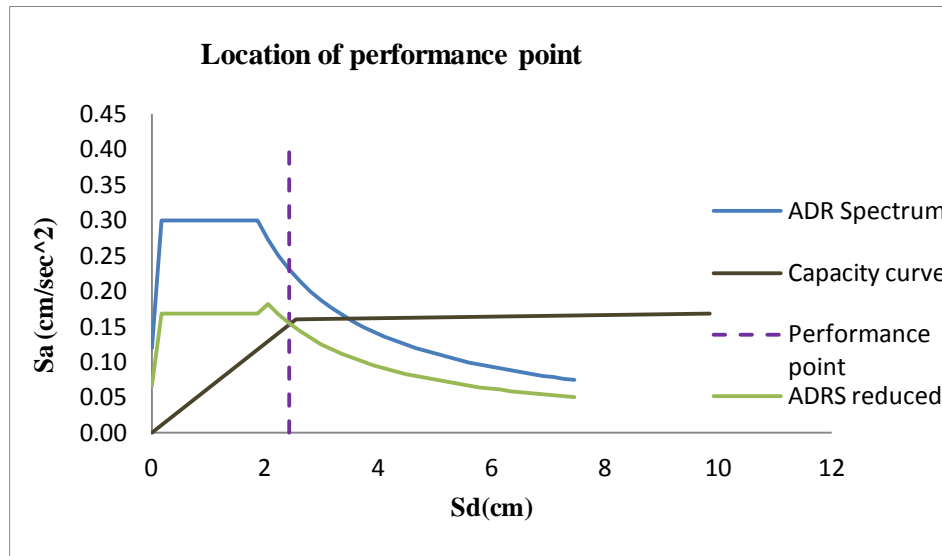


Figure 2.21 Spectral capacity - based vulnerability. The performance point is the intersection of the capacity curve and the reduced ADRS.

After determining the performance point, probabilities of exceedance of four damage states are calculated from the appropriate displacement-based fragility curves, using the performance point as displacement. The performance point intersects the curves, so percentage for each damage state is calculated (see Figure 2.22 and Table 2.5).

$$P_{\text{none}} = 1.0 - P(ds \geq DS1) = 1.0 - 0.68 = 0.32$$

$$P_{\text{slight}} = P(ds \geq DS1) - P(ds \geq DS2) = 0.68 - 0.43 = 0.25$$

$$P_{\text{moderate}} = P(ds \geq DS2) - P(ds \geq DS3) = 0.43 - 0.11 = 0.32$$

$$P_{\text{extensive}} = P(ds \geq DS3) - P(ds \geq DS5) = 0.11 - 0.03 = 0.08$$

$$P_{\text{complete}} = P(ds \geq DS1) = 0.03$$

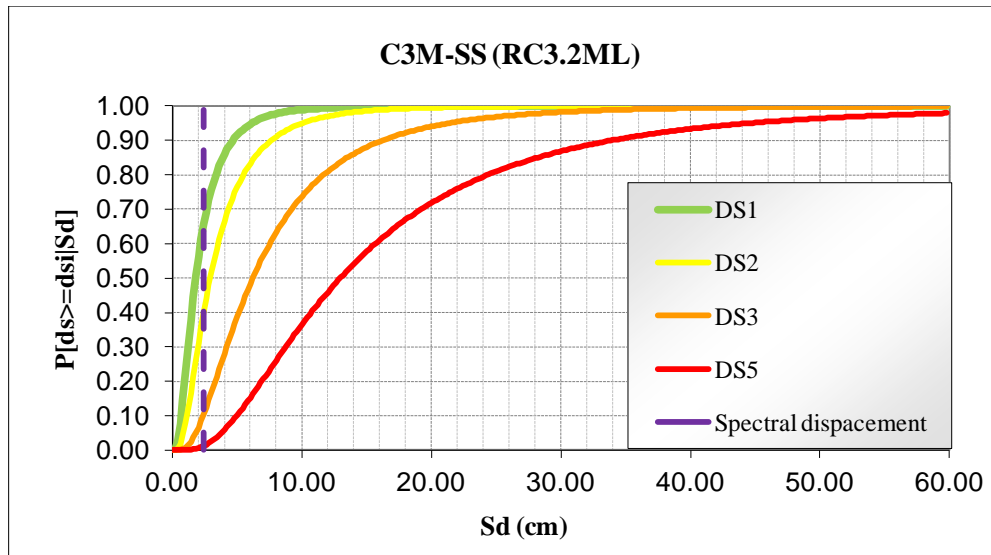


Figure 2.22 Damage assessment methodology. Fragility curves are taken from (Kappos et al., 2006)

Table 2.5 Damage percentages for each damage state for building typology RC3.2ML in GridID 348

None	Slight	Moderate	Extensive	Collapse	Total	
32	25	32	8	3	100	%
2.56	2	2.56	0.64	0.24	8	number of buildings

Finally, the diagram in Figure 2.23 depicts the discrete percentage of each damage state.

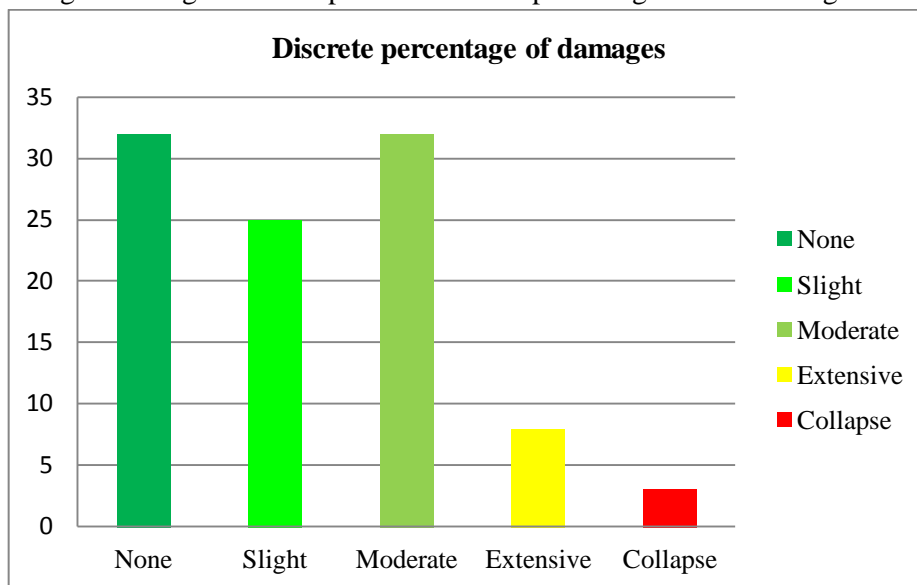


Figure 2.23 Damage percentages for each damage states for building typology RC3.2 ML in GridID 348

2.2.7 Casualty Model

Once the definition of a grid based building inventory and a grid based population distribution is completed, the software calculates the number of dwelling units (using user defined estimated number of dwellings per building type) and an average population per dwelling unit for each cell. Then, casualties for each building type, building damage level and injury severity level can be calculated by the following equation:

$$K_{ij} = \text{Population per Building} * \text{Number of Damaged Building in damage state } j * \text{Casualty Rate for severity level } i \text{ and damage state } j$$

Three casualty models are included in ELER. These are HAZUS99 (FEMA, 1999), HAZUS-MH (FEMA, 2003) and the KOERI (2002) casualty models. All studied scenarios use HAZUS MH approach. The output from the module consists of a casualty breakdown by injury severity level, defined by a four level injury severity scale (Durkin and Thiel, 1993; Coburn and Spence, 1992; Cheu, 1994). Table 2.6 defines the injury classification scale used in the methodology.

Table 2.6 Injury severity levels

INJURY SEVERITY	INJURY DESCRIPTION
Level 1	Injuries requiring basic medical aid without requiring hospitalization
Level 2	Injuries requiring medical care and hospitalization, but not expected to progress into a life threatening status
Level 3	Injuries that pose an immediate life threatening condition if not treated adequately and expeditiously. The majority of these injuries result because of structural collapse and subsequent collapse or impairment of the occupants.
Level 4	Instantaneously killed or mortally injured

3. Application to Istanbul

3.1 Buildings and population data for Zeytinburnu district of Istanbul

3.1.1 Classification of buildings in Istanbul (Zeytinburnu)

The Zeytinburnu District is selected for this application. The data for building assets in the Zeytinburnu District were collected in the framework title of the “Urban Transformation” project of the Istanbul Metropolitan Municipality (IMM) and it is considered to be of high quality and accuracy. Due to the detailed and complete database the loss assessment analysis is expected to be more reliable.

In ELER, the building inventory should be associated with geographical coordinates in order to perform an urban loss estimation study resulting from the ground motion generated by a specific earthquake.

The grid based building inventory of Marmara region is based on the year 2000 census, which has been carried out by Turkish Statistical Institute (TUIK). The data for buildings include the construction year, the occupational type, the construction type and the number of floors of each building. Since the seismic design code applicable in Turkey improved particularly after 1975, buildings were classified as pre-1979 (included) and post-1980 reflecting the state of seismic design applications. The inventory is classified in the following way in accordance with the EMS building classification system.

The construction type was selected as the basic parameter to be distributed to geocells. Next, the number of floors and the age of building were added using a logic tree and the district based ratios of these two parameters (Table 3.1).

Table 3.1 The logic tree to obtain the numbers for each of building class (taken from ELER)

Construction Type	The story Number of Buildings	Construction Year
RC1	Low Rise	Pre – 1980
M1- Rubble	Mid Rise	Post - 1980
M2- Adobe	High Rise	
M5 – Unreinforced Masonry		

For this purpose, a more detailed inventory is provided for the Zeytinburnu district of Istanbul (Figure 3.1) as an input to be used in Level 2. This inventory was based on the 1/5000 scale building footprint maps of the Istanbul Metropolitan Municipality (IBB) and TUIK year 2000 building census (KOERI, 2002). The building inventory is classified both in terms of the European Building Classification System and also a HAZUS similar system considering the construction type, the height and the construction year of the buildings, as it is shown in Table 3.2. The building inventory is provided in 0.005°x0.005° geocell (Figure 3.2 and Figure 3.3).

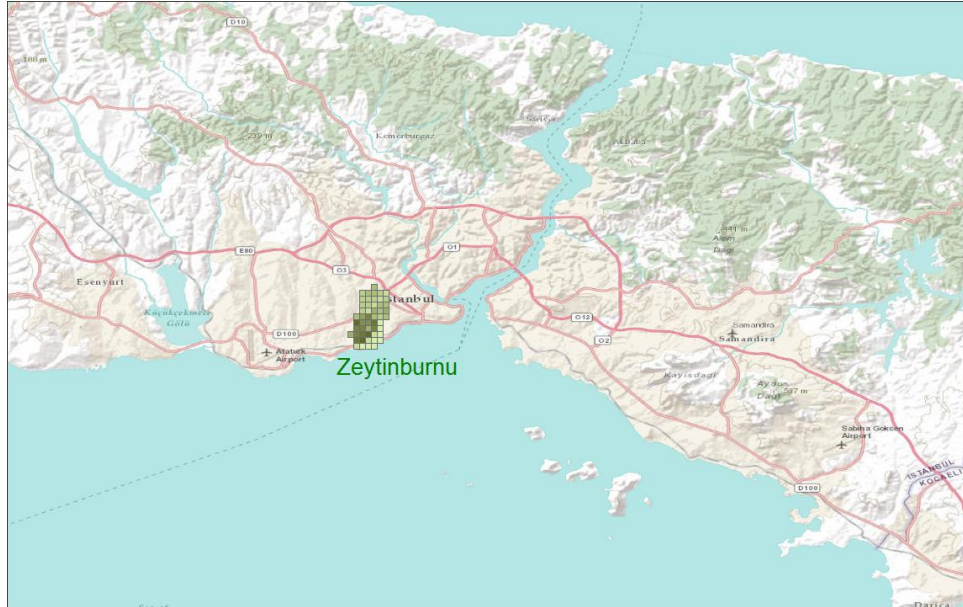


Figure 3.1 Location of Zeytinburnu district in Istanbul Metropolitan Municipality

Table 3.2 Building inventory of Zeytinburnu based on RISK-UE Building Taxonomy

Type	Corresponding to European Building Class	Structural System	Number of Floors	Construction year
B111	M7_L	Other-Unknown	1--4	-1979
B121	M7_M	Other-Unknown	5--8	-1979
B131	M7_H	Other-Unknown	9+	-1979
B112	M7_L	Other-Unknown	1--4	1980-2000
B122	M7_M	Other-Unknown	5--8	1980-2000
B132	M7_H	Other-Unknown	9+	1980-2000
B211	M7_L	Masonry	1--4	-1979
B221	M7_M	Masonry	5--8	-1979
B231	M7_H	Masonry	9+	-1979
B212	M7_L	Masonry	1--4	1980-2000
B222	M7_M	Masonry	5--8	1980-2000
B232	M7_H	Masonry	9+	1980-2000
B311	RC3_DCL_II_M	Precast	1--4	-1979
B321	RC3_DCL_II_M	Precast	5--8	-1979
B331	RC3_DCL_II_M	Precast	9+	-1979
B312	RC3_DCL_II_M	Precast	1--4	1980-2000

B322	RC3_DCL_II_M	Precast	5--8	1980-2000
B332	RC3_DCL_II_M	Precast	9+	1980-2000
B411	S	Steel	1--4	-1979
B421	S	Steel	5--8	-1979
B431	S	Steel	9+	-1979
B412	S	Steel	1--4	1980-2000
B422	S	Steel	5--8	1980-2000
B432	S	Steel	9+	1980-2000

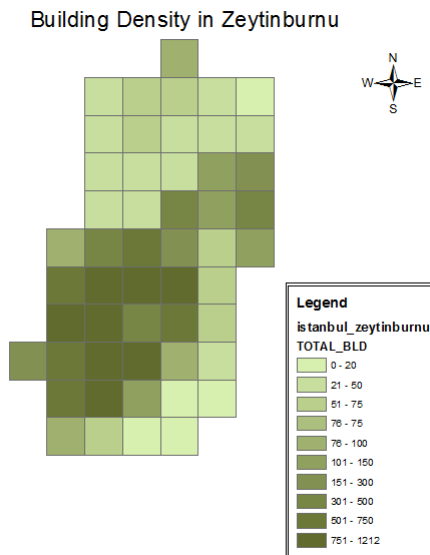


Figure 3.2 Building density in Zeytinburnu

- Total number of buildings (all types): 14482
- Total population: 243188

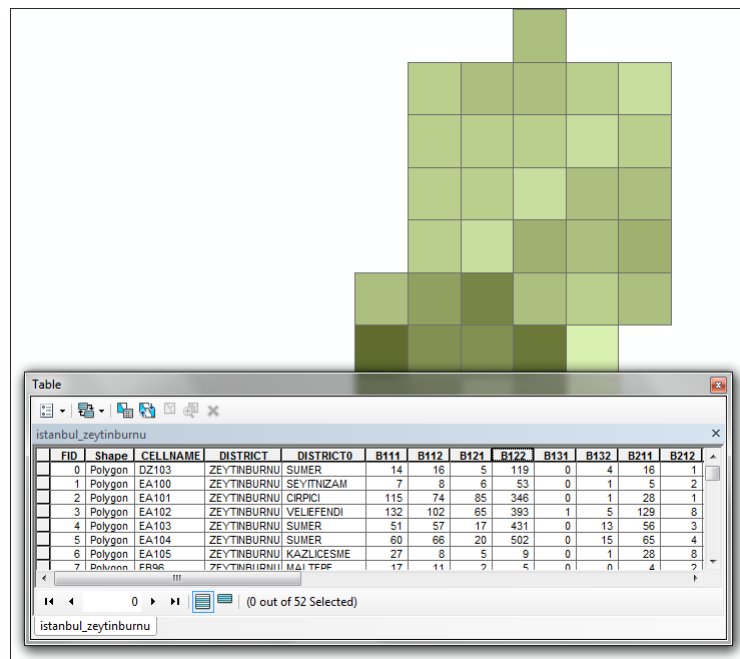


Figure 3.3 ArcGIS shape file with its attribute table; data refers to cells

3.2 Fragility and Capacity Curves for Istanbul building stock

3.2.1 Structural Damage Levels

Structural damage levels definitions for RC buildings in Istanbul are given below:

- *slight damage*: In some columns, beams and near joints, there may be some hairline cracks. In dual systems (shear-wall), there may be also some small shear cracks.
- *moderate damage*: Cracking in most of beams and columns. In some ductile frames, ultimate capacity reached in some elements, so wider cracks are formed (approximately 2mm). In non-ductile frame elements and in dual systems diagonal shear cracks are formed rather than small cracks.
- *extensive damage*: Most of the ductile frame elements reach to their limit capacities and wider cracks are formed (approximately 3mm or wider). Some re-bar may buckle.
- *complete damage*: Complete or impending collapse.

Structural damage levels definitions for Masonry buildings are described below:

- *Structural slight damage*: In the surface of structural walls there may be small cracks, wider cracks may occur between door and window gaps. Cracks may occur on the base of parapets, and movements can be seen on lentos.
- *Structural moderate damage*: There may be cracks in diagonal direction on surface of the most of the structural walls. In some parts walls are dispatched from floors. Severe cracks on window below parapets may be seen and fall of bricks can be seen.
- *Structural heavy damage*: In almost all of the structural walls there may be very wide cracks. In many parapets and walls brick falls are seen. Floors and roofs move. Permanent deformations and displacements are observed.
- *Structural very heavy damage*: Structure collapses due to the extreme deformation or become in a condition near to collapse.

3.2.2 Fragility curves

The fragility curve parameters as well as capacity curve parameters are provided in the ELER database (Figure 3.4 and Figure 3.5) for the building classes in Istanbul, based on RISK-UE building typologies.

	I	J	H (m)	α_2	Slight			Moderate			Extensive			Complete		
					D_s (%)	$S_{d,s}$ (cm)	β_s	D_m (%)	$S_{d,m}$ (cm)	β_m	D_e (%)	$S_{d,e}$ (cm)	β_e	D_c (%)	$S_{d,c}$ (cm)	β_c
K = 1	1	1	6	0.75	0.40	1.80	0.95	0.80	3.60	0.91	2.00	9.00	0.85	4.00	18.00	0.97
	1	2	15	0.75	0.35	3.94	0.70	0.80	9.00	0.74	1.60	18.00	0.86	3.00	33.75	0.98
	1	3	30	0.65	0.30	6.75	0.70	0.80	18.00	0.81	1.20	27.00	0.89	2.50	56.25	0.98
	2	1	6	0.75	0.30	1.35	0.99	0.70	3.15	1.05	1.60	7.20	1.10	3.20	14.40	1.08
	2	2	10	0.75	0.35	2.63	0.70	0.80	6.00	0.74	1.60	12.00	0.86	3.00	22.50	0.98
	3,4	1	6	0.75	0.40	1.80	0.95	0.80	3.60	0.91	2.00	9.00	0.85	4.00	18.00	0.97
	3,4	2	15	0.75	0.30	3.38	0.70	0.60	6.75	0.74	1.20	13.50	0.86	2.67	30.04	0.98
K = 2	1	1	6	0.75	0.50	2.25	0.89	1.00	4.50	0.90	2.50	11.25	0.90	5.00	22.50	0.89
	1	2	15	0.75	0.40	4.5	0.70	1.00	11.25	0.70	2.00	22.50	0.70	4.00	45.00	0.89
	1	3	30	0.65	0.40	9.00	0.66	1.00	22.50	0.66	1.60	36.00	0.76	3.20	72.00	0.91
	2	1	6	0.75	0.40	1.80	0.99	0.90	4.05	1.05	2.00	9.00	1.10	4.00	18.00	1.08
	2	2	10	0.75	0.40	3.00	0.70	1.00	7.50	0.70	2.00	15.00	0.70	4.00	30.00	0.89
	3,4	1	6	0.75	0.50	2.25	0.89	1.00	4.50	0.90	2.50	11.25	0.90	5.00	22.50	0.89
	3,4	2	15	0.75	0.40	4.50	0.70	0.70	7.88	0.70	1.60	18.00	0.70	3.33	37.46	0.89
3,4	3	30	0.60	0.40	9.00	0.66	1.00	22.50	0.66	1.60	36.00	0.76	3.20	72.00	0.91	

Figure 3.4 Spectral displacement- based fragility curves parameters

A	B	C	D	E	F	G	H	I	J	K	L	M	N	O	P	Q	R	S	T	U	V
Building Name	Fragility Curves				Capacity Curve				Economic Loss	Structural Behaviour Degradation Factor			Building Cost	Structural Behaviour Degradation Factor			Ductility Value	Building Characteristics			
	Slight Median Beta	Moderate Median Beta	Extensive Median Beta	Complete Median Beta	Yield Displacement	Ultimate Acceleration	Elastic Displacement	Damping		Short	Moderate	Long		CO coefficient	Period						
B111	0.018	0.95	0.036	0.91	0.09	0.85	0.18	0.97	0.007753097	1.913	0.015506194	1.913	0.006590132	5	1000	0.8	0.4	0.2	2	1.1	0.211
B211	0.0394	0.7	0.09	0.74	0.18	0.86	0.3375	0.98	0.024108109	1.692	0.048216218	1.692	0.020491893	5	1500	0.9	0.6	0.3	3	1.3	0.355
B221	0.018	0.95	0.036	0.91	0.09	0.85	0.18	0.97	0.007753097	1.913	0.015506194	1.913	0.006590132	5	1000	0.8	0.4	0.2	2	1.1	0.211
B212	0.0394	0.7	0.09	0.74	0.18	0.86	0.3375	0.98	0.024108109	1.692	0.048216218	1.692	0.020491893	5	1500	0.9	0.6	0.3	3	1.3	0.355

Figure 3.5 Example excel document for fragility and capacity curves in Istanbul

3.2.3 Capacity curves

A building capacity curve is the plot of the building's lateral load resistance as a function of a characteristic lateral displacement and quantifies the inelastic structural capacity of the structure. Each building type in Istanbul has its own capacity curve quantified by the spectral acceleration (S_a) and spectral displacement (S_d).

3.3 Hazard Scenarios for Istanbul; the 1999 Kocaeli Earthquake (scenario A)

3.3.1 Introduction

The Marmara Sea region housing one third of Turkey's population is one of the most tectonically active regions in Eurasia. In the last century, this region witnessed seismic activities with nine district events having $M_w > 7.0$ (M_w stands for moment magnitude). In 1999, two destructive earthquakes (Kocaeli and Duzce) occurred in the eastern part of the Marmara region on the North Anatolian Fault (NAF) system. This strike-slip fault system cuts across northern Turkey for more than 1500 km, and accommodates 25 mm/year right-lateral slip between Anatolia and Eurasian plate (Straub et al., 1997; McClusky et al., 2000). Based on the renewal model, the probability of occurrence of M7.0 and greater earthquakes in the Marmara Sea region (which would directly affect the Istanbul Metropolitan area) was computed as 44 ± 18 percent in the next 30 years (Parsons, 2004). As implied by the level of hazard exposure in the Marmara region, and especially in the Istanbul Metropolitan area due to its socio-economic importance, critical assessment of the regional seismic hazard retains paramount priority for preparedness and other regional earthquake engineering applications.

3.3.2 Regional seismicity and tectonic setting

The Marmara Sea region, limited in this study within latitudes 39-43 deg. N and longitudes 26-32 deg. E, is one of the most seismically active regions of the continent as manifested by the number of large earthquakes (M 6.0) that occurred during 1509-1999. The epicenters of these events are depicted in Figure 3.6. Many of these events ruptured on or in proximity of the NAF system. A moderate to large earthquakes with M 6.0 also occurred on fault segments situated well away from the NAF. For regional seismic hazard formulation, all potential sources of seismic activity that could produce significant ground motions were identified and characterized based on geologic, tectonic, historical and instrumental evidences. Two major ingredients of hazard computation that follow are the earthquake catalog and fault segmentation data (Kalkan et al., 2008). The current regulatory seismic zoning map in Turkey including the Marmara Sea region is based on a study (Gulkan et al., 1993) using then available earthquake catalog and attenuation expressions originally developed for western U.S. ground motion data. In the past 14 years, a large number of additional strong motion records were obtained in Turkey, which has allowed development of regional attenuation relationships (Gulkan and Kalkan, 2002; Kalkan and Gulkan, 2004a, b; Ulusay et al., 2004). In addition, tracing of new fault segments beneath the Marmara Sea augments our understanding of the seismotectonic environment of the Marmara basin (e.g., Le Pichon et al., 2001; Armijo et al., 2002).

For Istanbul an earthquake scenario is determined to take place on the Main Marmara Fault. For the estimation of earthquake hazard, geotechnical, geological, topographical data as well as the appropriate attenuation relationships are taken into consideration.

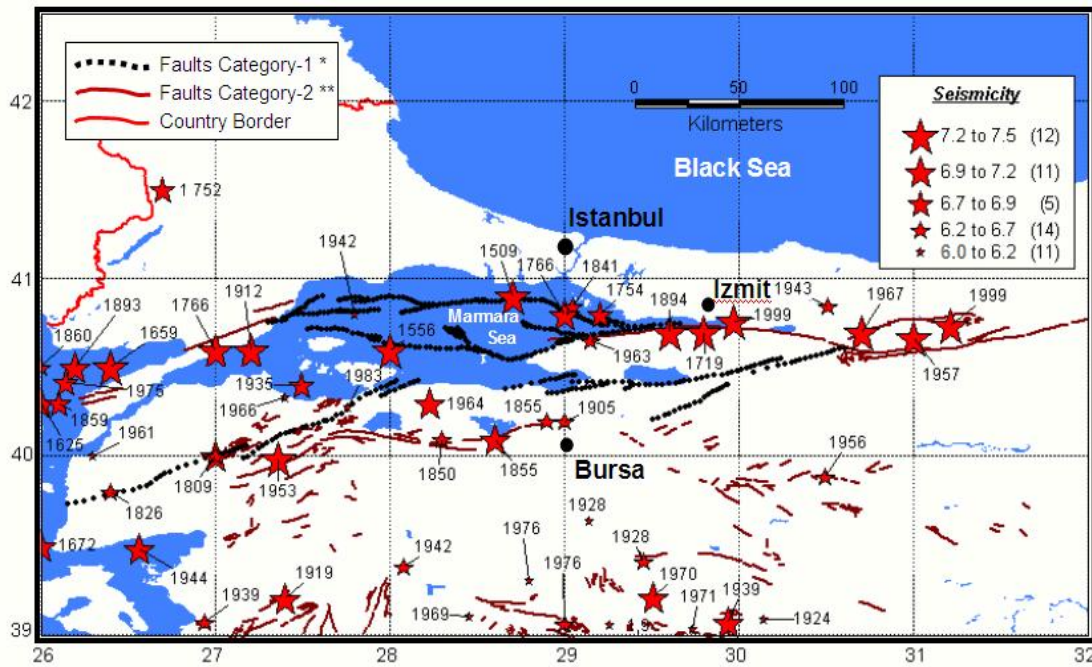


Figure 3.6 Locations of M 6.0 earthquakes (A.D. 1509-1999) (Note: Parentheses in the legend denote the breakdown of earthquakes; Category-1 faults were recently visualized using bathymetric images and seismic reflection survey; Category-2 faults indicate the previously known faults) (Kalkan et al., 2008)

The selected attenuation relationships provide earthquake intensities, peak ground acceleration, velocity and displacement and, spectral acceleration, at specific frequencies and damping ratios, for given earthquake magnitude, distance, fault mechanism and local geology (KOERI, 2002).

The North Anatolian Fault (NAF) with a length of 1500 km is the most active component in the tectonic evolution of Anatolia, and is one of the most active and largest strike-slip faults in the world. Within this century, 8 destructive earthquakes have occurred between Erzinçan and Istanbul (Figure 3.7). The last destructive earthquakes in NAF were the 1999 Izmit (Mw 7.4) and the 1999 Duzce (Mw 7.2) earthquakes. Figure 3.8 shows the North Anatolian fault system in the Marmara region and the surface ruptures of the Izmit and Duzce earthquakes.

The August 17, 1999 Izmit earthquake ruptured about 125 km of the surface. The epicenter was Izmit at the eastern end of the Marmara Sea. This event affected the highly developed urban and industrialized area surrounding the Gulf of Izmit and Adapazari. The focal mechanism solution shows a right lateral strike slip movement on the fault.

The fault mechanism for earthquakes that have occurred on the North Anatolian Fault System in Northwestern Turkey is predominantly strike-slip. Various authors analyzed the fault mechanisms of the thirty largest aftershocks of the Izmit earthquake and found strike-slip dominance in most of these events and a normal faulting type in some cases.

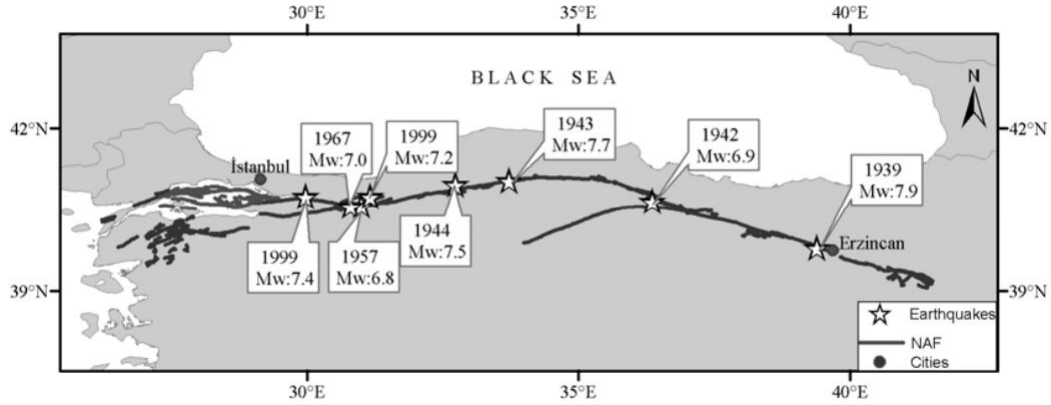


Figure 3.7 Destructive earthquakes along the North Anatolian fault between Erzincan and Istanbul in this century (Ulutas & Ozer, 2009)

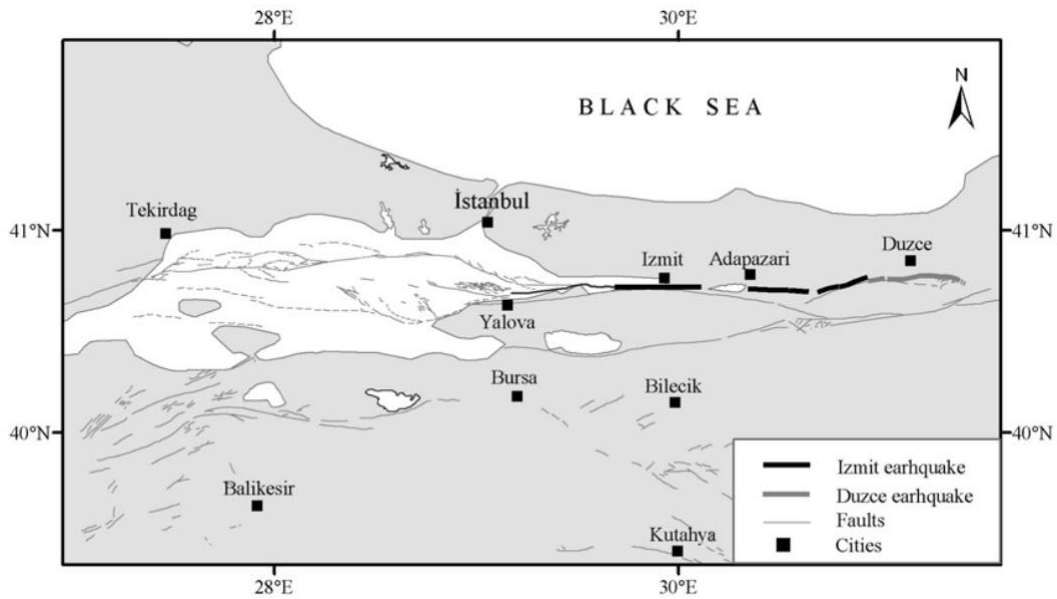


Figure 3.8 North Anatolian Fault system in Marmara region and the surface ruptures after Izmit and Duzce earthquakes (Ulutas & Ozer, 2009)

3.3.3 Input data for ELER

Event Data

Details for the input data of the 1999 Kocaeli earthquake are given in Figure 3.9.

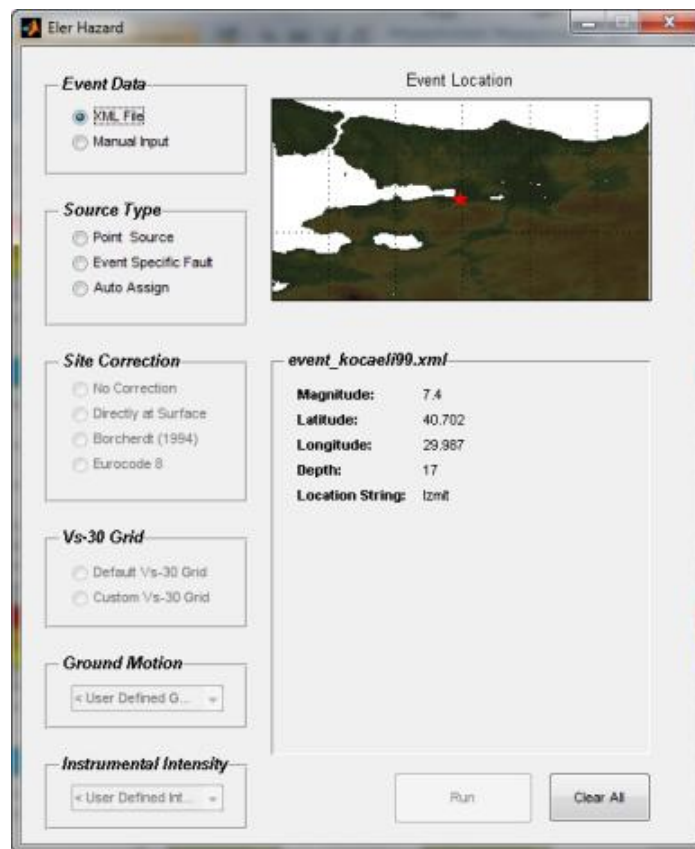


Figure 3.9 Event Location of the 1999 Kocaeli earthquake. Red star in the figure denotes the epicenter of the event.

Source type

Kocaeli Fault had a (pure) dextral strike-slip mechanism reflecting the overall characteristic of the North Anatolian Fault Zone (NAFZ). In the case of the Izmit event the rupture extended from the eastern Sea of Marmara to the Duzce area.

Another important remark is that surface projections of the fault planes are modeled like linear segmentations in ELER. Generally, the region has a very complex fault system. All these faults systems are examined with segments. The segmentation model of Kocaeli fault is illustrated in Figure 3.10, Figure 3.11. Table 3.3 summarizes the main information regarding the Kocaeli fault.

Table 3.3 The 1999 Kocaeli Earthquake Fault Identity

General Information			
Country:	Turkey		
Name:	North Anatolian Fault		
Parametric Information			
Parameter	Qualification Key	Evidence	
Fault type	right-lateral strike slip		focal mechanisms
Depth (km)	17	OD	co-seismic ruptures and seismological data (various authors)
Strike (deg)	268	OD	inferred from microseismic spatial and field measurements (various authors)
Dip (deg)	86	OD	focal mechanisms (various authors)
Rake (deg)	180	OD	kinematic indicators, focal mechanisms and regional stress field (various authors)
Max magnitude (Mw)	7.4	OD	monitoring/seismological data
Epicenter (Lat/Long)	40.702/29.987	OD	monitoring/seismological data
Length (km)	125	OD	co-seismic ruptures and seismological data (various authors)
Associated Earthquake			
Latest earthquake	17/8/1999	Mw=7.4 (instrumental recordings)- The 1999 Kocaeli Earthquake	

*Acronyms: OD=Original Data

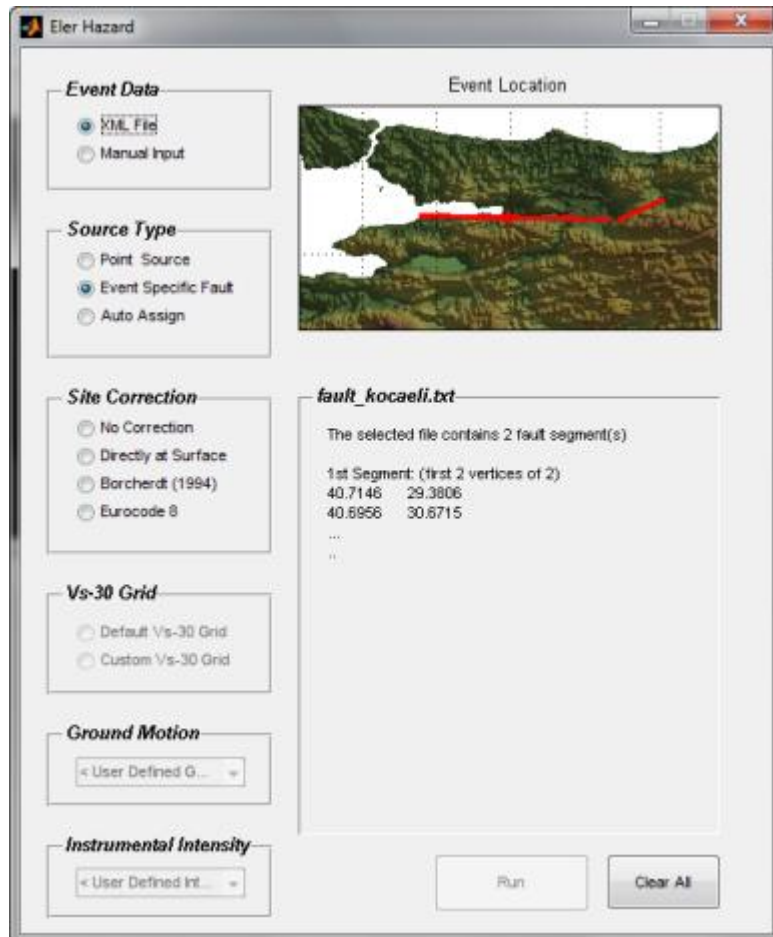


Figure 3.10 Segmentation model of Kocaeli fault

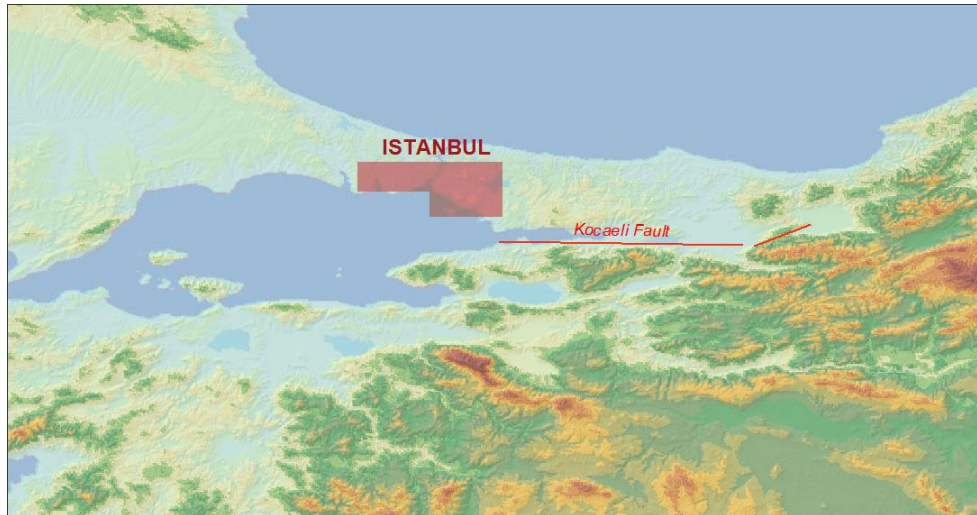


Figure 3.11 The segments of the Kocaeli fault considered in the analysis

Site correction

Local site effects are taken into account with Vs30 parameter, which is the average shear velocity down to 30m. Using Next Generation Attenuation relations (NGA), ground motion parameters are calculated directly at surface.

Site condition

The Quaternary Tertiary Mesozoic (QTM) map developed by the Turkish Republic’s General Directorate of Mineral Research and Exploration was used in addition to average shear wave velocity down to 30m depth (Vs30). Vs30-QTM correlations are given in Wills and Silva (1998) to obtain site specific PGA for Istanbul Metropolitan Area. Vs30-QTM is grouped into three units of Vs30 values. Vs30 maps of Turkey and Istanbul Metropolitan Region are given in Figure 3.12 and Figure 3.13 respectively.

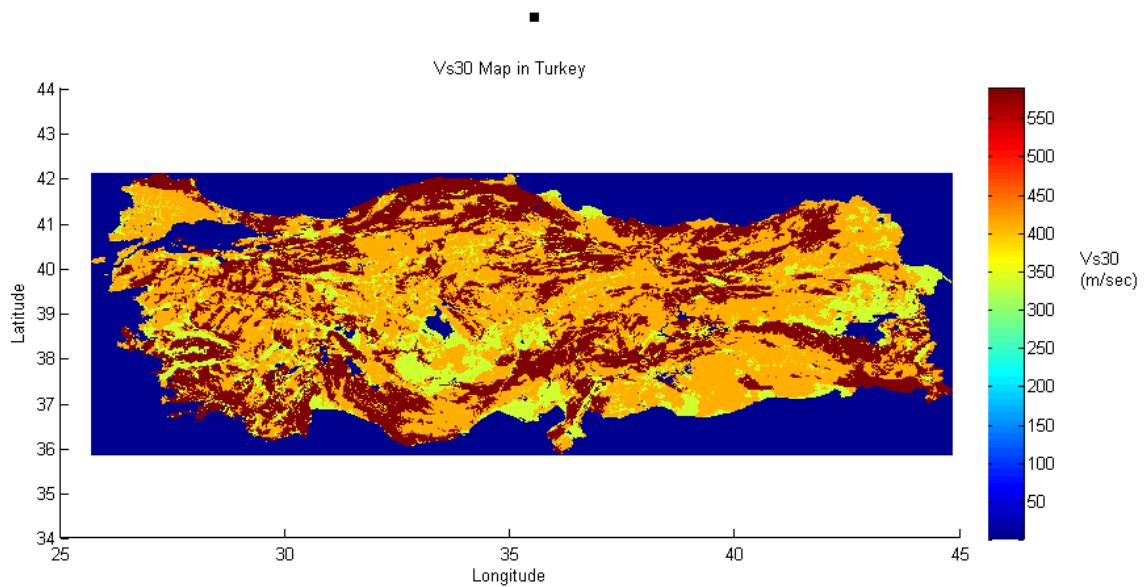


Figure 3.12 Distribution of Vs30 in Turkey

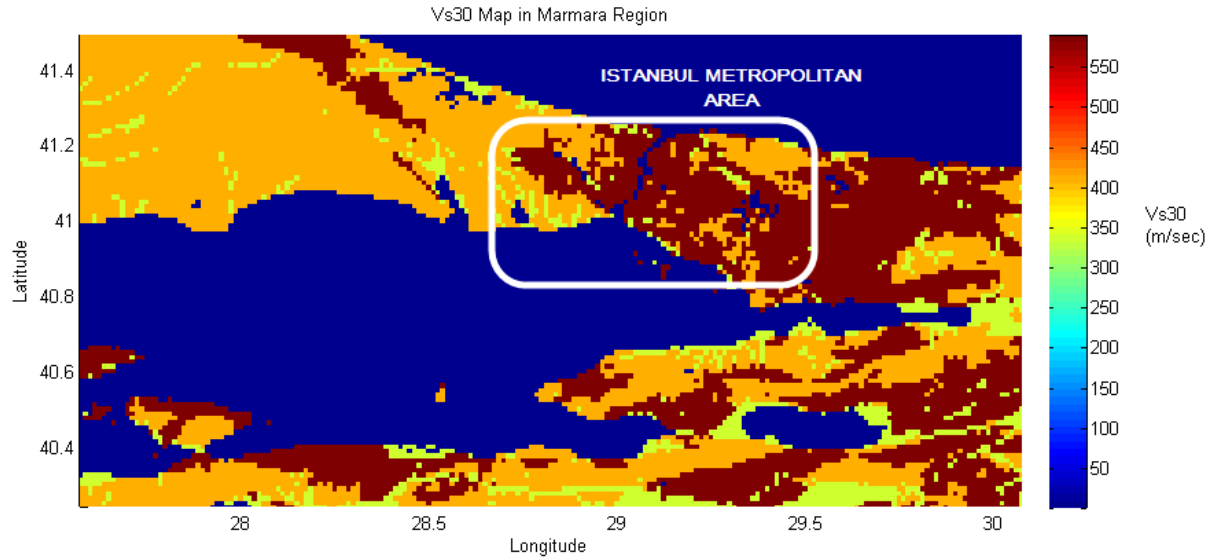


Figure 3.13 Distribution of Vs30 in Marmara Region. The main focus of the white frame is on the Metropolitan Area of Istanbul

Ground Motion Prediction Equations

As it is mentioned above, using NGA relations all calculation for the ground motion can be given directly at the surface.

Campbell and Bozorgnia (2008) GMPE estimates peak ground acceleration (PGA) and spectral acceleration (S_a) at different periods depending on the information on magnitude, distance, fault type and average shear wave velocity down to 30m depth (Vs30). In this study, Campbell and Bozorgnia (2008) GMPE has been used in the estimation of PGA, S_a (T=0.2sec) and S_a (T=1.0sec) distribution.

The general equation of the model is as follows:

$$\ln Y = f_{mag} + f_{dis} + f_{flt} + f_{hng} + f_{site} + f_{sed}$$

where Y represents ground motion parameters of estimated PGA, PGV, PGD and SA. The other parameters which are used in the model are as follows:

f_{mag} : Magnitude parameter:

$$f_{mag} = \begin{cases} c_0 + c_1M & M \leq 5.5 \\ c_0 + c_1M + c_2(M - 5.5) & 5.5 \leq M \leq 6.5 \\ c_0 + c_1M + c_2(M - 5.5) + c_3(M - 6.5) & M > 6.5 \end{cases}$$

F_{dis} : Distance parameter:

$$f_{dis} = (c_4 + c_5M) \ln \left(\sqrt{R_{RUP}^2 + C_6^2} \right)$$

F_{flt} : Fault type parameter:

$$f_{flt} = c_7 F_{RV} f_{flt,Z} + c_8 F_{NM}; f_{flt,Z} = \begin{cases} Z_{TOR}; & \dots Z_{TOR} < 1 \\ 1; & Z_{TOR} \geq 1 \end{cases}$$

F_{site} : Site effect parameter:

$$f_{site} = \begin{cases} c_{10} \ln\left(\frac{V_{S30}}{k_1}\right) + k_2 \left\{ \ln\left[A_{1100} + c \left(\frac{V_{S30}}{k_1}\right)^n \right] - \ln[A_{1100} + c] \right\}; & \dots V_{S30} < k_1 \\ (c_{10} + k_2 n) \ln\left(\frac{V_{S30}}{k_1}\right) & \dots k_1 \leq V_{S30} < 1100 \\ (c_{10} + k_2 n) \ln\left(\frac{V_{S30}}{k_1}\right) & \dots V_{S30} \geq k_1 \end{cases}$$

In these equations the parameters from c_0 to c_{12} and k_1 to k_3 are coefficients, V_{S30} is the average shear wave velocity down to 30m depth, f_{img} and f_{sed} are the parameters of hanging wall and basin effect. R_{RUP} is the closest distance to surface rupture, F_{RV} , F_{NM} , are slip parameters, Z_{TOR} is depth of the rupture surface from ground surface.

Regression Standard deviation (σ_T) for each ground motion parameter is also provided.

In order to estimate PGA distribution of the 1999 Kocaeli earthquake with $M_w=7.5$, median +0.5 standard deviation is selected, as it shown in Figure 3.14. Other parameters are calculated through specific commands in ELER (Figure 3.15):

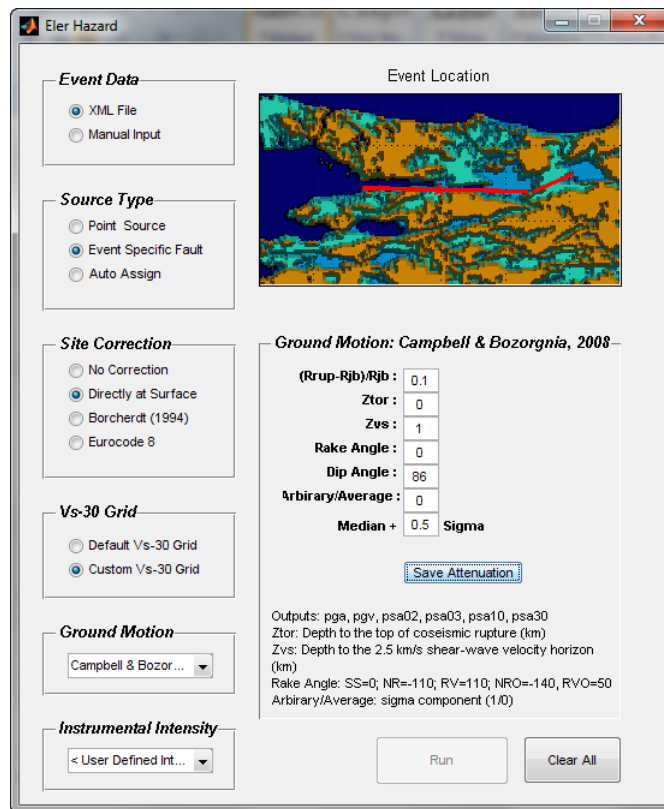


Figure 3.14 GMPE input screen (Campbell & Bozorgnia, 2008)

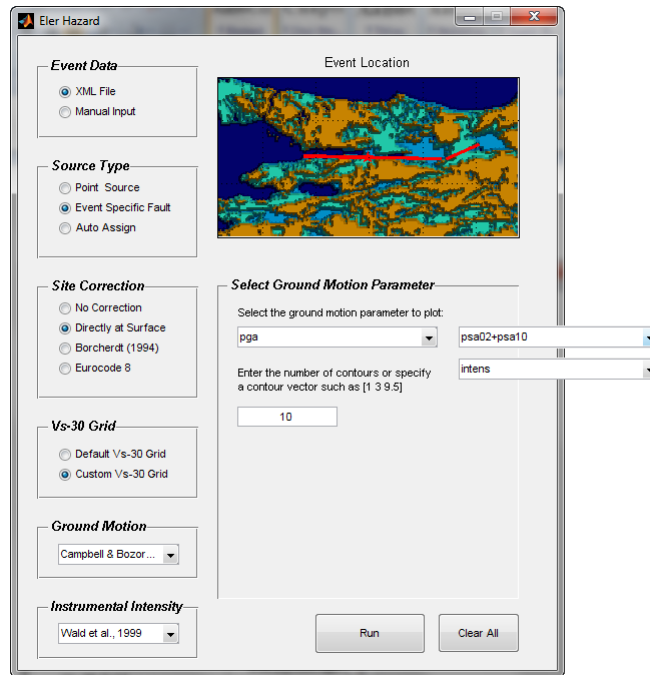


Figure 3.15 Alternative ground motion parameters

3.3.4 Output results

Deterministic seismic hazard is computed to understand the spatial distribution of the earthquake ground motion that would result from a given (Scenario) earthquake. Simulating the 1999 Kocaeli earthquake with the selected attenuation relationships and site response quantification, output results are given in Figure 3.16. Parameters for the selected scenario are summarized in Table 3.4. Figure 3.4.

Table 3.4 Input Parameters for Istanbul- the 1999 Kocaeli earthquake (scenario A)

Analysis-50*	
SEISMIC HAZARD	
Event Data	Kocaeli99
Source type	Kocaeli
Site correction	directly at surface
Vs30	qtm_turkey_cor
GMPE	Campbell & Bozorgnia 08
median+__sigma	0.7
PGA at Zeytinburnu	0.115g
Sa0.2 at Zeytinburnu	0.27g
Sa1.0 at Zeytinburnu	0.15g
Comments	
phantom grid 2km, interpolation grid 0.005	

*Analysis vol. denotes just the priority of the results done by the author in his personal database

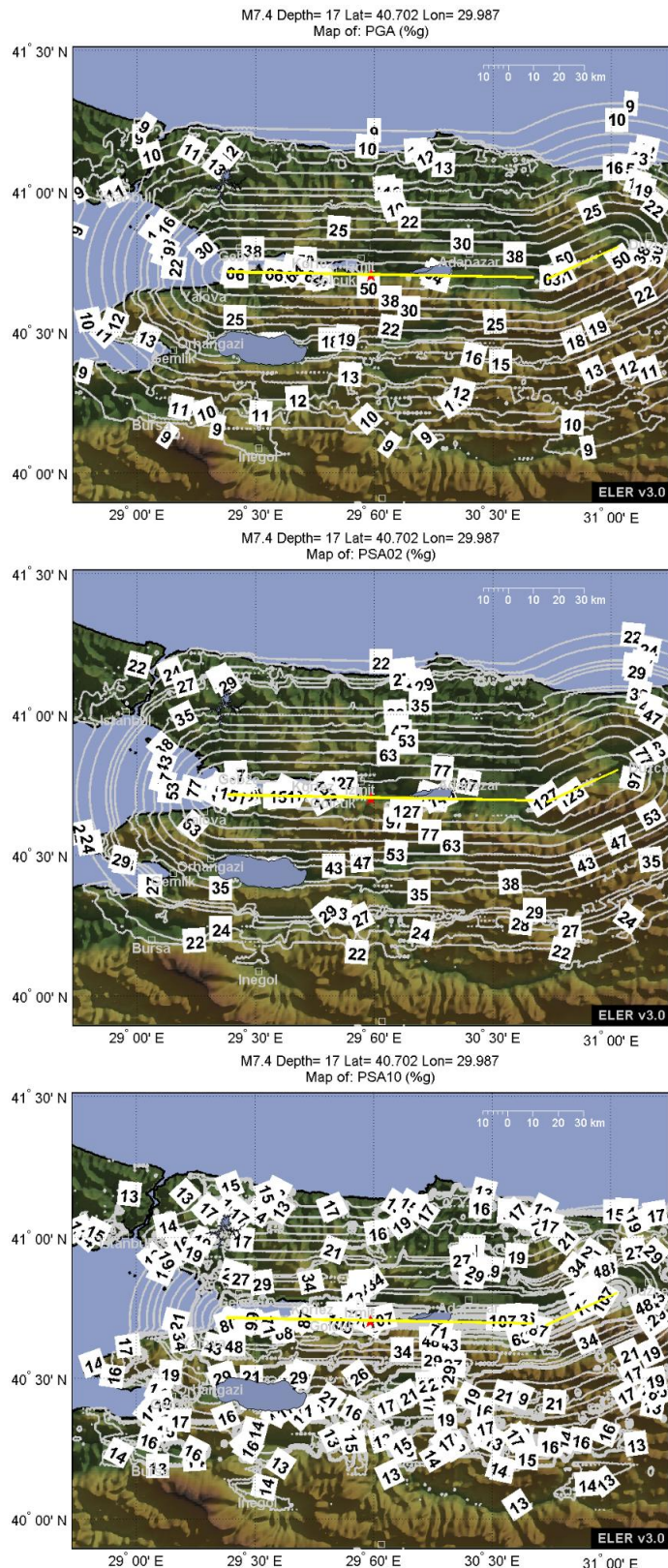


Figure 3.16 PGA (%g) and Spectral Accelerations (%g) at $T=0.2\text{sec}$ and $T=1.0\text{sec}$ obtained from the Campbell and Bozorgnia (2008) GMPE for Scenario A

3.4 Hazard Scenarios for Istanbul; The “Credible Worst Case” Scenario Earthquake for Istanbul (scenario B)

3.4.1 Introduction

In Istanbul province a scenario earthquake is determined to take place on the Main Marmara Fault, as the “Credible Worst Case” Scenario event. Based on recent findings a fault segmentation model is developed for the Marmara Sea region as shown in Figure 3.17. The segmentation provided relies on the discussion of several portions of the Main Marmara Fault, given in Le Pichon et al. (2000, 2003), based on bathymetric, sparker and deep-towed seismic reflection data and interprets it in terms of fault segments identifiable for different structural, tectonic and geometrical features. The studied fault consists of three active segments close to the city, determined as a right-lateral fault. For given earthquake magnitude, distance, local geology, and fault mechanism, the selected ground motion prediction equations provide earthquake intensities, peak ground acceleration, and spectral acceleration.

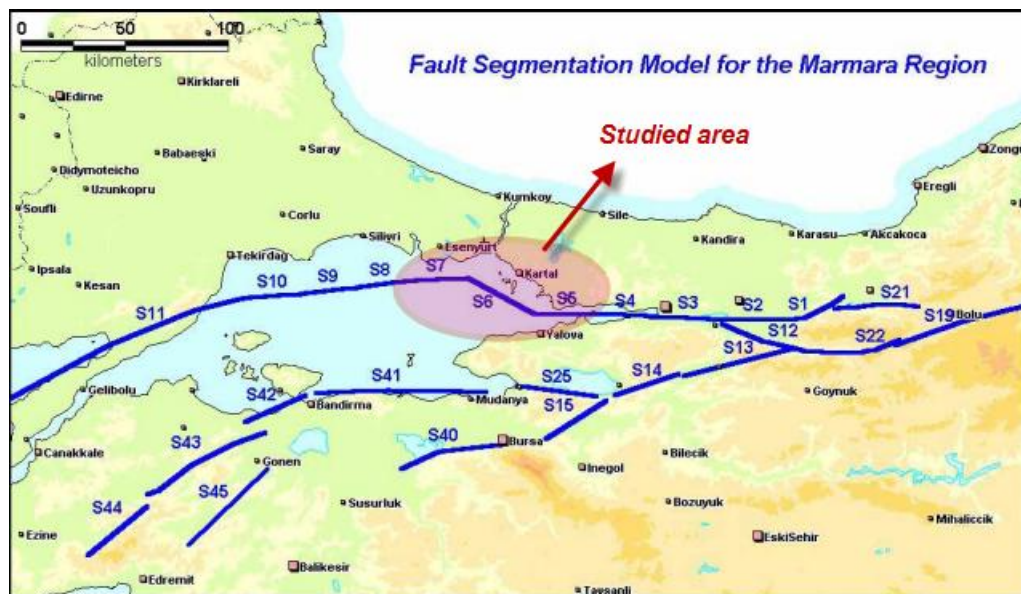


Figure 3.17 Fault segmentation model proposed for the Marmara region. Studied area consists of three segments S5, S6 and S7 (Erdik et al., 2004)

3.4.2 Input data for ELER

Event Data

Similar to 1999 Kocaeli earthquake, this scenario is considered to have magnitude $M_w=7.5$ as well as the same total rupture length. Distance between hypocenter and surface is about 27.2 km according to various authors. In this study, a different location of epicenter is selected closer to Ataturk International Airport (Figure 3.18). Fault Identity is given in Table 3.5.

Table 3.5 The Main Marmara Fault Identity (studied segments)

General Information			
Country:	Turkey		
Name:	Main Marmara Fault		
Parametric Information			
Parameter	Qualification Key	Evidence	
Fault type	right-lateral strike slip		focal mechanisms
Depth (km)	27.2	EJ	estimation of Credible worst case scenario earthquake for Istanbul
Strike (deg)	81.5	LD	inferred from microseismic spatial and field measurements (Okay et al, 2000)
Dip (deg)	90	LD	focal mechanisms (Okay et al, 2000)
Rake (deg)	180	LD	kinematic indicators, focal mechanisms and regional stress field (Okay et al, 2000)
Max magnitude (Mw)	7.5	AR	estimation of Credible worst case scenario earthquake for Istanbul
Epicenter (Lat/Long)	40.947/28.871	EJ	estimation of Credible worst case scenario earthquake for Istanbul
Length (km)	120	LD	geological/geophysical studies
Associated Earthquake			
Latest earthquake	02/09/1754	Mw=7.4 (historical event), associated with segment S6	
	22/05/1766	Mw=7.1 (historical event), associated with segment S7, S8	
	10/07/1894	Mw=7.3 (historical event), associated with segment S3, S4, S5	

*Acronyms: EJ=Expert Judgement, LD=Literature Data, AR=Analytical Relationship

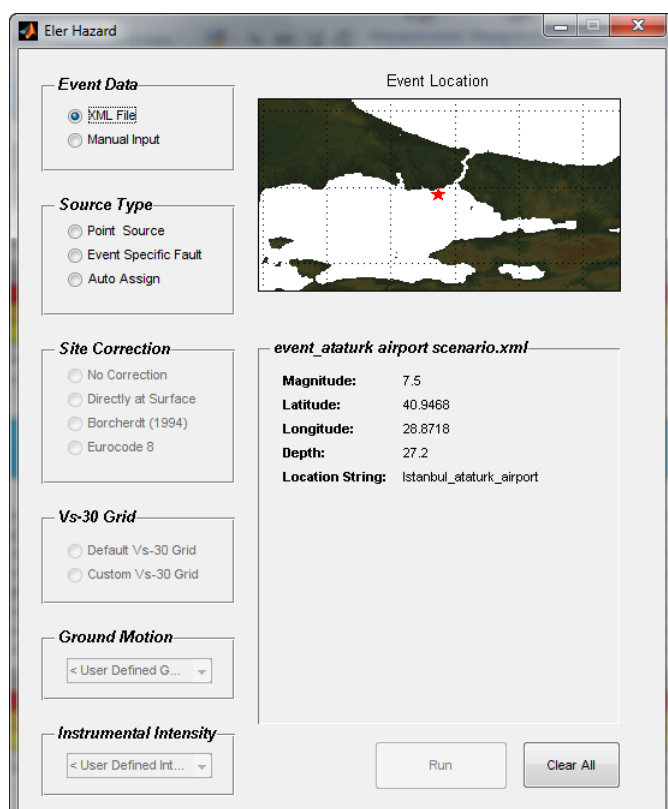


Figure 3.18 Event Epicenter for Scenario B (close to Ataturk International Airport)

Source type

Three segments are selected for the scenario B in Istanbul, as it is shown in Figure 3.19.

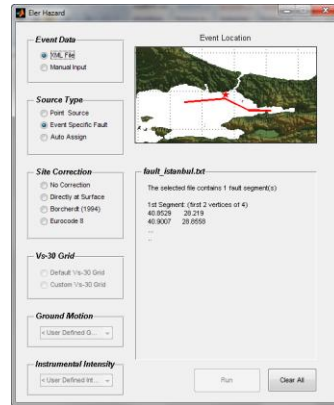


Figure 3.19 Segmentation model of the fault considered in Scenario B

Site correction

Local site effects are taken into account with Vs30 parameter. Using Next Generation Attenuation relations (NGA), ground motion parameters are calculated directly at surface.

Site condition

The QTM-Vs30 map created for the scenario A is also used for the scenario B.

Ground Motion Prediction Equations

Campbell and Bozorgnia (2008) ground motion estimation equation has been used in the estimation of PGA, Sa (T=0.2sec) and Sa (T=1.0sec) distribution.

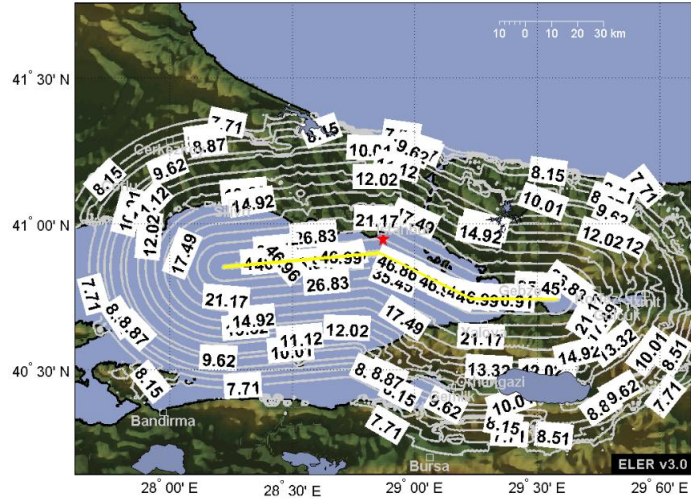
3.4.3 Output results

Earthquake hazard in the Istanbul region is essentially controlled by the Main Marmara Fault (part of the North Anatolian Fault) passing about 20 km south of the city in the Marmara Sea. In order to estimate the regional hazard, a scenario based on Main Marmara Fault (Table 3.6), is studied.

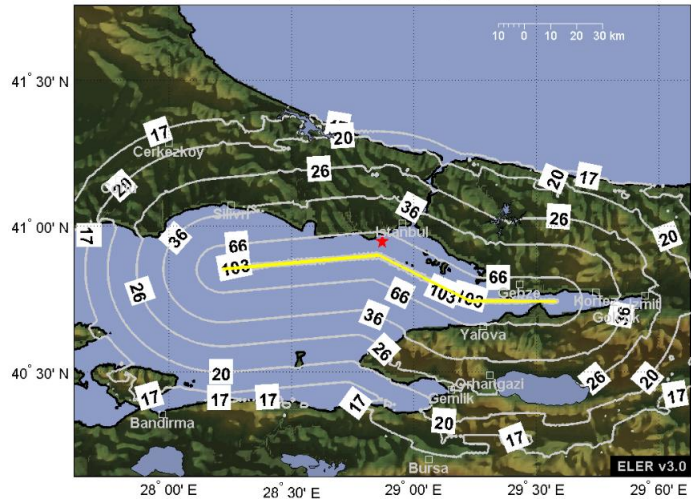
Table 3.6 Input Parameters for Scenario B

Analysis-56	
SEISMIC HAZARD	
Event Data	Istanbul Worst Scenario-Ataturk Airport
Source type	North Marmara Fault
Site correction	directly at surface
Vs30	qtm_turkey_cor
GMPE	Campbell & Bozorgnia 08
median+___sigma	0
PGA at Zeytinburnu	0.24g
Sa0.2 at Zeytinburnu	0.54g
Sa1.0 at Zeytinburnu	0.30g
Comments	
phantom grid 2km, interpolation grid 0.005	

M7.5 Depth= 27.2 Lat= 40.9468 Lon= 28.8718
 Map of: PGA (%)



M7.5 Depth= 27.2 Lat= 40.9468 Lon= 28.8718
 Map of: PSA02 (%)



M7.5 Depth= 27.2 Lat= 40.9468 Lon= 28.8718
 Map of: PSA10 (%)

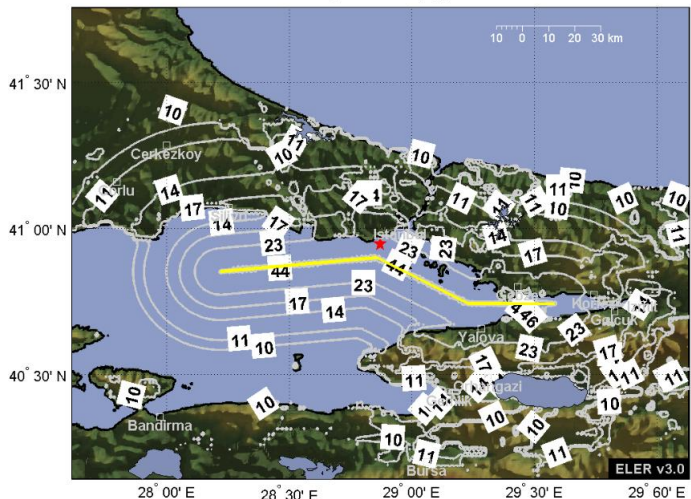


Figure 3.20 PGA (%) and Spectral Accelerations (%) at $T=0.2\text{sec}$ and $T=1.0\text{sec}$ obtained from the Campbell and Bozorgnia (2008) GMPE for Scenario B

3.5 Building damages & casualties for Scenario A

3.5.1 Building damages (analysis results)

The analysis is conducted for the Zeytinburnu district using the building inventory of Istanbul. The distribution of damages obtained from Level 2 module for the different damage states is presented in Table 3.7.

Calculations were performed by using:

i. One Ground Motion Prediction Equation (GMPE):

-Campbell & Bozorgnia (2008) ----Analysis 50*

** Analysis vol. denotes just the priority of the results done by the author in his personal database*

ii. Two demand spectrums:

-International Building Code (IBC)

-Eurocode 8 (EC8)

iii. Two different approaches for the computation of the demand spectrum and the performance point:

-Capacity Spectrum Method (CSM)

-Coefficient Method (CM)

As a result, comparisons of different methods are given in the following diagrams. Figure 3.21 shows that EC8 demand spectrum overestimates the damages in moderate, extensive and complete level compared to IBC demand spectrum.

Spatial distributions of damaged buildings at each discrete damage level, namely slight, moderate, extensive and complete, are given in Figure 3.22. Indicative results from this scenario are:

Number of complete damage building: 182

Number of extensive damage building: 363

Number of moderate damage building: 1337

Table 3.7 Damage estimation results for Zeytinburnu Scenario A, using the GMPE by Campbell & Bozorgnia (2008)

Analysis-50		LEVEL 2							LEVEL 2								
SEISMIC HAZARD		IBC-International building code							EC8								
Event Data	Kocaeli99	Demand Spectrum	IBC-International building code							Demand Spectrum	EC8						
Source type	Kocaeli	Classification	Istanbul							Classification	Istanbul						
Site correction	directly at surface	Building DB	Zeytinburnu							Building DB	Zeytinburnu						
Vs30	qtm_turkey_cor	Magnitude	7.4							Magnitude	7.4						
GMPE	Campell & Bozorgnia 08	Vs30	qtm_turkey_cor							Vs30	qtm_turkey_cor						
median	0.7	PGA	-							PGA	0						
PGA at Zeytinburnu	0.115g	Sa0.2	0.27g							Sa0.2	-						
Sa0.2 at Zeytinburnu	0.27g	Sa1.0	0.15g							Sa1.0	-						
Sa1.0 at Zeytinburnu	0.15g	Method	CSM-Capacity Spectrum Method	percentage (%)	CM-Coefficient method	percentage (%)	Average	Average perc (%)	Method	CSM-Capacity Spectrum Method	percentage (%)	CM-Coefficient method	percentage (%)	Average	Average perc (%)		
Comments		Complete	182	1.3	50	0.3	116	0.8	Complete	187	1.3	72	0.5	130	0.9		
phantom grid 2km, interpolation grid 0.005'		Extensive	363	2.5	108	0.7	236	1.6	Extensive	355	2.5	148	1.0	252	1.7		
		Moderate	1337	9.2	1030	7.1	1184	8.2	Moderate	1370	9.5	1272	8.8	1321	9.1		
		Total	14482	13.00	14482	8.2	14482	10.6	Total	14482	13.20	14482	10.3	14482	11.8		

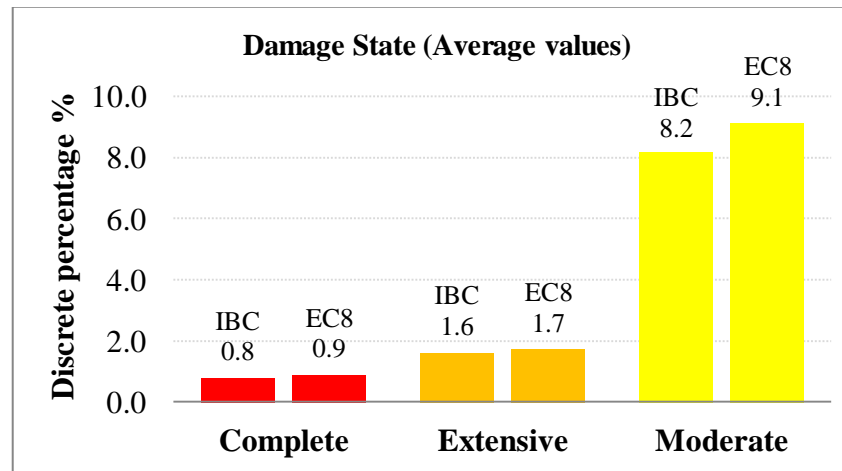


Figure 3.21 Discrete damage probabilities under Analysis 50 (Scenario A)

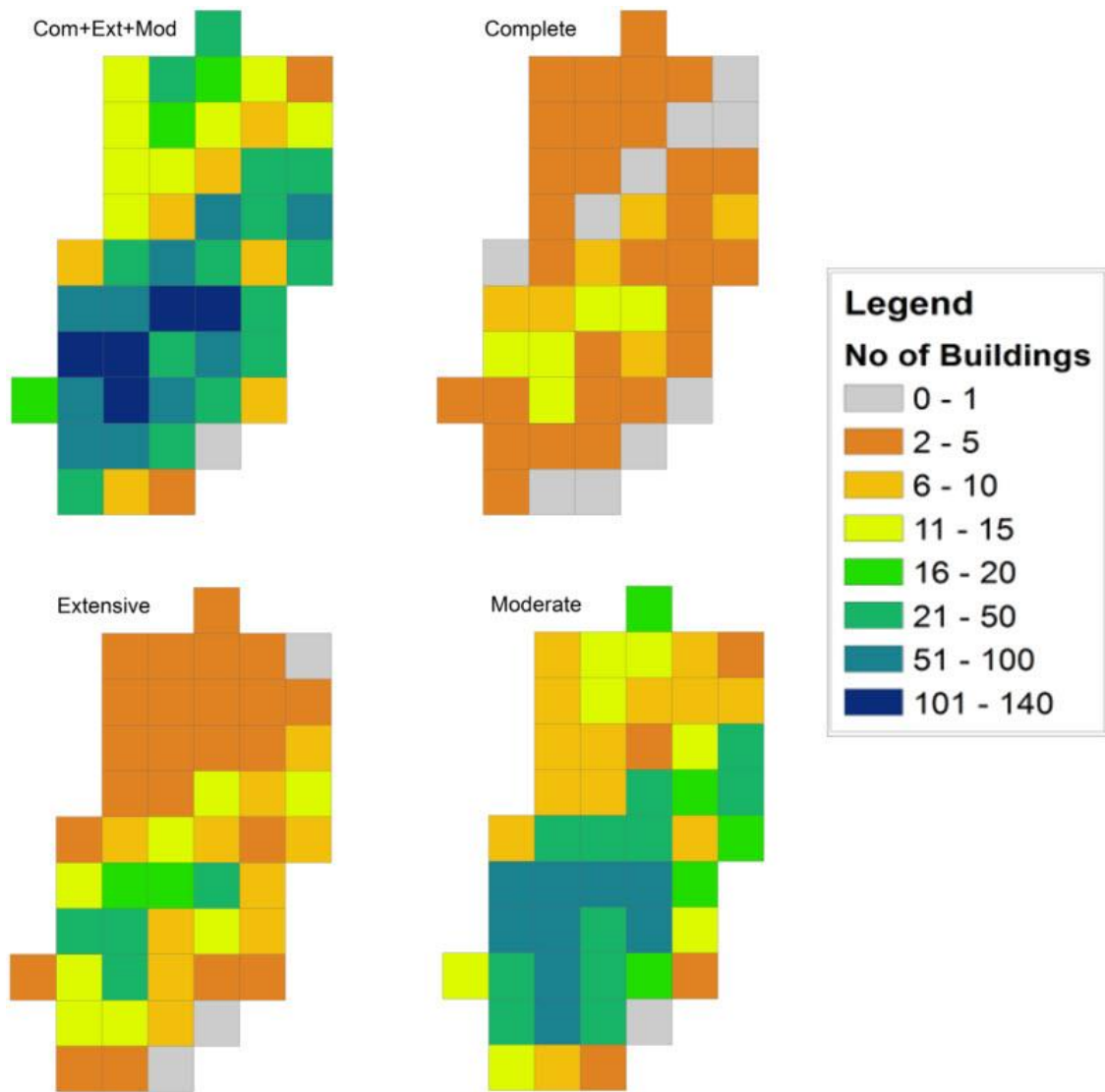


Figure 3.22 The distribution of damaged buildings in Zeytinburnu resulting from Analysis 50, IBC demand spectrum and CSM as selected method-Level 2 Analysis (Scenario A)

3.5.2 Comparison with observed damages from the 1999 Kocaeli Earthquake

Recorded damages from Kocaeli earthquake, are available for Istanbul region. In Zeytinburnu district, damaged buildings were limited to moderate damage state (Figure 3.23)

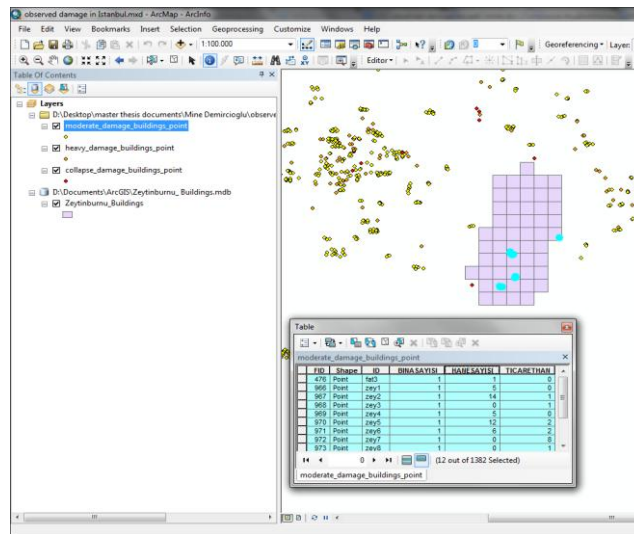


Figure 3.23 Distribution of moderate damaged buildings in Istanbul due to August 17, 1999 Kocaeli earthquake (Scenario A)

- Total number of moderate damaged buildings in Zeytinburnu: 84

Comparison between observed and calculated damages is not consistent, as ELER seems to overestimate the damages from this specific seismic event. Fragility curve parameters are not dated, thus uncertainty is inherent.

3.5.3 Casualties

ELER calculates the human losses due to the damaged buildings using the Hazus approach.. Results are shown in Figure 3.24. The total number of expected deaths is 19 in total 243188 or 0.08%.

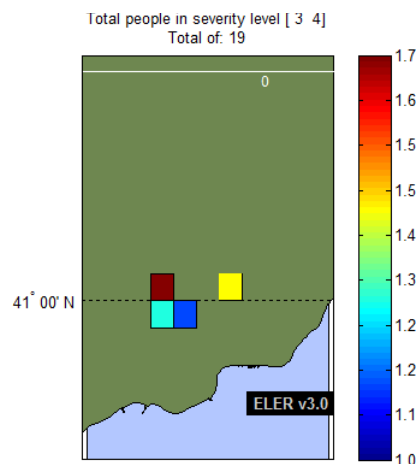


Figure 3.24 The distribution of casualties in Zeytinburnu district resulting from the 1999 Kocaeli earthquake scenario

3.6 Building damages & casualties for Scenario B

3.6.1 Building damages (analysis results)

In this case, the seismic hazard of Main Marmara Fault in Zeytinburnu district is studied. The results are summarized in Table 3.8.

Table 3.8 Damage estimation results for Zeytinburnu Scenario B, using the GMPE by Campbell & Bozorgnia (2008)

Analysis-56		LEVEL 2							LEVEL 2								
SEISMIC HAZARD		IBC-International building code							EC8								
Event Data	Istanbul Worst Scenario-aturk	Demand Spectrum								Demand Spectrum							
Source type	North marmara fault	Classification	Istanbul							Classification	Istanbul						
Site correction	directly at surface	Building DB	Zeytinburnu							Building DB	Zeytinburnu						
Vs30	qtm_turkey_cor	Magnitude	7.4							Magnitude	7.4						
GMPE	Campell & Bozorgnia 08	Vs30	qtm_turkey_cor							Vs30	qtm_turkey_cor						
median	0	PGA	-							PGA	0						
PGA at Zeytinburnu	0.24g	Sa0.2	0.54g							Sa0.2	-						
Sa0.2 at Zeytinburnu	0.54g	Sa1.0	0.30g							Sa1.0	-						
Sa1.0 at Zeytinburnu	0.30g	Method	CSM-Capacity Spectrum Method	percentage (%)	CM-Coefficient method	percentage (%)	Average	Average perc (%)	Method	CSM-Capacity Spectrum Method	percentage (%)	CM-Coefficient method	percentage (%)	Average	Average perc (%)		
<u>Comments</u>		Complete	715	4.9	434	3.0	575	4.0	Complete	1051	7.3	630	4.4	841	5.8		
phantom grid 2km, interpolation grid 0.005'		Extensive	1044	7.2	861	5.9	953	6.6	Extensive	1359	9.4	1169	8.1	1264	8.7		
		Moderate	3140	21.7	3653	25.2	3397	23.5	Moderate	3542	24.5	4046	27.9	3794	26.2		
		Total	14482	33.83	14482	34.2	14482	34.0	Total	14482	41.10	14482	40.4	14482	40.7		

Figure 3.25 and Figure 3.26 shows the graphical display of the previous results in bar chart and in map.

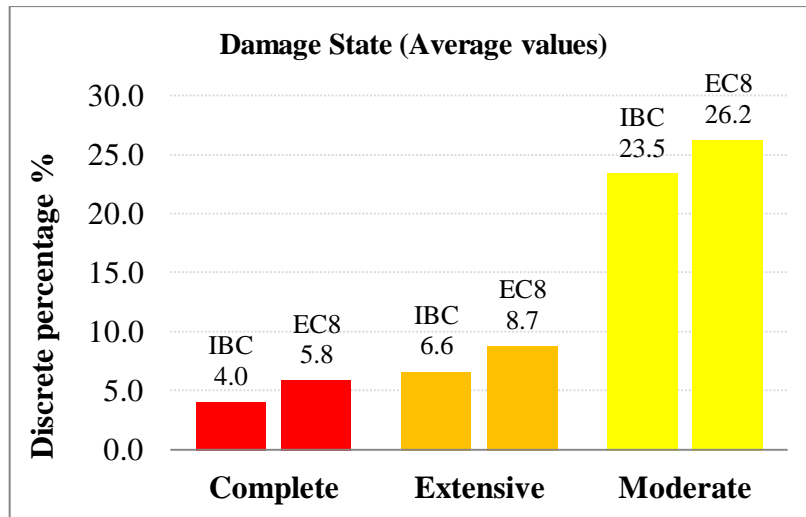


Figure 3.25 Discrete damage probabilities under Analysis 56 (Scenario B)

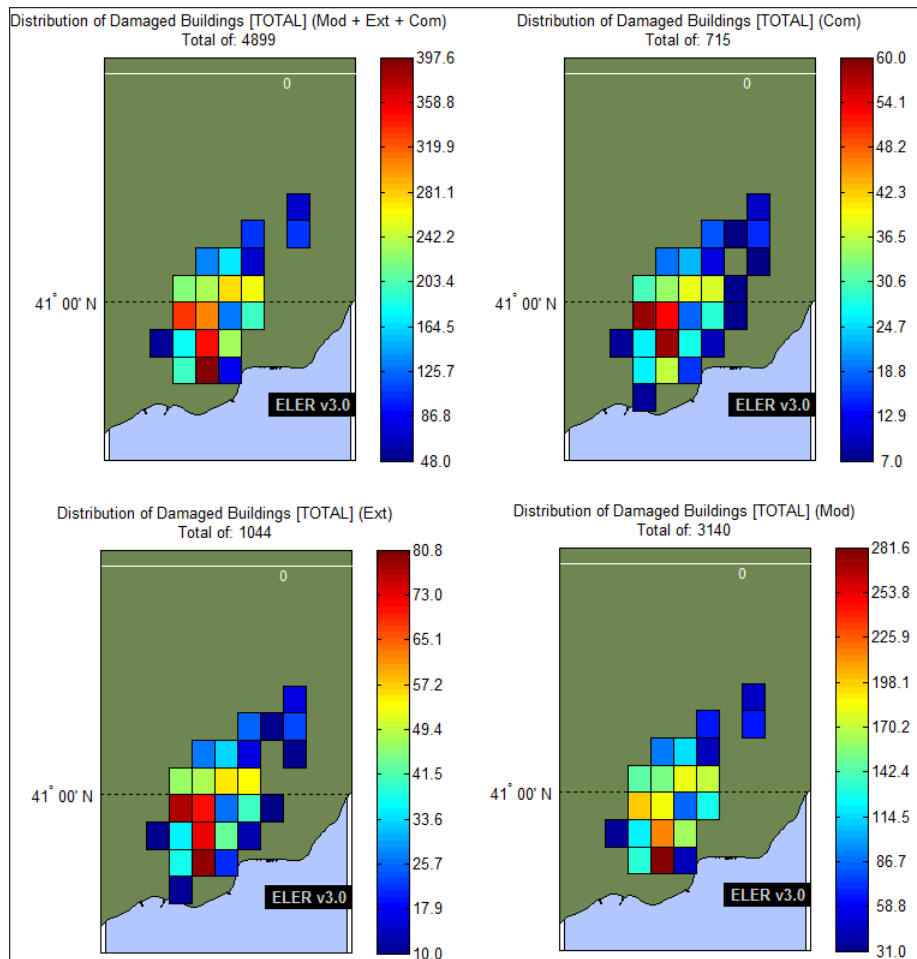


Figure 3.26 The distribution of damaged buildings in Zeytinburnu resulting from Analysis 56, IBC demand spectrum and CSM as selected method-Level 2 Analysis (Scenario B)

3.6.2 Casualties

Human losses are estimated based on Hazus Method and it was found that 93 people would suffer of severe injury or be unsaveable for this specific earthquake scenario.

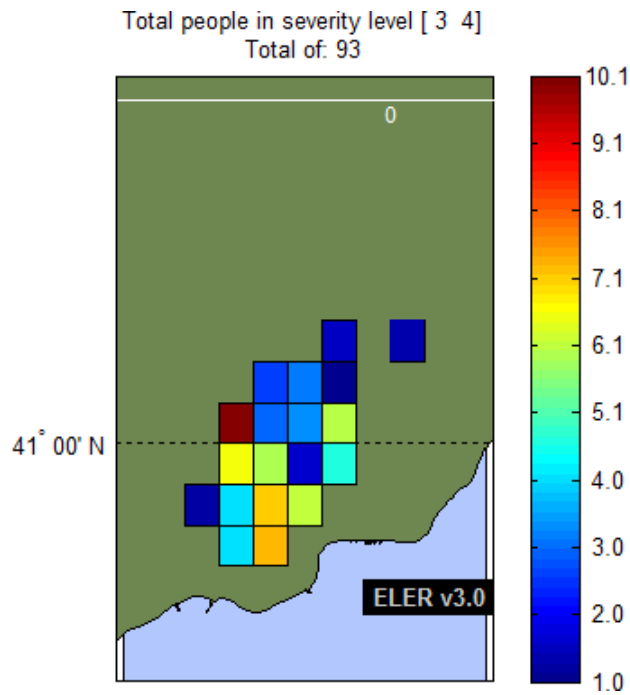


Figure 3.27 The distribution of casualties in Zeytinburnu district resulting from earthquake scenario B

4. Application to Thessaloniki

Thessaloniki is located in the eastern part of Mediterranean in the Northern Greece (Macedonia, Thrace) in a strategic geographical location. It is the second city in population in Greece with almost one million inhabitants (included suburban areas), after Athens and an important administrative, economic, industrial, academic and cultural centre at national scale. The city was stroked from several earthquakes as its urban area is located on the Axios-Vardar seismogenic zone, which is adjacent to Servomacedonian massif, one of the most seismotectonically active regions in Europe. The latest major earthquake occurred in Thessaloniki in June 1978 with an epicenter located at a distance of about 25km NE of the city, a focal depth of about 8 km and a magnitude of $M=6.5$. Especially, the urban area of Thessaloniki is situated on three (3) main large-scale geology structures. The first formation includes the metamorphic substratum, the second is composed by alluvial deposits and the third formation composed by recent deposits. The purpose of this application is to implement ELER to Euro-Mediterranean City, as Thessaloniki is, in order to predict potential losses after an earthquake.

4.1 Manipulation of Vs30 data in Geographical Information Systems

4.1.1 The Thessaloniki Vs30 map from point to polygon

GIS can provide an effective solution for integrating different layers of information, thus providing a useful input for city planning and in particular input to earthquake resistant design of structures in an area. According to recent researches, seismic microzonation includes delineation of the ground zones that are homogenous in geological and seismological characteristics in specific region as a city. As a result of that, classification ground motion parameters are varied relatively.

For the seismic microzonation, geotechnical site characterization need to be assessed at local scale grouped at geo-cells, which is further used to assess of the site response and liquefaction susceptibility of the sites. Another crucial point is the quality and quantity of input data. To classify the ground in a city, a detailed study of penetration holes is needed for that. To improve the quality of data, 0.0045x0.0045 degree sized grid cell is selected to gather the appropriate information.

The first step for the Thessaloniki study is to map the distribution of Vs30 in 0.0045x0.0045 grid cells gathering available data. At this point it is important to note that the average shear-wave velocity of the upper 30 meters of a soil profile (Vs30) is a key indicator of site response dominating the ground-motion amplification.

Vs30 values are taken from the microzonation study of Thessaloniki (Figure 4.1). For this purpose, a detailed model of the surface geology and geotechnical characteristics, for site effect studies, was generated for the city of Thessaloniki. The resulted geotechnical map (Anastasiadis et al. 2001) was based on numerous data provided by geotechnical investigations, geophysical surveys, microtremors measurements, classical geotechnical and special soil dynamic tests (Pitilakis et al. 1992, Pitilakis and Anastasiadis 1998, Raptakis et al. 1994a, Raptakis et al. 1994b, Raptakis 1995, Apostolidis et al. 2004). The dynamic properties of the main soil formations have been defined from an extended laboratory testing including resonant column and cyclic tri-axial tests (Pitilakis et al. 1992, Pitilakis and Anastasiadis 1998, Anastasiadis 1994).

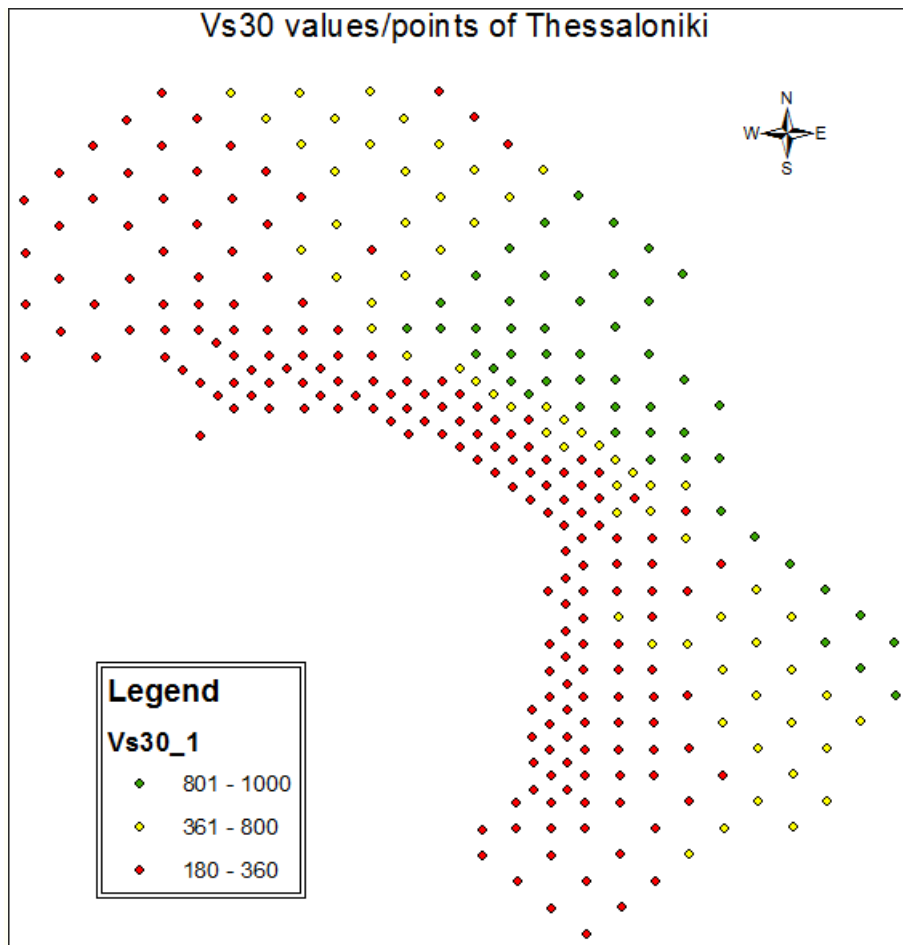


Figure 4.1 Distribution of Vs30 in the city

For the study area, the available information data for Thessaloniki is referred to city blocks, so the user has to manipulate it and convert the files to the appropriate format; geo-cells, recognisable to ELER software (Figure 4.2).

It is noted that during the manipulation of data in GIS environment, it is important to keep the same unique grid ID (identity) for each cell.

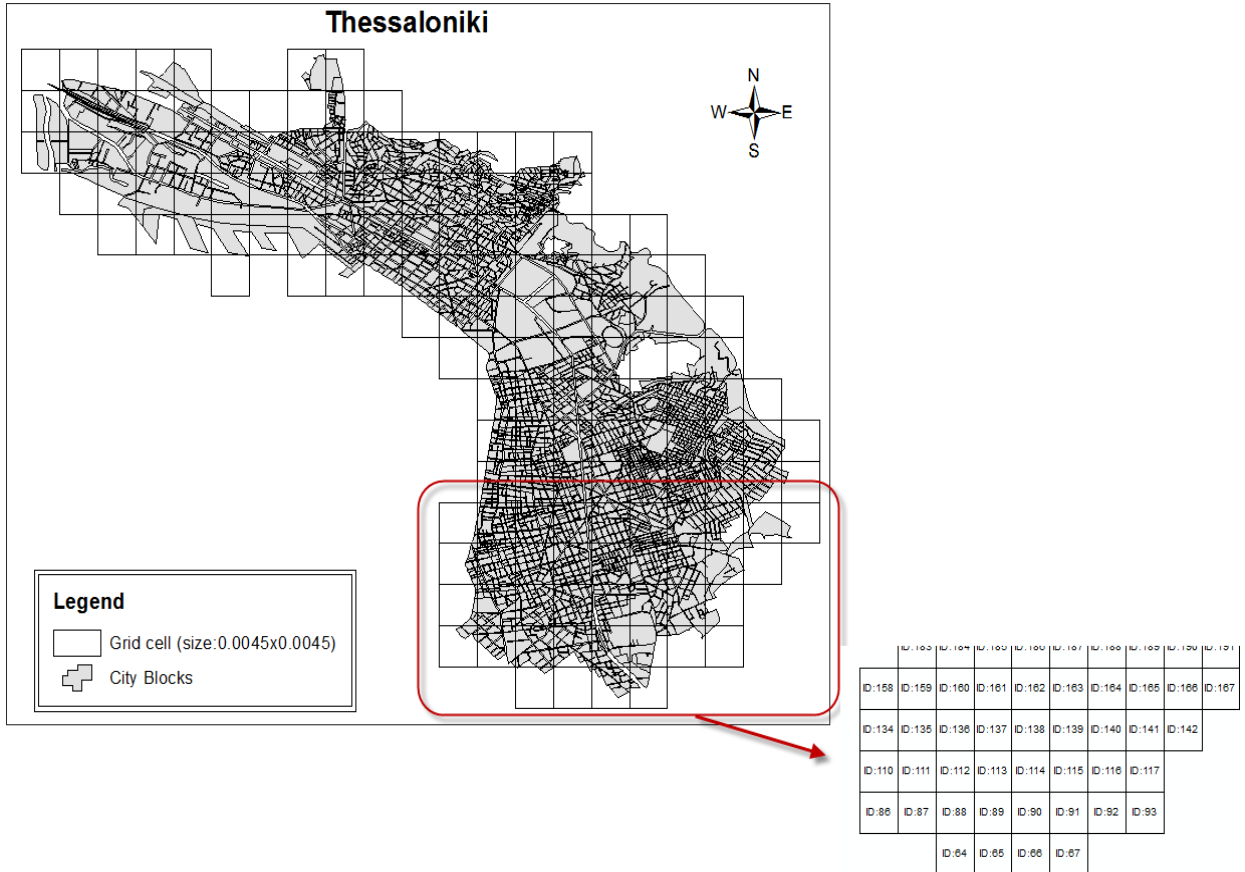


Figure 4.2 Municipality of Thessaloniki; Manipulation of available data. Each cell has its unique GridID.

Custom site condition maps should be in form of Vs30 grids. To achieve that, 215 Vs30 values are selected to define the site conditions under the city (Figure 4.3). Next step is to group the values in each cell in order to take one single average value for each 0.0045 degree gridded cell. Regarding the cells that are not intersected with any Vs30 value, an interpolation with the neighbour cells is done to obtain values for the rest of the grid. Manipulation of data is succeeded through ArcGIS software. Figure 4.4 illustrates the resultant Vs30 map for Thessaloniki that is used for the following analysis in ELER.

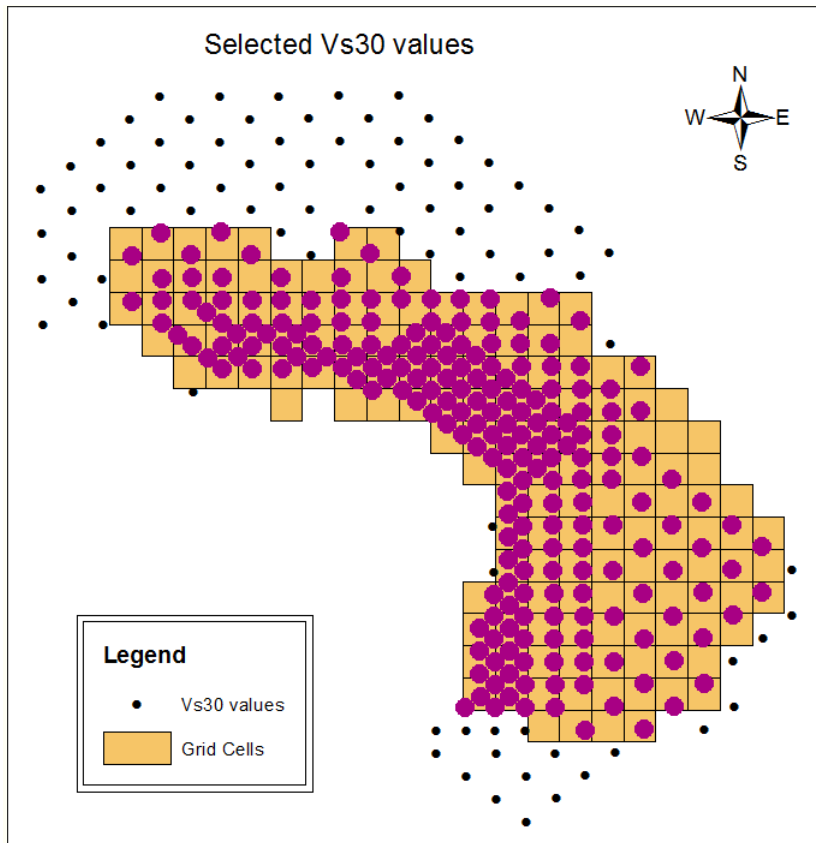


Figure 4.3 Selected Vs30 values that correspond to the studied region

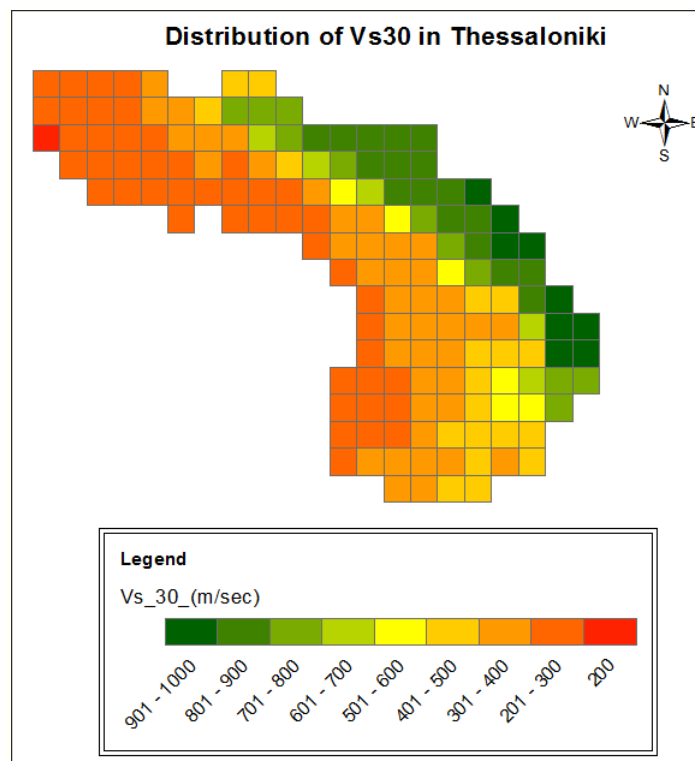


Figure 4.4 Distribution of Vs30 in Thessaloniki

A qualitative comparison is attempted in Figure 4.5 between the EC8 Site Classification taken from microzonation study of Thessaloniki and the resultant Vs30 gridded map.

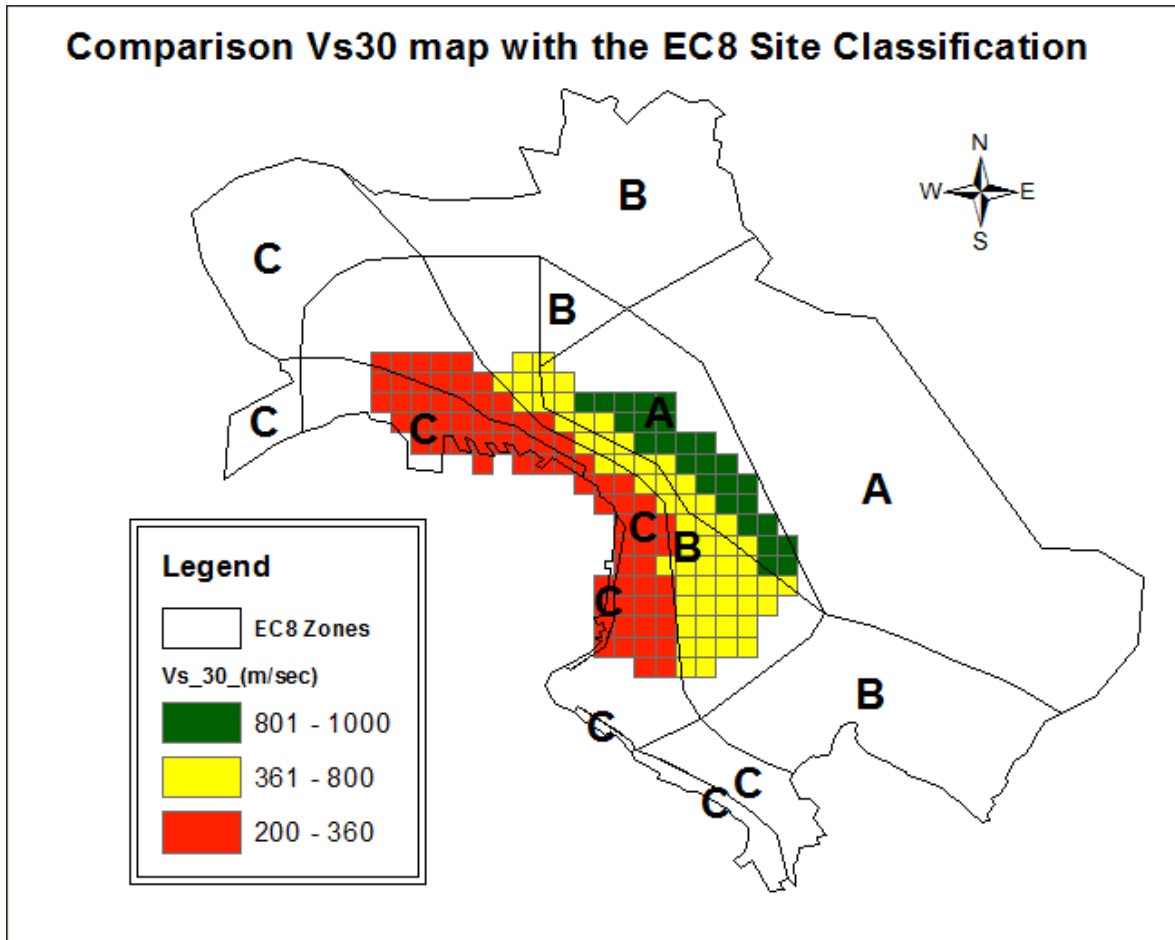


Figure 4.5 Eurocode 8 Site classification of Thessaloniki ground

4.1.2 The Central Macedonia Vs30 map generated by USGS

ELER software uses maps of Vs30 grids for extended areas, so in order to use the above values of Thessaloniki, it is necessary to incorporate them into a more extended Vs30 model. The USGS Vs30 maps, available for the whole world, were used for this purpose.

However, Vs30 maps provided by USGS are based on a simplified approach and should not be considered accurate for every location or region. As stated in USGS website:

“The maps and grids are provided for general purpose use, and are not intended to supplant or supersede existing, detailed Vs30 maps or measurements. Wald and Allen (2007) note significant limitations to this simplified approach. Users should be aware of these limitations and should exercise caution in using this approach for anything other than regional scale Vs30-based site amplification estimates. As always, site-specific Vs30 values should be used at finer scales or at particular locations.”

Figure 4.6 shows the generated Vs30 map for Central Macedonia including the city of Thessaloniki.

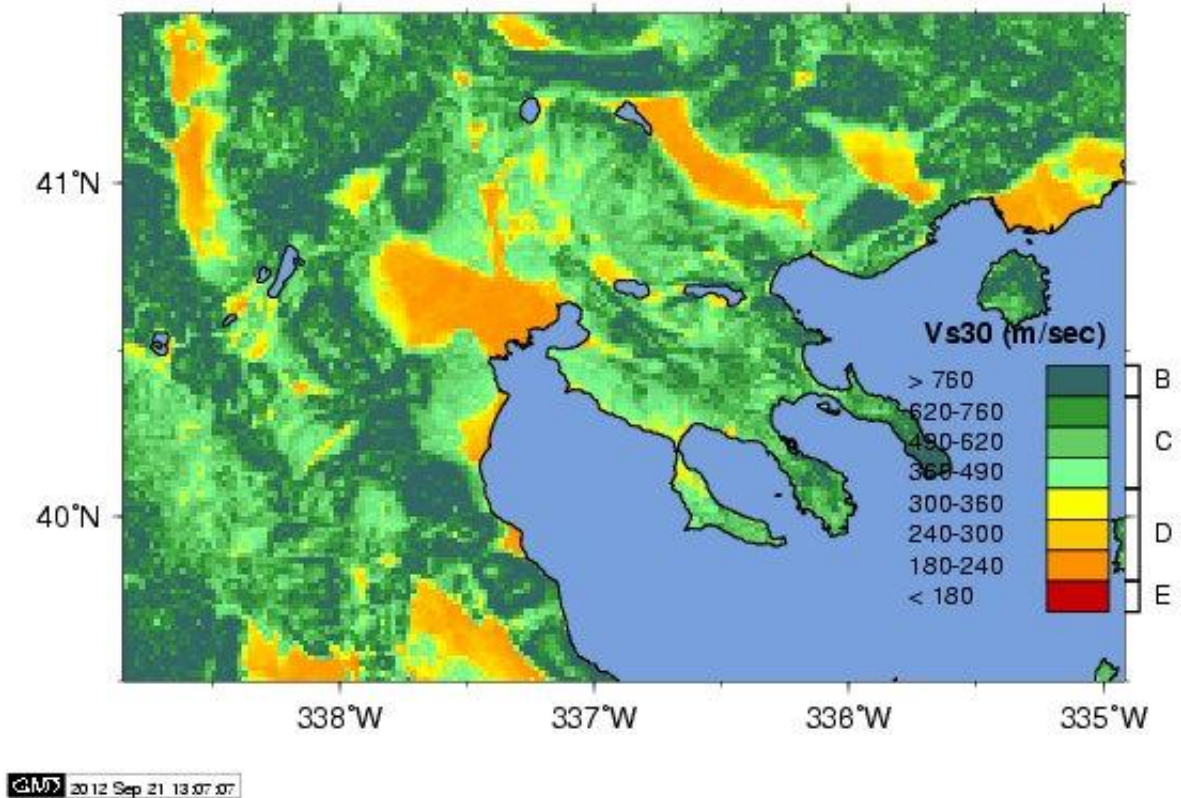


Figure 4.6 Distribution of Vs30 in Central Macedonia (generated by USGS)

4.1.3 Interpolation of USGS Vs30 map

One of the main problems is to transfer the USGS values from point to polygon. Input data for ELER is given in grid format, so the user has to create a new map where the information refers to 0.0045 degree sized grid. To achieve this, a new fishnet is created containing all the points.

The default grid provided by USGS is 0.0083 degree, thus the user has to decrease the size of the grid, because ELER can recognise only one grid interval for the input data. Figure 4.7 and Figure 4.8 illustrate the above problem.

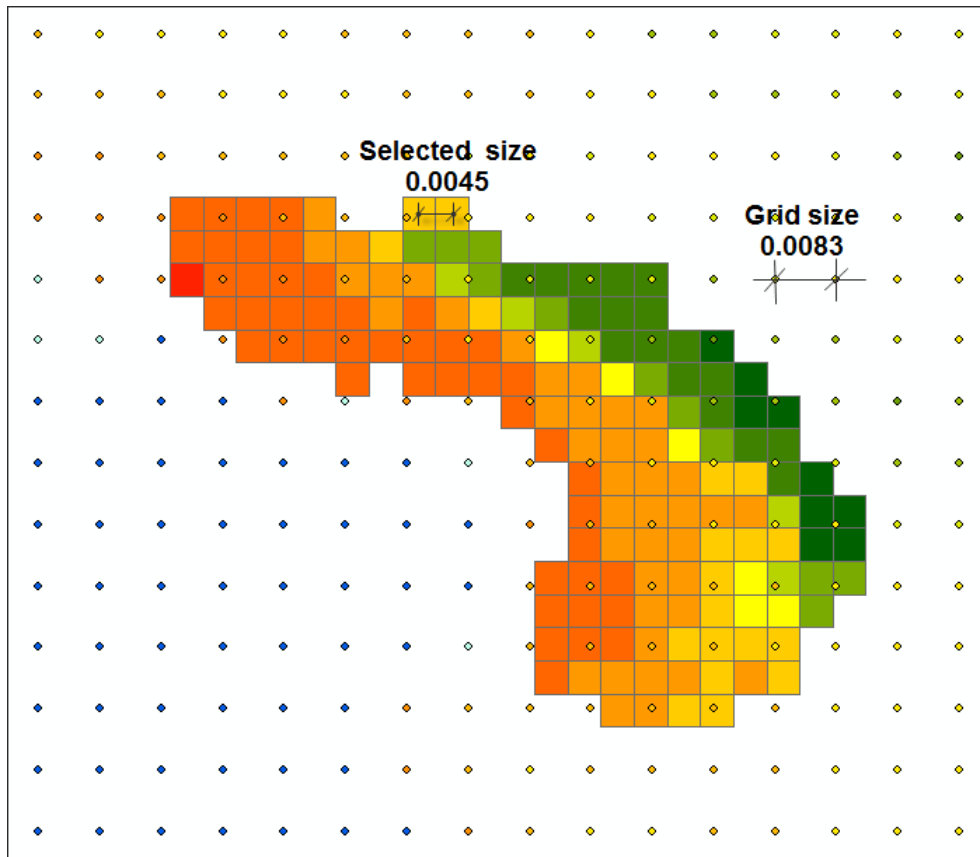


Figure 4.7 Selected and default by USGS grid interval

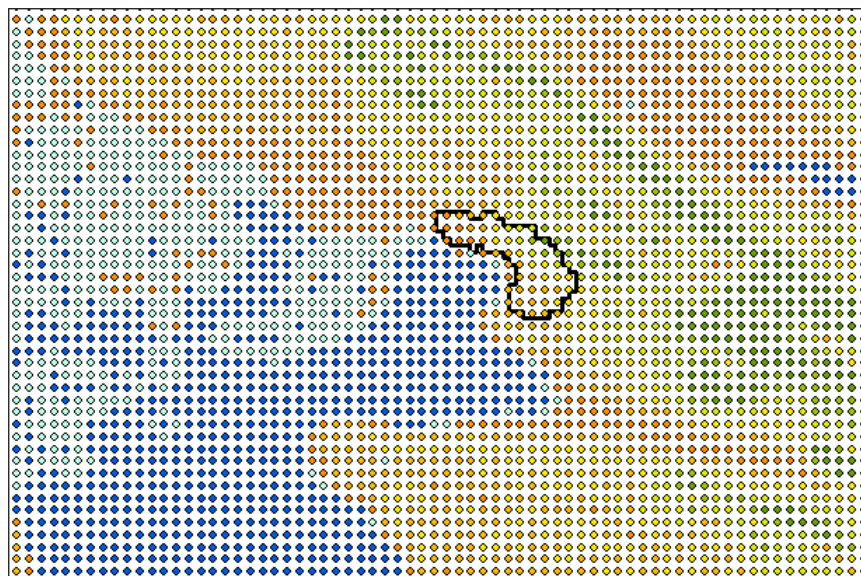


Figure 4.8 USGS Vs30 grids. The focus of the black frame is on the Municipality of Thessaloniki

4.1.4 Joining to a single map

The final phase of the procedure is to combine the two Vs30 maps; the simplified one from USGS that refers to the whole Central Macedonia region, and the second, more detailed one, from the microzonation study that refers to the city of Thessaloniki. Figure 4.9 depicts the final Vs30 map of Central Macedonia that contains values from both above maps.

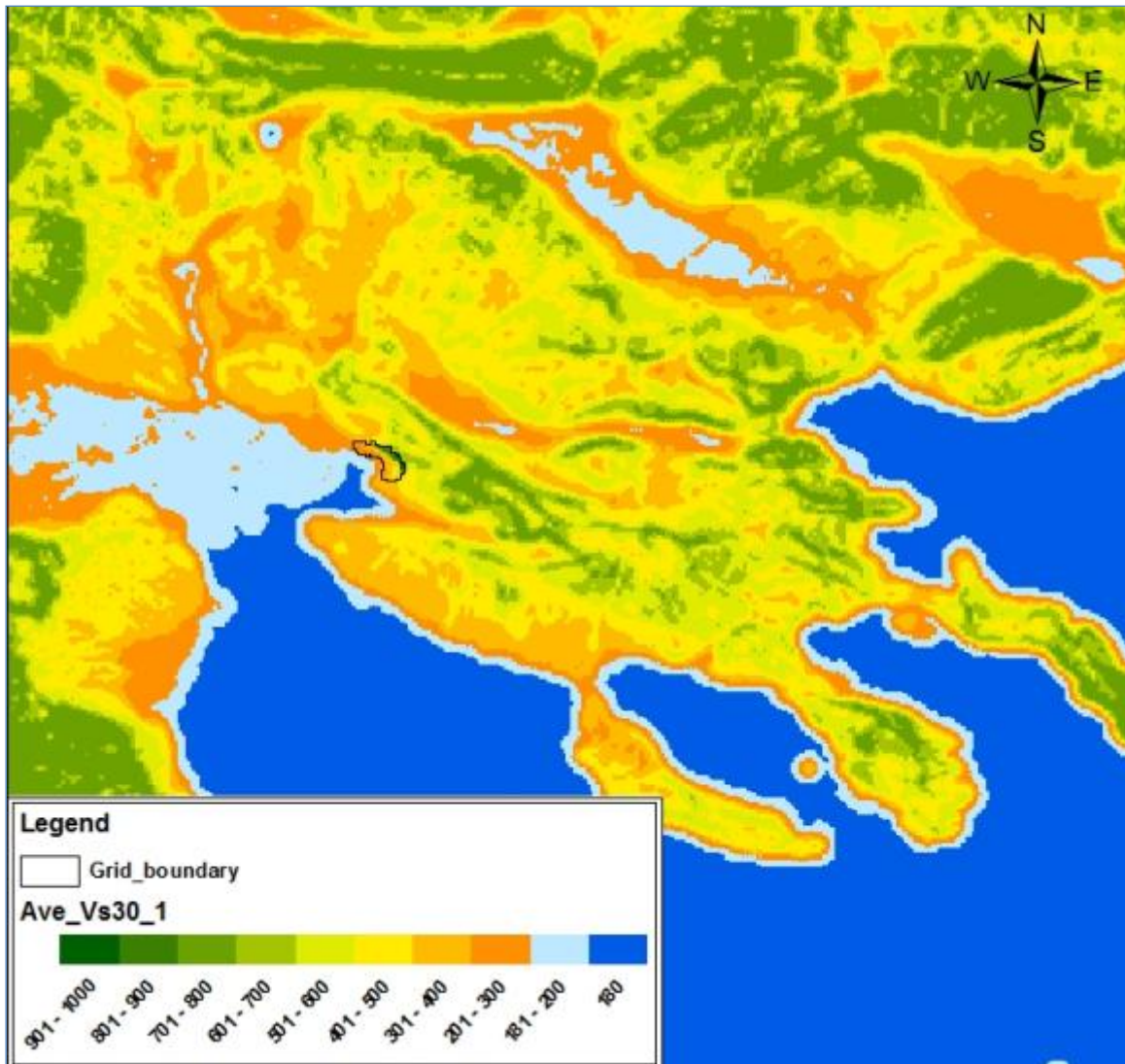


Figure 4.9 The final Vs30 map of Central Macedonia

Following this, ELER provides tools for external data integration. After extracting the Vs30 values from each cell and their coordinates to a text (.txt) files, the txt file can now be converted to a MATLAB file.

Figure 4.10 and Figure 4.11 show the Text2Grid tool, the input text file and the figure obtained from the converted MATLAB matrix, respectively. The Header lines parameter defines the number of lines to be ignored when processing the text file.

The Grid interval parameter specifies the density at which the points in the text file are located. These points do not need to be sorted in any particular order, but the x y z columns should be separated by a whitespace or a tab. The resulting MATLAB matrix file is saved automatically with the same name as the input file, with a .mat extension.

The Text2Grid tool can be used for creating ground motion grids to be used in Level 2 or for creating custom site condition maps for use in the Hazard module.

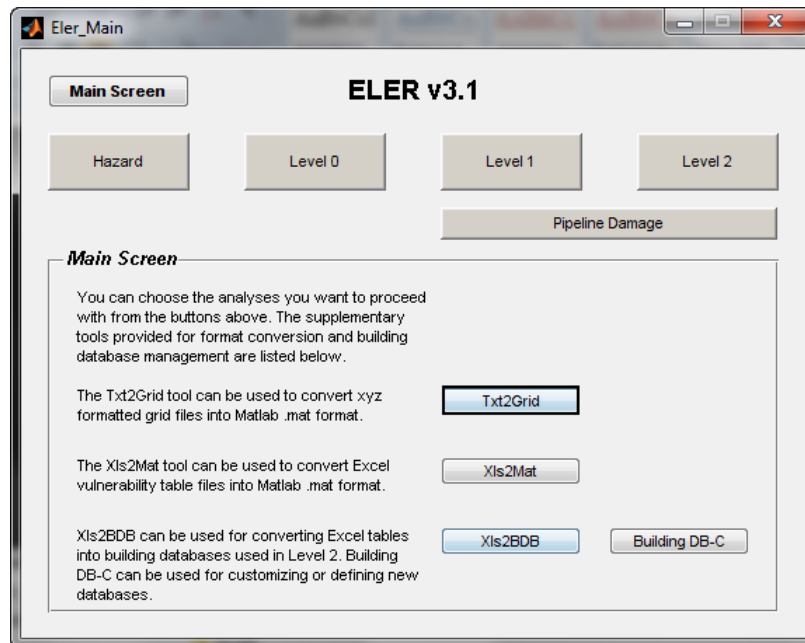


Figure 4.10 Text2Grid for external data integration

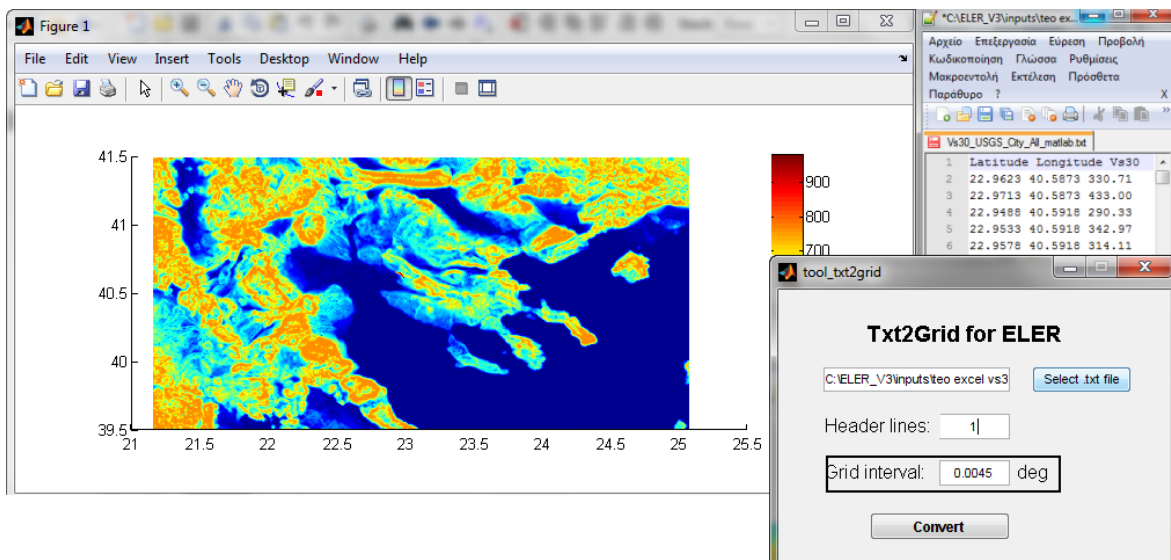


Figure 4.11 Text2Grid GUI, input and output

4.2 Buildings and population data for Thessaloniki

4.2.1 Division into grids; from blocks to grid-cells

The building inventory for Thessaloniki has been developed by the Laboratory of Reinforced Concrete and Masonry Structures in Aristotle University of Thessaloniki (Kappos et al., 2008). The inventory which was introduced in a GIS platform during the RISK-UE project is based on a combination of the 1991 census data from the Statistics Agency of Greece, those from a previous project and a recent in-situ survey of appropriately selected blocks. The inventory includes information about material, code level, and number of storey, structural type and volume for each building. The building database has been updated during SYNER-G EC project covering the entire municipality. The population data is obtained from SRM-LIFE project based on the 2001 census.

Each record represents one block, and the total number of records is 2985 (Figure 4.12). The available information includes information of building type, construction year, number of floors and population.

- Total number of buildings (all types): 27725
- Total population: 362570

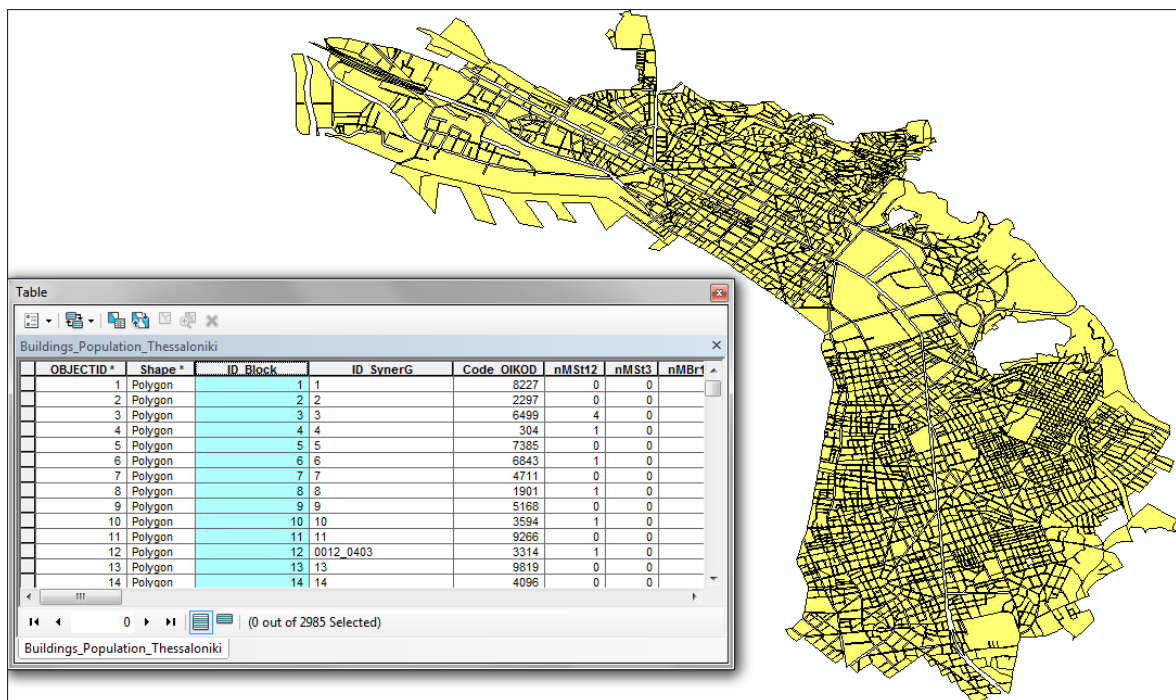


Figure 4.12 Shape file with its attribute table; data refers to blocks

In order to produce 0.0045 degree grid based building inventory, building area geometry data have been converted into a polygon geometry data, as it is shown in Figure 4.13, step 4. Number of total polygon of this covered area set is 155.

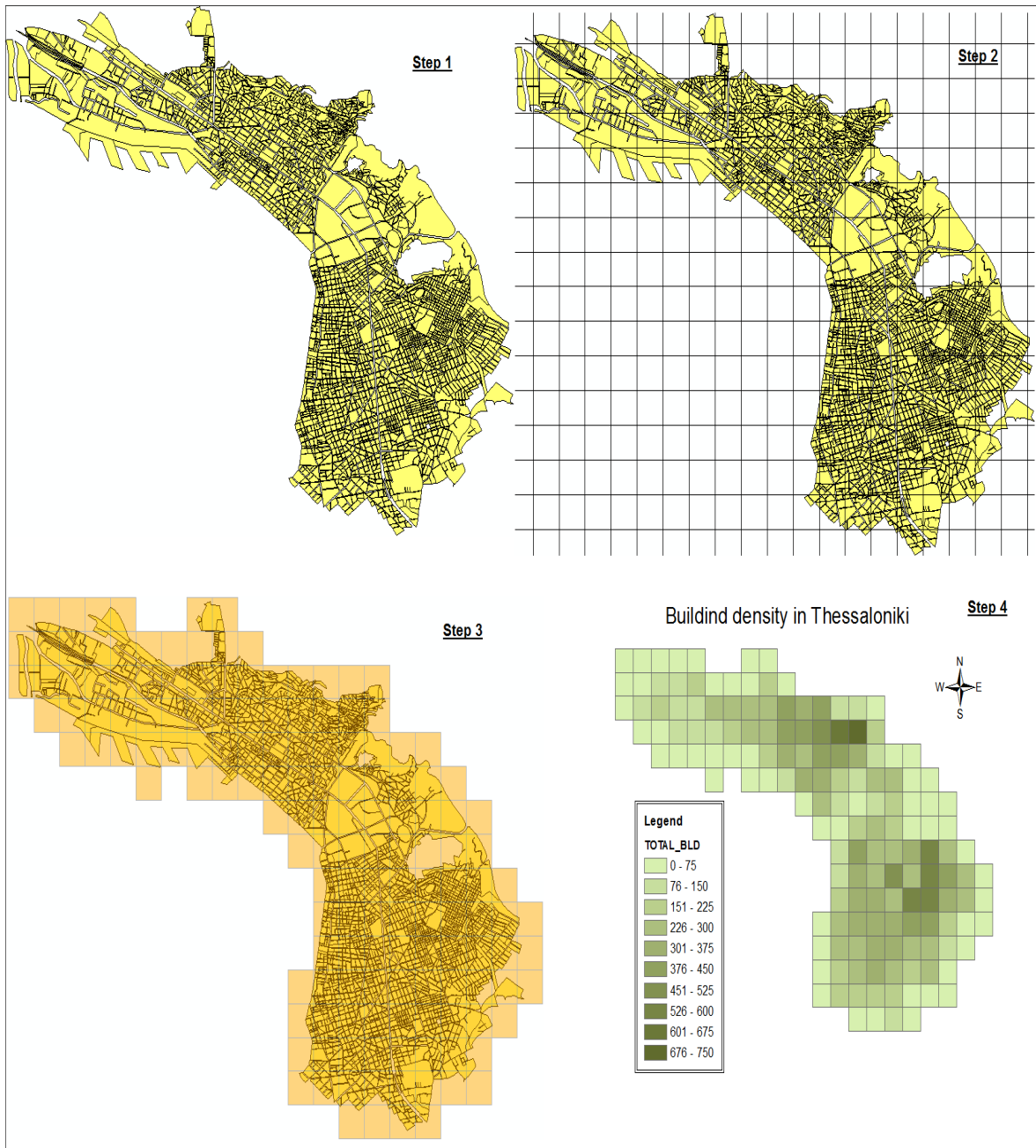


Figure 4.13 Preparation of compiled building data

As it was mentioned before, ELER can recognise shape files that contain the data based on grid. The available data for Thessaloniki refer to blocks (Figure 4.13, step 1), so it is important to compile the data to 0.0045 degree grid-cells, similar to Vs30 map. Next step is to create a fishnet sized 0.0045 degree (Figure 4.13, step 2) and trim the rest of the fishnet that doesn't intersect the layer of the blocks. Then, the data from the source layer is pasted to grid-cells. For those blocks that belong to more than one cell, the information they contain is divided according to their geometry percentages (Figure 4.13, step 3). Once the data are summed in each cell, the resultant model is then ready, as an input file in Level 2 in ELER (Figure 4.13, step 4; Figure 4.14)

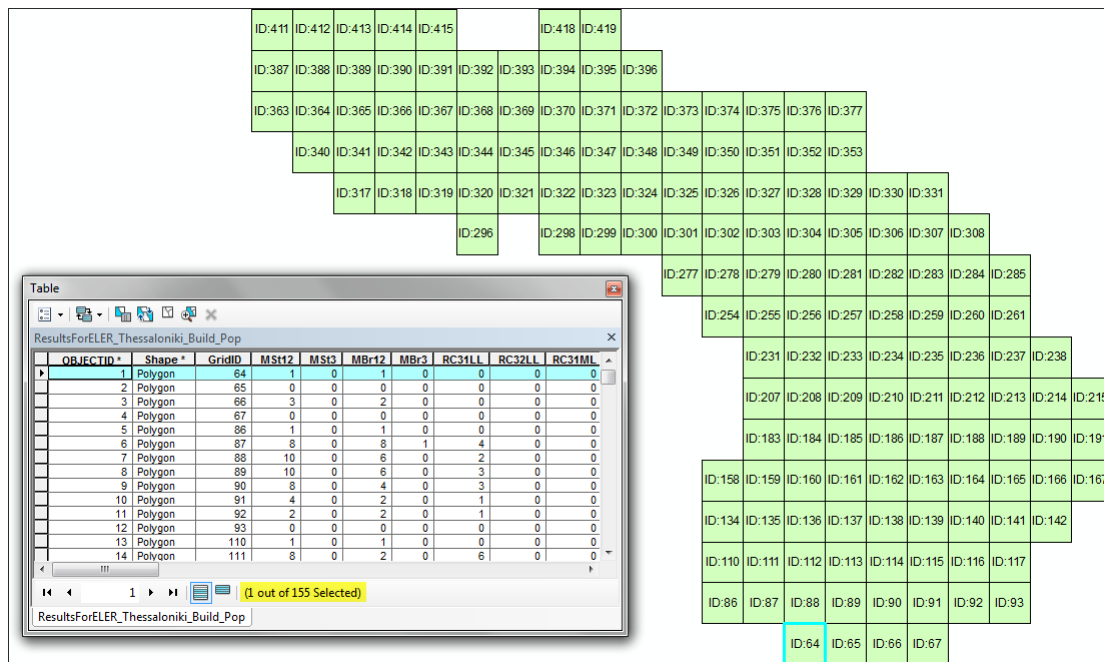


Figure 4.14 Shape file input with its attribute table; data now refers to grid-cells

4.2.2 Classification of buildings in Thessaloniki

RC Buildings

For RC buildings the building typology matrix proposed by Kappos et al. (2006) has been applied. Referring to the height of the buildings, 2-storey, 4-storey, and 9-storey R/C buildings were selected as representative of Low-rise, Medium-rise and High-rise, respectively. Regarding the structural system, both frames and dual (frame & shear wall) systems were addressed. Each of the above buildings was assumed to have three different configurations, “bare” (without masonry infill walls), “regularly infilled” and “irregularly infilled” (soft ground storey, usually pilotis), (Kappos et al, 2006).

Regarding the level of seismic design and detailing, four subclasses could be defined, as follows (Table 4.1):

Table 4.1 Specific building types and design levels for R/C building analysis (Kappos et al., 2006)

Type	Structural system	Height (number of storeys)	Seismic design level
RC1	Concrete moment frames		
RC3	Concrete moment frames with unreinforced masonry infill walls		(N)o/pre code
3.1	Regularly infilled frames	(L)ow-rise (1–3)	(L)ow code
3.2	Irregularly infilled frames (pilotis)	(M)id-rise (4–7)	(M)edium code
RC4	RC dual systems (RC frames and walls)	(H)igh-rise (8+)	(H)igh code
4.1	Bare frames (no infill walls)		
4.2	Regularly infilled dual systems		
4.3	Irregularly infilled dual systems (pilotis)		

- No code (or pre-code): R/C buildings with very low level of seismic design or no seismic design at all, and poor quality of detailing of critical elements
- Low code: R/C buildings with low level of seismic design (roughly corresponding to pre-1980 codes in S. Europe, e.g., the 1959 Code for Greece)
- Moderate code: R/C buildings with medium level of seismic design (roughly corresponding to post-1980 codes in S. Europe, e.g., the 1985 Supplementary Clauses of the Greek Seismic Codes) and reasonable seismic detailing of R/C members.
- High code: R/C buildings with enhanced level of seismic design and ductile seismic detailing of R/C members according to the new generation of seismic codes (similar to Eurocode 8) (Kappos et al., 2006)

Masonry buildings

For unreinforced masonry bearing walls buildings (URM in Hazus format) the building typology matrix proposed by Kappos et al. (2009) has been applied. Referring to the height of the buildings, 1-storey, 2-storey, and 3-storey masonry buildings were selected as representative of Low-rise. Regarding the structural system, the unreinforced masonry bearing walls system was only addressed. There are two sub-categories for URM buildings in Thessaloniki; the first only refers to structures built by stone and the second one built by brick.

As a result, the building inventory for Thessaloniki contains data for 27 categories based on Building Type, Number of Floors and Construction Year. Building categories are shown in Table 4.2 in detail, containing both URM and RC buildings.

Table 4.2 RISK-UE building typology matrix; contains only the building types used in Thessaloniki

	Type	Structural system	Height (number of stories)	Seismic design level
URM	Unreinforced Masonry			
	MSt12	stone	(L)ow rise (1-3)	(L)ow code
	MSt3			
	MBr12	bricks		
	MBr3			
RC3	Concrete Moment frames with unreinforced masonry infill walls			
	RC31LL	regularly infilled frames	(L)ow rise (1-3)	(L)ow code
	RC31ML		(M)id-rise (4-7)	
	RC31HL		(H)igh-rise (8+)	
	RC32LL	irregularly infilled frames (pilotis)	(L)ow rise (1-3)	
	RC32ML		(M)id-rise (4-7)	
	RC32HL		(H)igh-rise (8+)	
RC4	Reinforced concrete dual systems (frames & walls)			
	RC42LL	regularly infilled dual systems	(L)ow rise (1-3)	(L)ow code
	RC42ML		(M)id-rise (4-7)	
	RC42HL		(H)igh-rise (8+)	
	RC42LM		(L)ow rise (1-3)	(M)edium Code
	RC42MM		(M)id-rise (4-7)	
	RC42HM		(H)igh-rise (8+)	
	RC42LH		(L)ow rise (1-3)	(H)igh code
	RC42MH		(M)id-rise (4-7)	
	RC42HH		(H)igh-rise (8+)	
	RC43LL	irregularly infilled dual systems (pilotis)	(L)ow rise (1-3)	(L)ow code
	RC43ML		(M)id-rise (4-7)	
	RC43HL		(H)igh-rise (8+)	
	RC43LM		(L)ow rise (1-3)	(M)edium Code
	RC43MM		(M)id-rise (4-7)	
	RC43HM		(H)igh-rise (8+)	
	RC43MH		(M)id-rise (4-7)	(H)igh code
	RC43HH		(H)igh-rise (8+)	

The distribution in Thessaloniki is given in Figure 4.15 and Figure 4.16. It can be seen that the majority of buildings were built with past design codes, so the building stock in Thessaloniki could be characterized as “old”. Moreover, the dominated structural system is regularly infilled dual system (RC42).

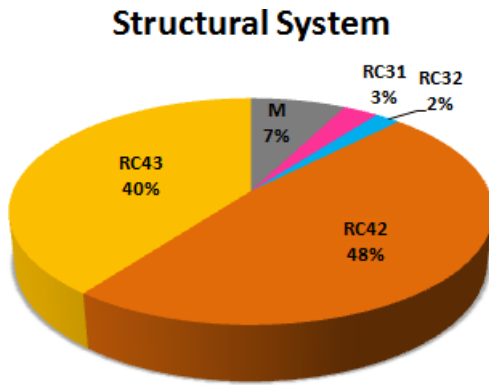


Figure 4.15 Building distribution based on structural system

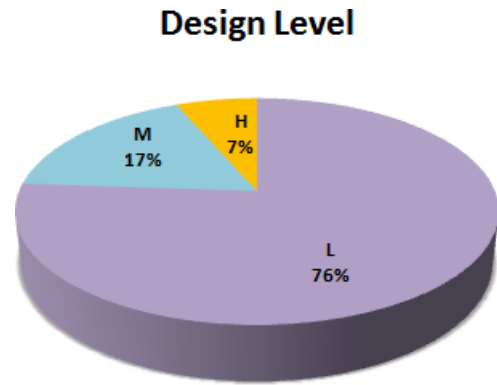


Figure 4.16 Building distribution based on design level

4.3 Fragility and capacity curves for Thessaloniki building stock

4.3.1 Structural Damage Levels

Structural damage levels for RC buildings in Thessaloniki are given below:

Table 4.3 Damage states and losses indices for R/C buildings (Kappos et al., 2006)

Damage state	Damage state label	Range of loss index-R/C	Central Index (%)
DS0	None	0	0
DS1	Slight	0--1	0.5
DS2	Moderate	1--10	5
DS3	Substantial to heavy	10--30	20
DS4	Very heavy	30--60	45
DS5	Collapse	60--100	80

4.3.2 Generate in ELER Software

For this purpose, fragility and capacity curves for Thessaloniki city derived by the 1978 Volvi earthquake are modified in order to create a user-defined building inventory database.

Building capacity curves are constructed for each model building type and represent different levels of lateral force design and building performance. Each curve is defined by two points: (1) the “yield” capacity and (2) the “ultimate” capacity. The yield capacity represents the strength level beyond which the response of the building is strongly nonlinear and is higher than the design strength, due to minimum code requirements, actual strength of materials being higher than the design one (mean values of concrete and steel strength were used in the nonlinear analyses) and, most important of all, due to the presence of the masonry infills (this influence is more pronounced in the case of frame systems), whenever such infills are present.

The ultimate capacity is related to the maximum strength of the building when the global structural system has reached a full mechanism (Kappos et al., 2006). An example for RC42LM building type is given in Figure 4.17.

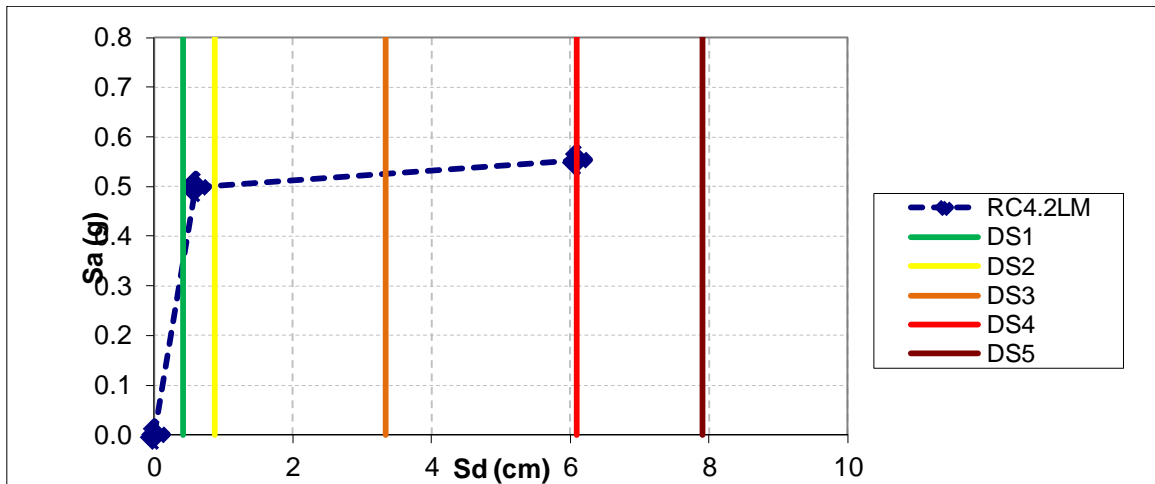


Figure 4.17 Capacity curve for RC42LM building type (Kappos et al., 2006)

ELER provides a tool *BDC-Building Database Creator*, which is able to make over the Thessaloniki data with the compatible format. Basic steps of Building Database Formation are:

- i. Definition of Building Taxonomy
- ii. Definition of Fragility Curve Parameters
- iii. Definitions of Analytical Methodology Parameters
- iv. Definition of Building Capacity Parameters

Figure 4.18 depicts the menu of BDC, where the number of building types and the corresponding design levels are entered as well as the working units are assigned.

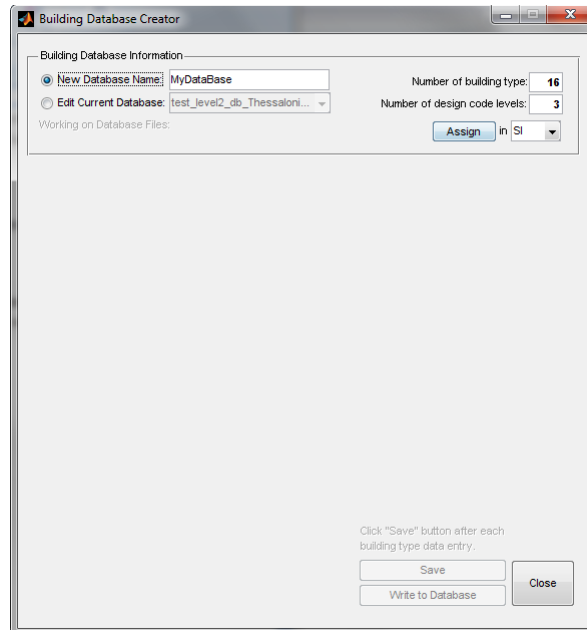


Figure 4.18 Main menu of Building database Creator

All parameters defined for Thessaloniki building inventory can be saved at each step as well as can be written to a new database as it is shown in Figure 4.21. Building type definition is done based on the number of building type and design Code levels.

Table 4.4,

Table 4.5 and Table 4.6 illustrate all parameters referred to three specific building types.

Table 4.4 Estimated S_d fragility curve parameters for Thessaloniki (median values in m), (Kappos et al, 2006)

	Building Name	Fragility Curves							
		Slight		Moderate		Extensive		Complete	
		Median	Beta	Median	Beta	Median	Beta	Median	Beta
14	RC42LM	0.004162	0.7	0.0086912	0.7	0.033401	0.7	0.079113	0.7
15	RC42MM	0.009319	0.7	0.0190124	0.7	0.070305	0.7	0.165485	0.7
16	RC42HM	0.033092	0.7	0.0576581	0.7	0.151111	0.7	0.331432	0.7

Table 4.5 Estimated capacity curves for Thessaloniki (displacement values in m, acceleration values in m/sec^2 , damping values in %), (Kappos et al, 2006)

	Building Name	Capacity Curve					
		Yield		Ultimate		Elastic	
		Displacement	Acceleration	Displacement	Acceleration	Displacement	Damping
14	RC42LM	0.0059	4.887	0.0609	5.424	0.0059	5
15	RC42MM	0.0133	2.671	0.1273	2.728	0.0133	5
16	RC42HM	0.0473	2.851	0.2549	3.030	0.0473	5

Table 4.6 Estimated additional parameters for analytical vulnerability analysis (period values in sec), (Kappos et al, 2006)

	Building Name	Structural Behaviour			Ductility Value	Building Characteristics	
		Degradation Factor					
		Short	Moderate	Long		C0 coefficient	Period
14	RC42LM	0.8	0.4	0.2	9.22	1.2	0.219
15	RC42MM	0.8	0.4	0.2	9.36	1.4	0.444
16	RC42HM	0.8	0.4	0.2	5.07	1.46	0.810

Fragility curves are shown in Figure 4.19 and Figure 4.20. It is noted that for high design level the vulnerability of building is lower (i.e. the curves are lower compared to the corresponding ones for the low seismic design).

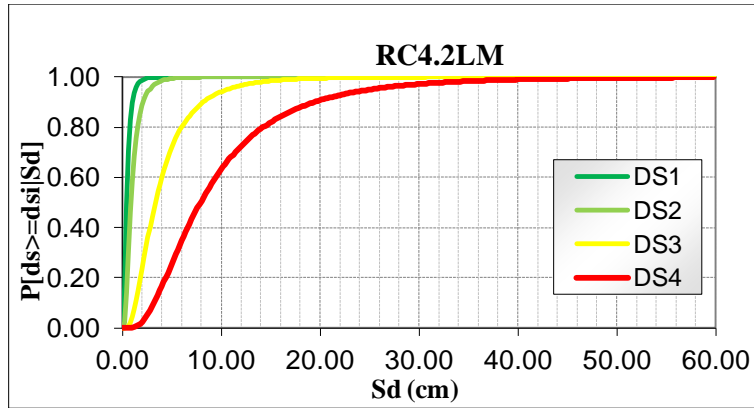


Figure 4.19 RC4.2LM fragility curves (Kappos et al., 2006)

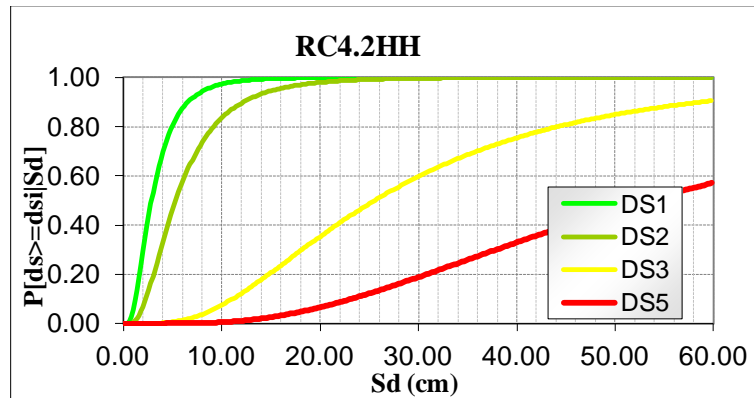


Figure 4.20 RC4.2HH fragility curves (Kappos et al., 2006)

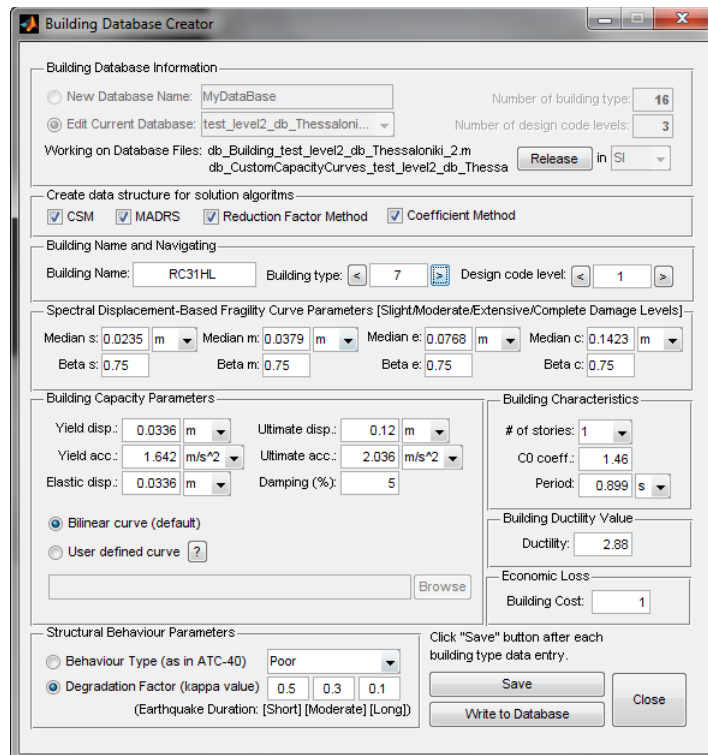


Figure 4.21 Definition of RC31HL building parameters in ELER

4.4 Hazard Scenarios for Thessaloniki; the 1978 Volvi Earthquake (scenario C)

4.4.1 Introduction

Greece is the most earthquake-prone country in Europe, as it located at the convergence of the Eurasian plate over the African one, as well as the western termination of the North Anatolian Fault Zone.

4.4.2 Regional seismicity and tectonic setting around Thessaloniki

The central sector of the Mygdonia is represented by the Gerakarou fault, which is the causative fault of the 1978 Volvi Earthquake. The earthquake, as well as the focal mechanism, has been thoroughly studied, due to its location close to the second largest city of Greece. Extended co-seismic ground ruptures were produced that splayed out in the Mygdonia Basin (Mercier et al., 1979; 1983; Papazachos et al., 1979; Soufleris and Stewart, 1981; Mountrakis et al., 1996a). The most significant ones occurred along the southern margin of the basin, coinciding with the principal N-dipping fault escarpment. All scientists agree showing roughly E(SE)-W(WN)-striking nodal planes (273°-289°), dipping between 43° and 55°, with a prevailing dip-slip kinematics and some left-lateral component (rake 272°-300°). Regarding the dimensions of the fault surface, fault length likely ranges between 18 and 22 km. Fault length has been constrained on the basis of seismological data suggesting a 25 km -long rupture plane (Roumelioti et al., 2007). Depth is proposed to be 8km (Carver and Bolligner, 1981). The maximum expected magnitude on the basis of the above parameters is $M_w=6.5$.

4.4.3 Input data for ELER

Event data

Preferred epicenter location is 40.710N and 23.270E (various authors)

Source type

Table 4.7 The Gerakarou Fault Identity

General Information			
Country:	Greece		
Name:	Gerakarou Fault (Mygdonia Basin)		
Parametric Information			
	Parameter	Qualification Key	Evidence
Fault type	normal		focal mechanisms
Depth (km)	8	LD	Carver & Bolligner (1981)
Strike (deg)	272	LD	geological/morphotectonic maps, foci and co-seismic ruptures (various authors)
Dip (deg)	50	LD	focal mechanism (various authors)
Rake (deg)	270	LD	kinematic indicators and focal mechanisms (various authors)
Max magnitude (Mw)	6.5	ER	after the relationships of Wells and Coppersmith (1994) and Hanks and Kanamori (1979)
epicenter (Lat/Long)	40.710/23.270	LD	AUTH Catalogue relocated by Karakostas
Length (km)	22.5	LD	co-seismic ruptures and seismological data (various authors)
Associated Earthquake			
Latest earthquake	20/6/1978	Mw=6.5 (instrumental recordings)-	The 1978 Volvi Earthquake or The Great Thessaloniki Earthquake

*Acronyms: EJ=Expert Judgement, LD=Literature Data, ER=Empirical Relationship



Figure 4.22 Segmentation model of Gerakarou Fault

Site correction

Local site effects are taken into account with Vs30 parameter. Using Next Generation Attenuation relations (NGA), ground motion parameters are calculated directly at surface.

Site condition

To take into consideration the local site effects of Thessaloniki, a new Vs30 map is used to calculate ground motion parameters at surface. The new map is integrated into USGS Vs30 map for Central Macedonia, as it is depicted in Figure 4.23.

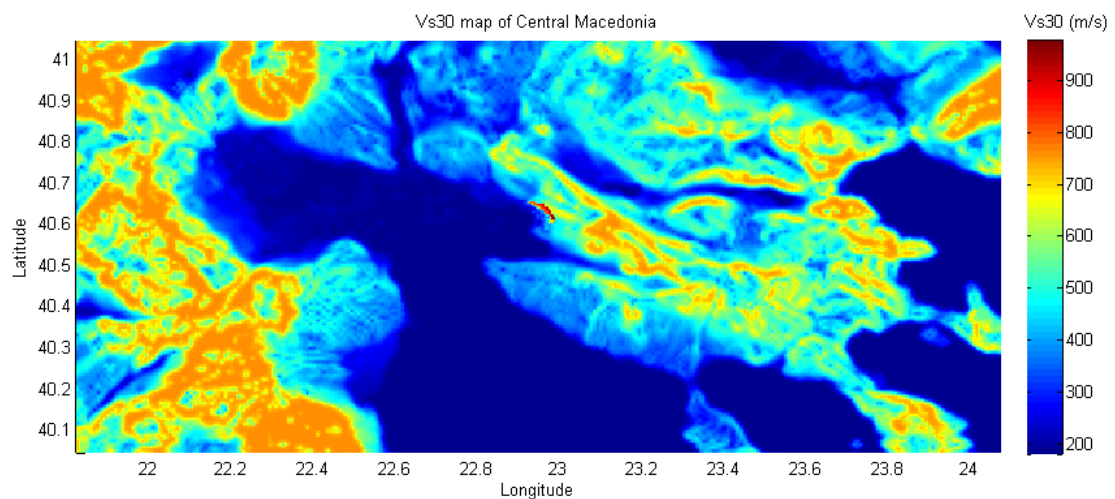


Figure 4.23 Vs30 distribution in Central Macedonia

Ground Motion Prediction Equations

For the application in Thessaloniki, it has been decided that both the Peak Ground Acceleration (PGA) and Spectral Acceleration will be examined for the damage estimation. The Boore & Atkinson (2008) model which was developed in NGA Project and the Akkar & Boomer (2007) and Campbell & Bozorgnia (2008) model have been selected.

The general equation of the Boore & Atkinson, 2008 model is as follows (taken from Douglas, 2011):

$$\begin{aligned}
 \ln Y &= F_M(M) + F_D(R_{JB}, M) + F_S(V_{S30}, R_{JB}, M) \\
 F_D(R_{JB}, M) &= [c_1 + c_2(M - M_{ref})] \ln(R/R_{ref}) + c_3(R - R_{ref}) \\
 R &= \sqrt{R_{JB}^2 + h^2} \\
 F_M(M) &= \begin{cases} e_1 U + e_2 SS + e_3 NS + e_4 RS + e_5 (M - M_h) + \\ e_6 (M - M_h)^2 & \text{for } M \leq M_h \\ e_1 U + e_2 SS + e_3 NS + e_4 RS + e_7 (M - M_h) & \text{for } M > M_h \end{cases} \\
 F_S &= F_{LIN} + F_{NL} \\
 F_{LIN} &= b_{lin} \ln(V_{S30}/V_{ref}) \\
 F_{NL} &= \begin{cases} b_{nl} \ln(\text{pga_low}/0.1) & \text{for } \text{pga4nl} \leq a_1 \\ b_{nl} \ln(\text{pga_low}/0.1) + c[\ln(\text{pga4nl}/a_1)]^2 + \\ d[\ln(\text{pga4nl}/a_1)]^3 & \text{for } a_1 < \text{pga4nl} \leq a_2 \\ b_{nl} \ln(\text{pga4nl}/0.1) & \text{for } a_2 < \text{pga4nl} \end{cases} \\
 c &= (3\Delta y - b_{nl}\Delta x)/\Delta x^2 \\
 d &= -(2\Delta y - b_{nl}\Delta x)/\Delta x^3 \\
 \Delta x &= \ln(a_2/a_1) \\
 \Delta y &= b_{nl} \ln(a_2/\text{pga_low}) \\
 b_{nl} &= \begin{cases} b_1 & \text{for } V_{S30} \leq V_1 \\ (b_1 - b_2) \ln(V_{S30}/V_2) / \ln(V_1/V_2) + b_2 & \text{for } V_1 < V_{S30} \leq V_2 \\ b_2 \ln(V_{S30}/V_{ref}) / \ln(V_2/V_{ref}) & \text{for } V_2 < V_{S30} < V_{ref} \\ 0.0 & \text{for } V_{ref} \leq V_{S30} \end{cases}
 \end{aligned}$$

where Y is in g, $M_h=6.75$ (hinge magnitude), $V_{ref}=760\text{m/s}$ (specified reference velocity corresponding to the NEHRP B/C boundary), $a_1=0.03\text{g}$ (threshold for linear amplification), $a_2=0.09\text{g}$ (threshold for nonlinear amplification), $\text{pga_low}=0.06\text{g}$ (for transition between linear and nonlinear behaviour), pga4nl is predicted PGA in g for V_{ref} with $F_s=0$, $V_1=180\text{m/s}$, $V_2=300\text{m/s}$, $b_{lin}=-0.360$, $b_1=-0.640$, $b_2=-0.14$, $M_{ref}=4.5$, $R_{ref}=1\text{km}$, $c_1=-0.66050$, $c_2=0.11970$, $c_3=-0.01151$, $h=1.35$, $e_1=-0.538004$, $e_2=-0.50350$, $e_3=-0.75472$, $e_4=-0.50970$, $e_5=0.28805$, $e_6=-0.10164$, $e_7=0.0$; $\sigma=0,502$ (intra-event); $\tau_U=0.265$, $\tau_M=0.260$ (inter-event); $\sigma_{TU}=0.566$, $\sigma_{TM}=0.56$ (total).

The general equation of the Akkar & Boomer, 2007 model is as follows (taken from Douglas, 2011):

$$\log y = b_1 + b_2 M + b_3 M^2 + (b_4 + b_5 M) \log \sqrt{R_{jb}^2 + b_6^2} + b_7 S_S + b_8 S_A + b_9 F_N + b_{10} F_R$$

where y is in cm/s^2 , $b_1 = 1.647$, $b_2 = 0.767$, $b_3 = -0.074$, $b_4 = -3.162$, $b_5 = 0.321$, $b_6 = 7.682$, $b_7 = 0.105$, $b_8 = 0.020$, $b_9 = -0.045$, $b_{10} = 0.085$, $\sigma_1 = 0.557 - 0.049M$ (intra-event) and $\sigma_2 = 0.189 - 0.017M$ (inter-event) when b_3 is unconstrained and $b_1 = 4.185$, $b_2 = -0.112$, $b_4 = -2.963$, $b_5 = 0.290$, $b_6 = 7.593$, $b_7 = 0.099$, $b_8 = 0.020$, $b_9 = -0.034$, $b_{10} = 0.104$, $\sigma_1 = 0.557 - 0.049M$ (intra-event) and $\sigma_2 = 0.204 - 0.018M$ (inter-event) when b_3 is constrained to zero (to avoid super-saturation of PGA).

- Use three site categories:

Soft soil $S_S = 1$, $S_A = 0$.

Stiff soil $S_A = 1$, $S_S = 0$.

Rock $S_S = 0$, $S_A = 0$.

- Use three faulting mechanism categories:

Normal $F_N = 1$, $F_R = 0$.

Strike-slip $F_N = 0$, $F_R = 0$.

Reverse $F_R = 1$, $F_N = 0$.

4.4.4 Output results

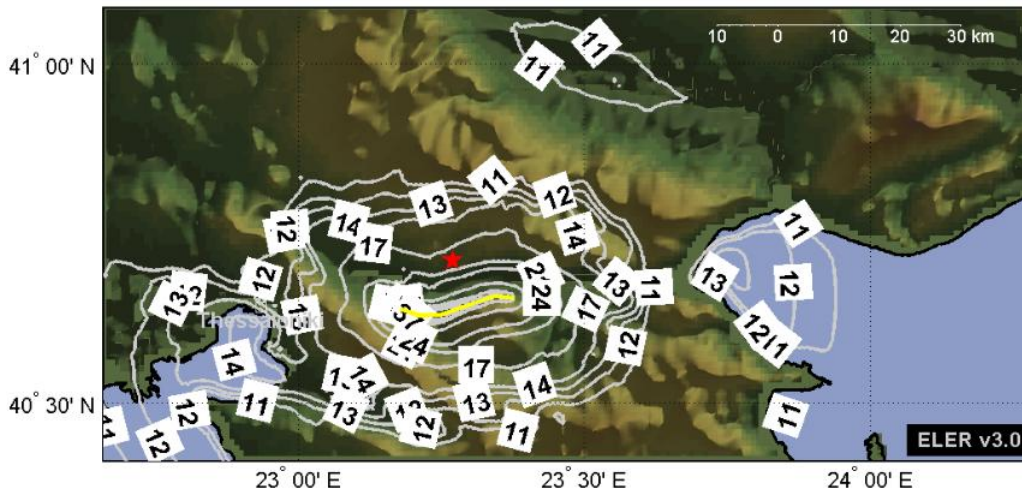
The selected equations have been analyzed and compared and their limitations were taken into consideration. Both equations exhibit advantages and disadvantages, so it is difficult to identify the most suitable. Despite the uncertainties, two criteria were taken into consideration to decide that Boore & Atkinson (2008) model is more suitable scenario the 1978 Thessaloniki earthquake (Volvi earthquake). The first criterion was the ground motion obtained during the verification process. PGA value at surface at the City Hotel during the 1978 Thessaloniki earthquake was recorded about 0.14g. Distribution of PGA obtained from Boore & Atkinson (2008) is close to the real one at City Hotel ($\approx 0.135\text{g}$). The second one is that using the previous equation, damages in Level 2 are comparable with the observed damages.

Figure 4.24 illustrates the spatial distribution of peak ground acceleration, and spectral accelerations.

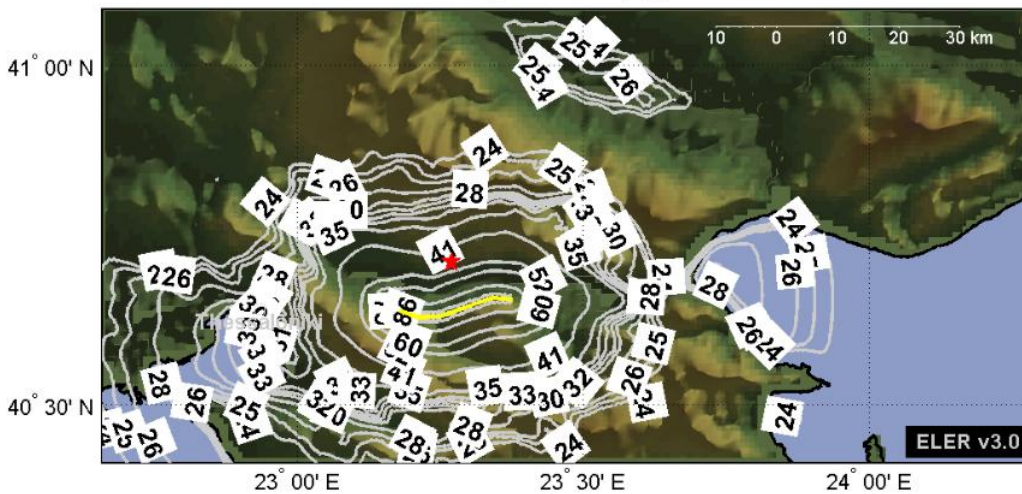
Table 4.8 Input parameters for Thessaloniki (Scenario C)

Analysis-59	
SEISMIC HAZARD	
Event Data	Thess78
Source type	Gerakarou-Stilvos fault
Site correction	directly at surface
Vs30	Vs30_Thess
GMPE	Boore & Atkinson 08
median+___sigma	0
PGA at City Hotel	0.1351g
Sa0.2 at City Hotel	0.3183g
Sa1.0 at City Hotel	0.1186g
Comments	
phantom grid 1km, interpolation grid 0.0045	

M6.5 Depth= 8 Lat= 40.71 Lon= 23.27
 Map of: PGA (%g)



M6.5 Depth= 8 Lat= 40.71 Lon= 23.27
 Map of: PSA02 (%g)



M6.5 Depth= 8 Lat= 40.71 Lon= 23.27
 Map of: PSA10 (%g)

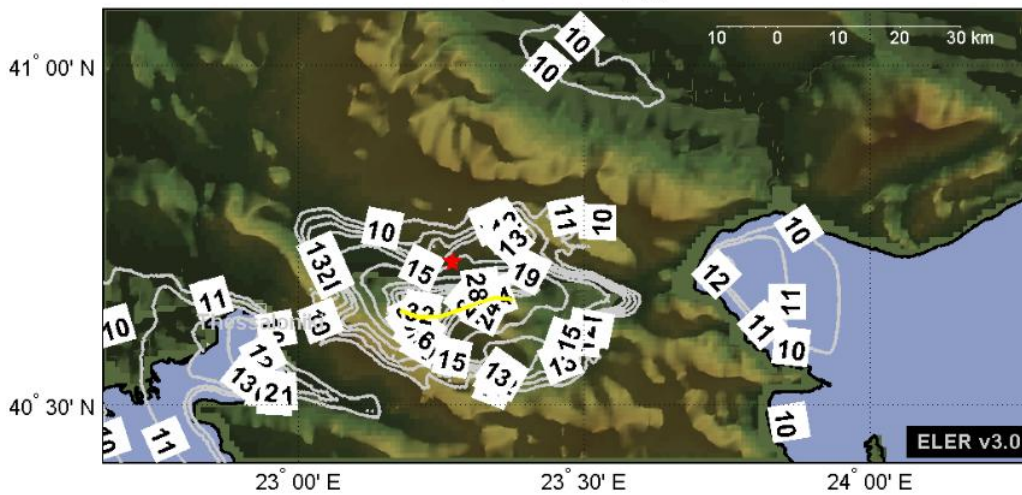


Figure 4.24 PGA (%g) and Spectral Accelerations (%g) at $T=0.2\text{sec}$ and $T=1.0\text{sec}$ obtained from the Boore & Atkinson (2008) GMPE for Thessaloniki (Scenario C)

In addition, Akkar & Bommer (2007) ground motion estimation equation was also used in the estimation of PGA distribution.

Table 4.9 Input parameters for Thessaloniki (Scenario C)

Analysis-66	
SEISMIC HAZARD	
Event Data	Thess78
Source type	Gerakarou-Stilvos fault
Site correction	Ec8
Vs30	Vs30_Thess
GMPE	Akkar & Bommer 07
median+__sigma	0.15
PGA at City Hotel	0.141g
Sa0.2 at City Hotel	-
Sa1.0 at City Hotel	-
Comments	
phantom grid 1km, interpolation grid 0.0045	

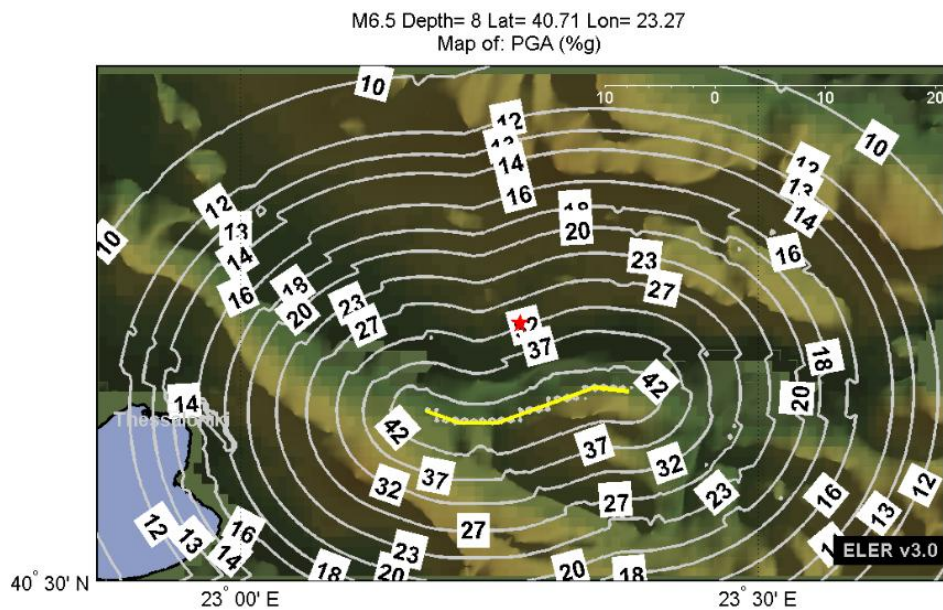


Figure 4.25 PGA (%g) obtained from the Akkar & Boomer (2007) GMPE for Thessaloniki (Scenario C)

The third GMPE for the estimation of ground motion is the Campbell and Bozorgnia (2008) equation depending on the information on magnitude, distance, fault type and average shear wave velocity at 30m depth ($V_{s,30}$). In this thesis, Campbell and Bozorgnia (2008) ground motion estimation equation has been used in the estimation of PGA, S_a (T=0.2s) and S_a (T=1.0s) distribution, as it summarized in Table 4.10.

Table 4.10 Input parameters for Thessaloniki (Scenario C)

Analysis-64	
SEISMIC HAZARD	
Event Data	Thess78
Source type	Gerakarou-Stilvos fault
Site correction	directly at surface
Vs30	Vs30_Thess
GMPE	Campbell & Bozorgnia 08
median+___sigma	0.2
PGA at City Hotel	0.137g
Sa0.2 at City Hotel	0.378g
Sa1.0 at City Hotel	0.145g

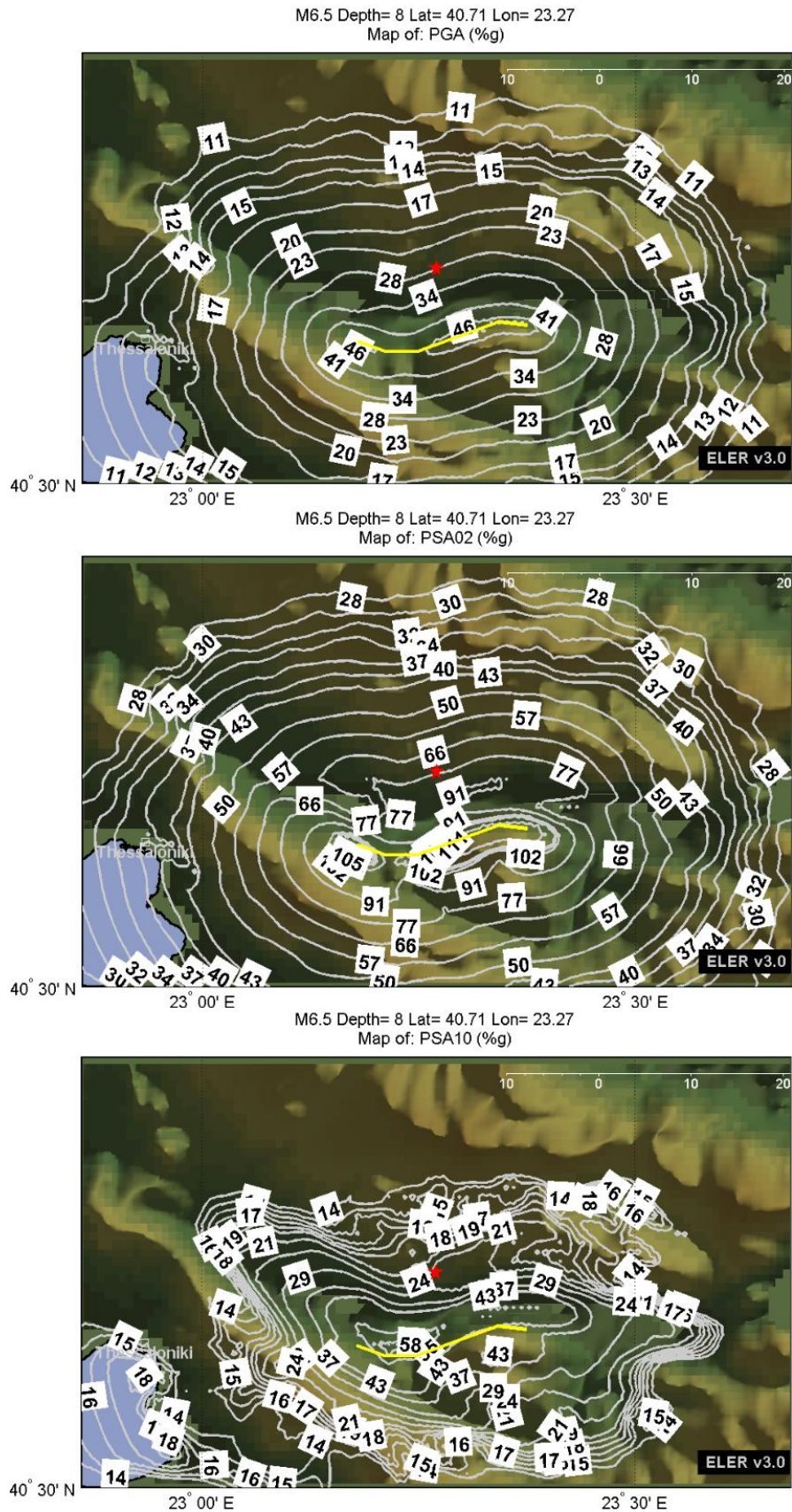


Figure 4.26 PGA (%g) and Spectral Accelerations (%g) at $T=0.2\text{sec}$ and $T=1.0\text{sec}$ obtained from the Campbell and Bozorgnia (2008) GMPE for Thessaloniki (Scenario C)

4.5 Hazard Scenarios for Thessaloniki; the Anthemountas Fault; one of the most hazardous earthquake sources for Thessaloniki (scenario D)

4.5.1 Introduction

Around Thessaloniki, there are a few active faults, which could cause a destructive earthquake similar to the 1978 one. Investigating the faults around the city of Thessaloniki, it is considered that Anthemountas fault in the southern side of the city could be a deterministic scenario for the seismic hazard of the region.

4.5.2 Regional seismicity and tectonic setting around Thessaloniki

The surface ruptures observed at Peraia are part of the longer active fault, known as the Anthemountas Fault (Neotectonic Map of Greece, Tranos et al 2003, Goldsworthy et al 2002). As it is shown in figure 2.23, the fault extends from the coastal area of Megalo Emvolo Cape, north of Angelochori village, with an E-W strike up to Galarinos village, with a total length of 32 km. About the fault type, it is a normal fault dipping to the north and divided into three segments (Fig. 2.23) based on the geometrical characteristics of the surface fault trace and the hypothetical extension to the sea area of Thermaikos Gulf.

- The first segment (1) extends from Galarinos to N. Risio with direction N110 and length 17 km.
- The second (2) segment extends from N. Risio village to Megalo Embolo Cape (Angelochori) with direction N90 and length 15 km.
- The third (3) part is the hypothetical extension of the fault into the sea with direction N90. The dip direction of the fault is 87 to the North near the surface, but deeper than 8km the dip decrease to 50 at 20km depth; it is therefore a listric fault.



Figure 4.27 The Anthemountas fault with red colour and its segments (Zervopoulou et al., 2007)

4.5.3 Input data for ELER

Event Data

Due to the fact that Thessaloniki is surrounded by active faults, a scenario is proposed for the seismic hazard of the region. Depth is proposed to be 6km, accordingly to the empirical relation by Mai et al. (2005). The maximum expected magnitude on the basis of the following parameters is $M_w=6.5$; calculated from the empirical relationships of Wells & Coppersmith (1994). Moreover, dimensions of the first segment are derived by Zervopoulou (2004), where length is 17-17.5 km and width 18km. Input parameters are depicted in Figure 4.28.

Maximum magnitude of this scenario is calculated below:

Normal rupture: $Mag=3.93+1.02\log(\text{Area})=3.93+1.02\log(17\times 18)=6.46$

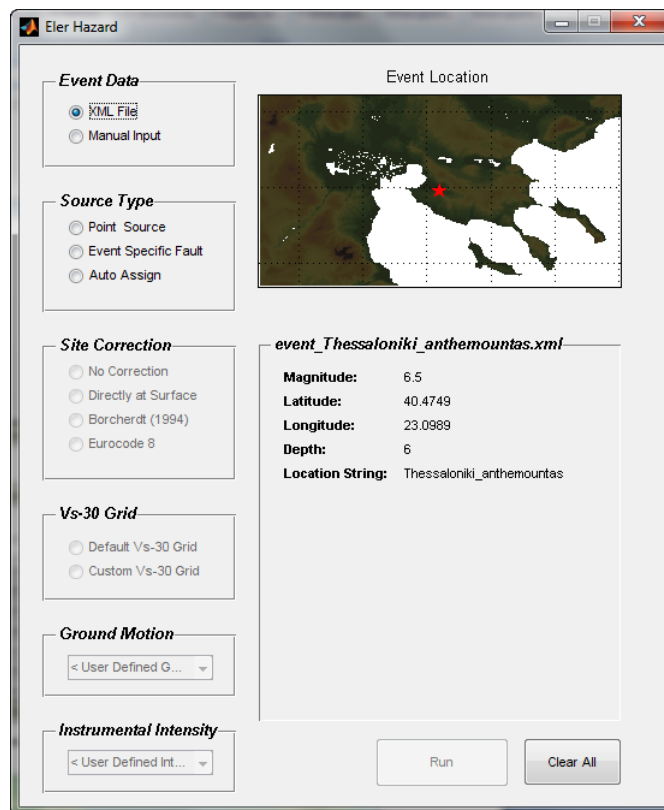


Figure 4.28 Event data for the forth scenario

Source type

Table 4.11 The Anthemountas Fault Identity

General Information			
Country:	Greece		
Name:	Anthemountas Fault		
Parametric Information			
	Parameter	Qualification Key	Evidence
Fault type	normal		focal mechanisms
Depth (km)	6	ER	empirical relations (various authors)
Strike (deg)	272	LD	various geological/morphotectonic maps
Dip (deg)	60	EJ	inferred from microseismic spatial and field measurements (Tranos et al, 2003)
Rake (deg)	270	LD	kinematic indicators, focal mechanisms and regional stress field (Mountrakis et al., 2006)
Max magnitude (Mw)	6.5	ER	calculated from the empirical relationships of Wells and Coppersmith (1994)
Epicenter (Lat/Long)	40.475/23.099	LD	various geological/morphotectonic maps
Length (km)	17	LD	morphotectonic maps (Zervopoulou, 2004)
Associated Earthquake			
Latest earthquake	03/07/1759	Mw=6.5 historical event	

*Acronyms: EJ=Expert Judgement, LD=Literature Data, ER=Empirical Relationship



Figure 4.29 Segmentation model of Anthemountas Fault

Site correction

The procedure used for the scenario C is also repeated in the scenario D.

Site condition

To take into consideration the local site effects of Thessaloniki, a new Vs30 map is used to calculate ground motion parameters at surface. The new map is integrated into USGS Vs30 map for Central Macedonia, as it is depicted in Figure 4.23, as in scenario C.

Ground Motion Prediction Equations

Using Boore & Atkinson (2008), Campbell & Bozorgnia (2008) and Akkar & Boomer (2007), spatial distribution of PGA and S_a is estimated Central Macedonia area.

4.5.4 Output results

In this paragraph, it is attempted to evaluate the ground motion produced by Anthemountas Fault. The ground motion was computed in Hazard module based on the Boore and Atkinson (2008) equation. Table 4.12 summarizes all necessary data for the analysis.

Table 4.12 Input parameters for Thessaloniki (Scenario D)

Analysis-67	
SEISMIC HAZARD	
Event Data	Anthemountas
Source type	Anthemountas Fault
Site correction	directly at surface
Vs30	Vs30_Thess
GMPE	Boore & Atkinson 08
median+___sigma	0
PGA	-
Sa0.2	-
Sa1.0	-
<u>Comments</u>	
phantom grid 1km, interpolation grid 0.0045, map extent 0.6/0.7	

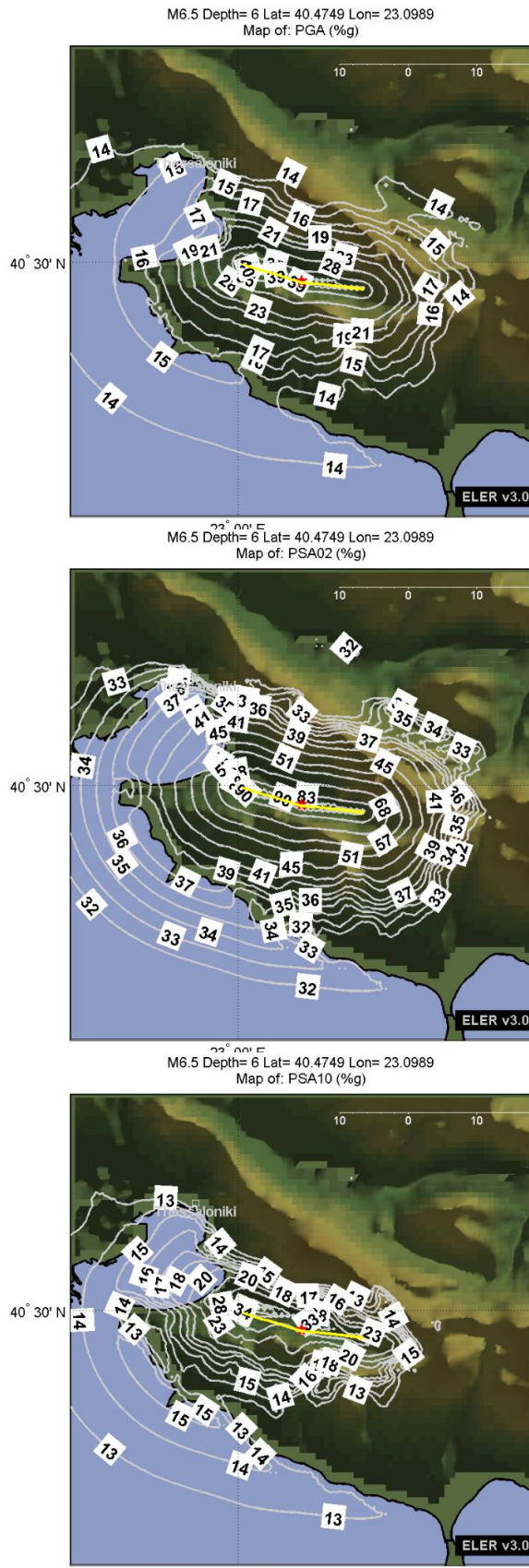


Figure 4.30 PGA (%g) and Spectral Accelerations (%g) at $T=0.2\text{sec}$ and $T=1.0\text{sec}$ obtained from the Boore & Atkinson (2008) GMPE for Thessaloniki (Scenario D)

Similar to the previous analysis, Campbell & Bozorgnia (2008) was also used to estimate the ground motion. Analysis parameters are summarized in Table 4.13.

Table 4.13 Input parameters for Thessaloniki (Scenario D)

Analysis-69	
SEISMIC HAZARD	
Event Data	Anthemountas
Source type	Anthemountas fault
Site correction	directly at surface
Vs30	Vs30_Thess
GMPE	Campbell & Bozorgnia 08
median+__sigma	0
PGA	-
Sa0.2	-
Sa1.0	-
<u>Comments</u>	
phantom grid 1km, interpolation grid 0.0045, map extent 0.6/0.7	

Ground motion distribution is mapped automatically by ELER, thus it is possible to compare the reliability of the values. PGA and spectral acceleration distribution are depicted in Figure 4.31.

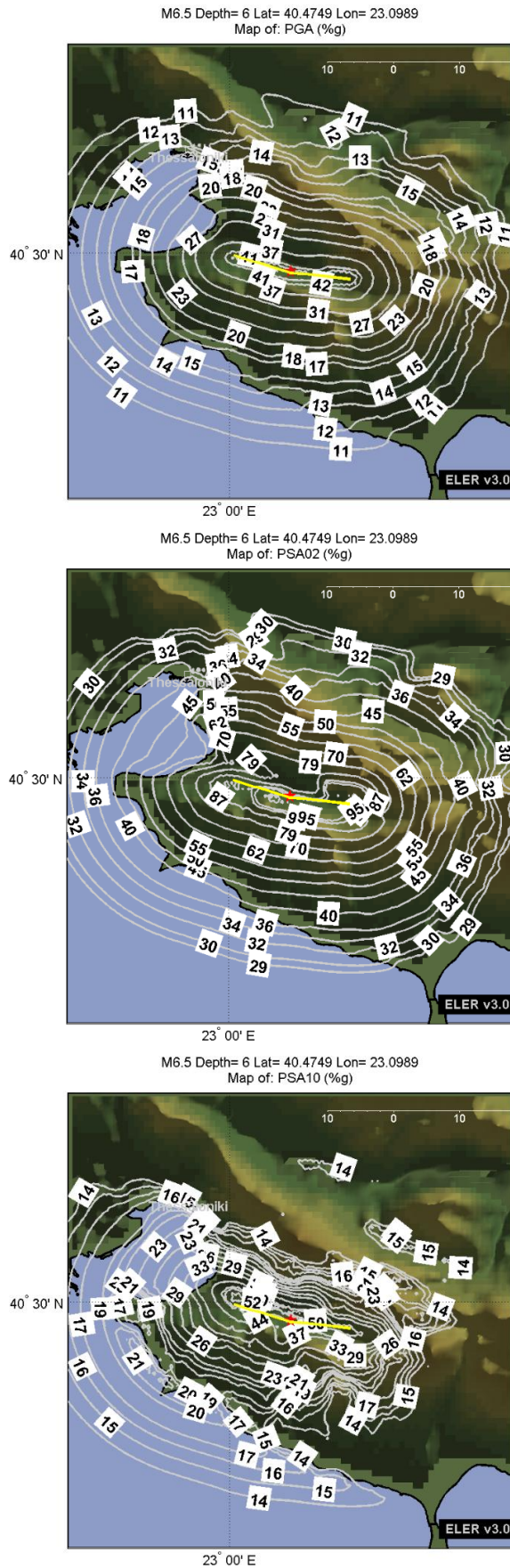


Figure 4.31 PGA (%g) and Spectral Accelerations (%g) at $T=0.2\text{sec}$ and $T=1.0\text{sec}$ obtained from the Campbell and Bozorgnia (2008) GMPE for Thessaloniki (Scenario D)

Last equation included in the analysis package is the Akkar & Bommer (2007).

Table 4.14 Input parameters for Thessaloniki (Scenario D)

Analysis-71	
SEISMIC HAZARD	
Event Data	Thess78
Source type	Gerakarou-Stilvos fault
Site correction	directly at surface
Vs30	Vs30_Thess
GMPE	Akkar & Bommer 07
median+__sigma	0
PGA	-
Sa0.2	-
Sa1.0	-
<u>Comments</u>	
phantom grid 1km, interpolation grid 0.0045, map extent 0.6/0.7	

PGA contours obtained from the aforementioned equation are shown in the Figure 4.32.

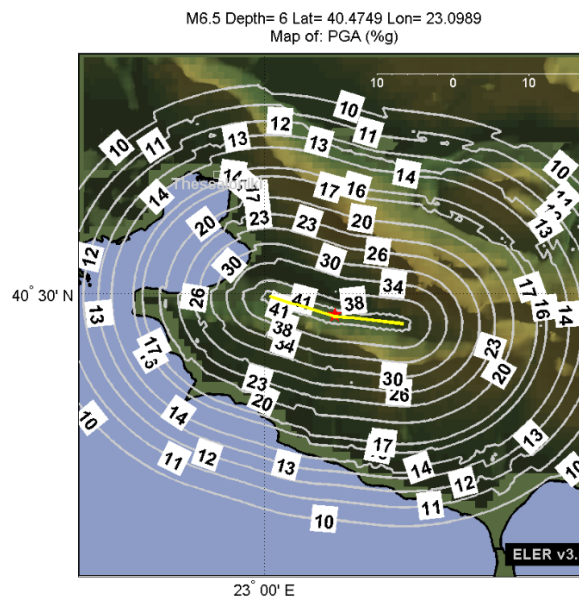


Figure 4.32 PGA (%g) obtained from the Akkar & Bommer (2007) GMPE for Thessaloniki (Scenario D)

4.6 Building damages and casualties from Scenario C

4.6.1 Building damages (analysis results)

In order to validate the applicability of the Level 2 module in an urban environment such as Thessaloniki, the building damage probabilities were calculated by CSM and CM. Average of total damaged number of buildings is given in Table 4.15 which was obtained for the scenario earthquake using the two aforementioned analytical methods (CSM and CM).

Calculations were done by using:

1. three Ground Motion Prediction Equations (GMPE's):

- Boore & Atkinson (2008)-----Analysis 59*
- Campbell & Bozorgnia (2008) ----Analysis 64
- Akkar & Bommer (2007) -----Analysis 66

**Analysis vol. denotes just the priority of the results done by the author in his personal database*

2. Two demand spectrums:

- International Building Code (IBC)
- Eurocode 8 (EC8)

3. Two different approaches for the computation of the demand spectrum and the performance point:

- Capacity Spectrum Method (CSM)
- Coefficient Method (CM)

As a result, comparisons of different methods are given in the following diagrams.

Spatial distributions of damaged buildings at each discrete damage level, namely slight, moderate, extensive and complete, are given in Figure 4.34.

Table 4.15 Damage estimation results for Thessaloniki (Scenario C), using the GMPE by Boore and Atkinson (2008)

Analysis-59		LEVEL 2							LEVEL 2								
SEISMIC HAZARD		IBC-International building code							EC8								
Event Data	Thess78	Demand Spectrum	Thess_2							Demand Spectrum	Thess_2						
Source type	Gerakarou-Stilvos fault	Classification	Thess_2							Classification	Thess_2						
Site correction	directly at surface	Building DB	Thess rounding							Building DB	Thess rounding						
Vs30	Vs30_Thess	Magnitude	6.5							Magnitude	6.5						
GMPE	Boore & Atkinson 08	Vs30	Vs30_Thess							Vs30	Vs30_Thess						
median	0	PGA	-							PGA	0.1351g						
PGA at City Hotel	0.1351g	Sa0.2	0.3183g							Sa0.2	-						
Sa0.2 at City Hotel	0.3183g	Sa1.0	0.1186g							Sa1.0	-						
Sa1.0 at City Hotel	0.1186g	Method	CSM-Capacity Spectrum Method	percentage (%)	CM-Coefficient method	percentage (%)	Average	Average perc (%)	Method	CSM-Capacity Spectrum Method	percentage (%)	CM-Coefficient method	percentage (%)	Average	Average perc (%)		
Comments		Complete	68	0.25	191	0.7	130	0.5	Complete	925	3.34	357	1.3	641	2.3		
phantom grid 1km, interpolation grid 0.0045		Extensive	881	3.18	1720	6.2	1301	4.7	Extensive	3802	13.71	2334	8.4	3068	11.1		
		Moderate	7407	26.71	9437	34.0	8422	30.4	Moderate	10566	38.11	10843	39.1	10705	38.6		
		Slight	8188	29.53	7964	28.7	8076	29.1	Slight	6254	22.55	7508	27.1	6881	24.8		
		None	11184	40.33	8416	30.4	9800	35.3	None	6181	22.29	6686	24.1	6434	23.2		
		Total	27728	100.00	27728	100.0	27728	100.0	Total	27728	100.00	27728	100.0	27728	100.0		

According to previous research, PGA at City Hotel in 1978 Thessaloniki was recorded approximately 0.14g. Using the GMPEs of Boore & Atkinson (2008), PGA value in the same geographical point is 0.135g, close to the recorded one.

	IBC	EC8
Com	0.5	2.3
Ext	4.7	11.1
Mod	30.4	38.6
Total	35.6 %	52%

Once the EC8 demand spectrum is selected, the number of unusable buildings (complete + extensive + moderate) is increased almost 1.5 times, overestimating the result compared to IBC spectrum.

Figure 4.33 illustrates the comparative difference using the two demand spectrums IBC and Ec8.

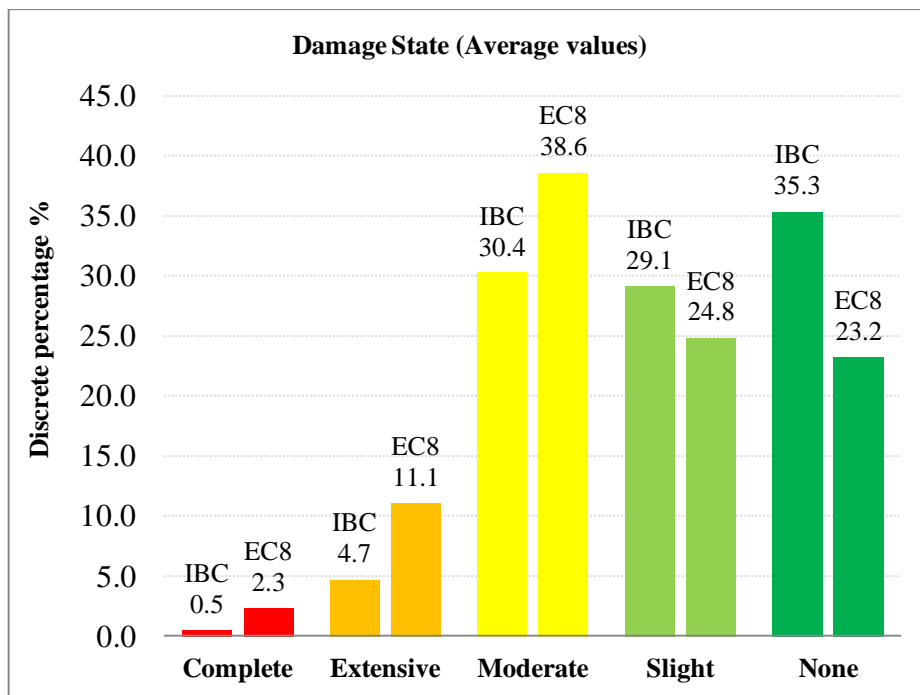


Figure 4.33 Discrete damage probabilities under Analysis 59

It is important to mention that ELER extracts the results to gridded maps with graduated colours. Figure 4.34 depicts the damage buildings in Thessaloniki after an earthquake similar to the ‘1978’ one.

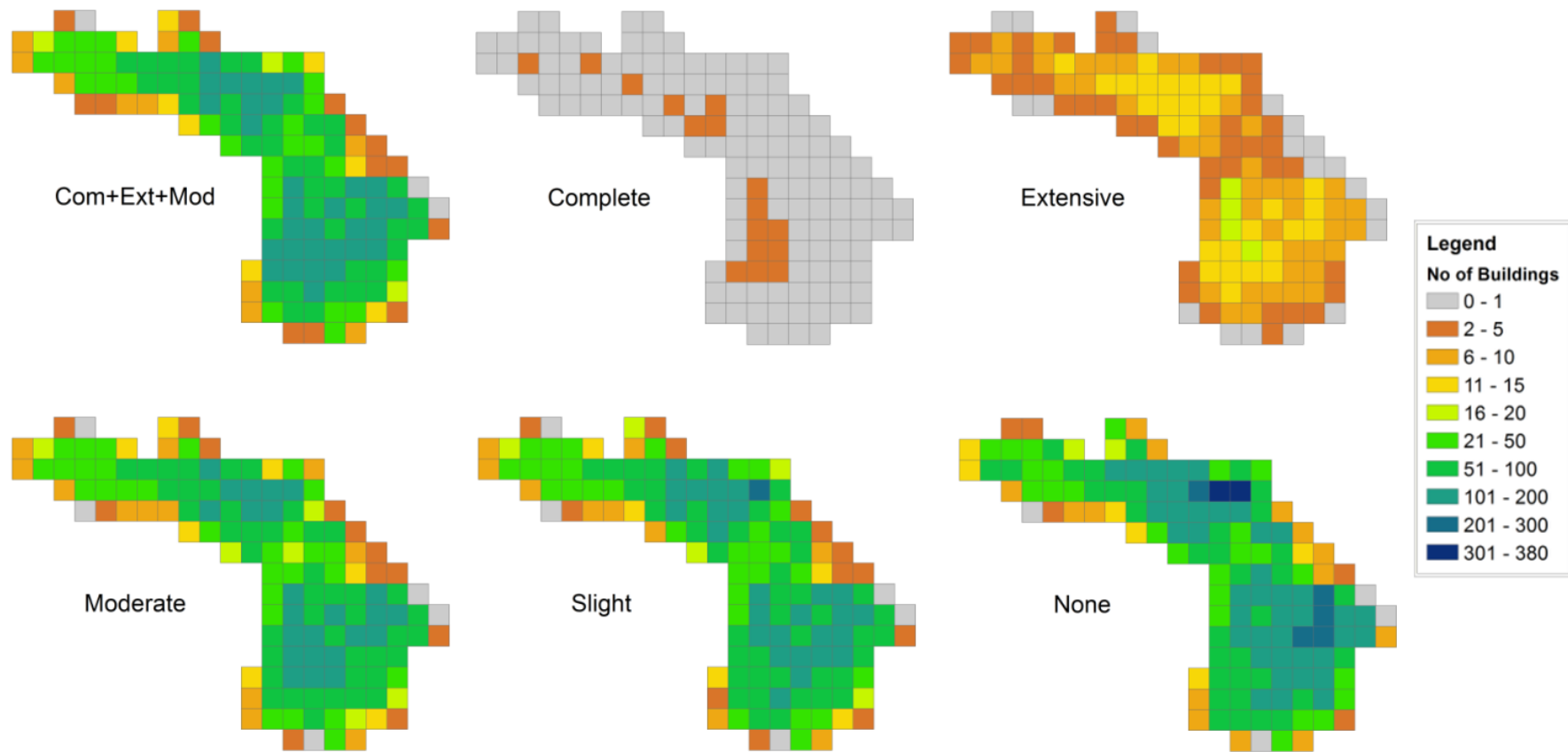


Figure 4.34 The distribution of damage buildings in Thessaloniki resulting from Analysis 59, IBC demand spectrum and CSM as selected method-Level 2 Analysis

Following the same concept, but changing the GMPE to Campbell & Bozorgnia (2008), the results are given in Table 4.16.

Table 4.16 Damage estimation results for Thessaloniki (Scenario C) using the GMPE by Campbell & Bozorgnia (2008)

Analysis-64		LEVEL 2						LEVEL 2							
SEISMIC HAZARD		IBC-International building code						EC8							
Event Data	Thess78	Demand Spectrum	IBC-International building code						Demand Spectrum	EC8					
Source type	Gerakarou-Stilvos fault	Classification	Thess_2						Classification	Thess_2					
Site correction	directly at surface	Building DB	Thess rounding						Building DB	Thess rounding					
Vs30	Vs30_Thess	Magnitude	6.5						Magnitude	6.5					
GMPE	Campbell & Bozorgnia 08	Vs30	Vs30_Thess						Vs30	Vs30_Thess					
median	0.2	PGA	-						PGA	0					
PGA at City Hotel	0.1369g	Sa0.2	0.3775g						Sa0.2	-					
Sa0.2 at City Hotel	0.3775g	Sa1.0	0.1450g						Sa1.0	-					
Sa1.0 at City Hotel	0.1450g	Method	CSM-Capacity Spectrum Method	percentage (%)	CM-Coefficient method	percentage (%)	Average	Average perc (%)	Method	CSM-Capacity Spectrum Method	percentage (%)	CM-Coefficient method	percentage (%)	Average	Average perc (%)
Comments		Complete	907	3.3	450	1.6	679	2.4	Complete	1186	4.3	440	1.6	813	2.9
phantom grid 1km, interpolation grid 0.0045		Extensive	2483	9.0	2963	10.7	2723	9.8	Extensive	3855	13.9	2741	9.9	3298	11.9
		Moderate	9476	34.2	11362	41.0	10419	37.6	Moderate	11189	40.4	11432	41.2	11311	40.8
		Slight	7623	27.5	7272	26.2	7448	26.9	Slight	6227	22.5	7237	26.1	6732	24.3
		None	7239	26.1	5681	20.5	6460	23.3	None	5271	19.0	5878	21.2	5575	20.1
		Total	27728	100.00	27728	100.0	27728	100.0	Total	27728	100.00	27728	100	27728	100.0

Figure 4.35 shows the comparative difference using the two demand spectrums IBC and EC8. Damages at each level are very close. Figure 4.36 summarizes in one single bar chart the damages using different GMPE's. It is obvious that the Campbell & Bozorgnia (2008) overestimates the number of unusable buildings (complete + extensive + moderate).

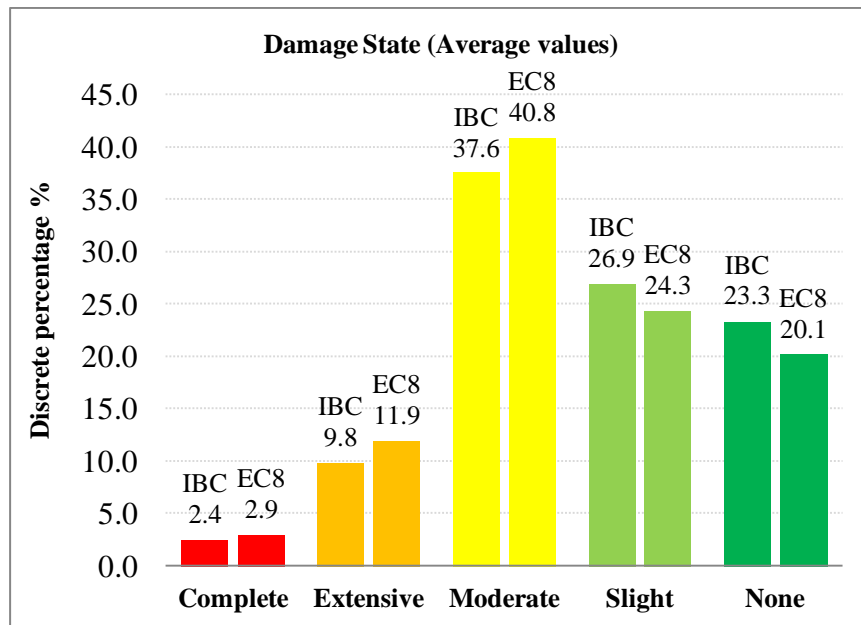


Figure 4.35 Discrete damage probabilities under Analysis 64

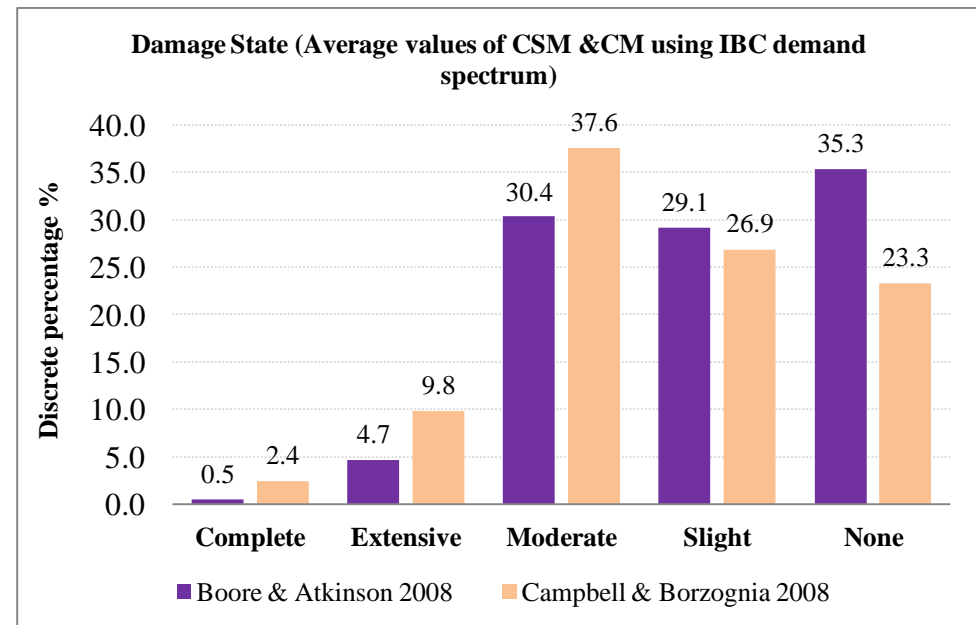


Figure 4.36 Comparison of damages between the selected GMPE

Estimated building damages from the analysis 66 based on the Akkar & Bommer (2007) equation is given in Table 4.17.

Table 4.17 Damage estimation results for Thessaloniki (Scenario C) using the GMPE by Akkar & Bommer (2007)

Analysis-66		LEVEL 2						
SEISMIC HAZARD		LEVEL 2						
Event Data	Thess78	Demand Spectrum	EC8					
Source type	Gerakarou-Stilvos fault	Classification	Thess_2					
Site correction	Ec8	Building DB	Thess rounding					
Vs30	Vs30_Thess	Magnitude	6.5					
GMPE	Akkar & Bommer 07	Vs30	Vs30_Thess					
median	0.15	PGA	0.141g					
PGA at City Hotel	0.141g	Sa0.2	-					
Sa0.2 at City Hotel	-	Sa1.0	-					
Sa1.0 at City Hotel	-	Method	CSM- Capacity Spectrum Method	percentage (%)	CM- Coefficient method	percentage (%)	Average	Average perc (%)
Comments		Complete	1769	6.4	570	2.1	1170	4.2
phantom grid 1km, interpolation grid 0.0045		Extensive	4400	15.9	3222	11.6	3811	13.7
		Moderate	11585	41.8	11951	43.1	11768	42.4
		Slight	5698	20.5	6871	24.8	6285	22.7
		None	4276	15.4	5114	18.4	4695	16.9
		Total	27728	100.00	27728	100.0	27728	100.0

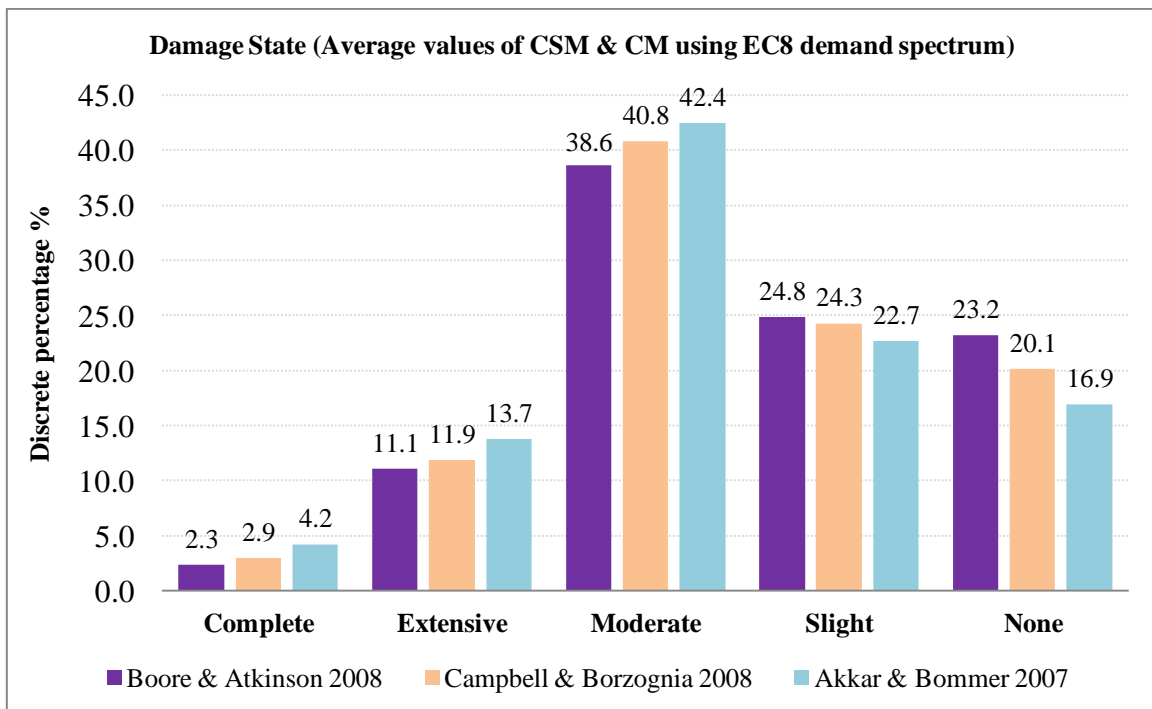


Figure 4.37 Damage results obtained from the ground motion of the three selected GMPE's

All three GMPE's produce highly comparable results, since the applied demand spectrum of EC8 overestimates the performance point and building stock data used are identical (see Figure 4.37). It should be noted that the aim of this comparative damage estimation exercise is to validate applicability of the Level 2 module in an urban loss assessment study.

4.6.2 Observed damage from the 1978 Thessaloniki earthquake

According to different references, forty-seven (47) people lost their lives during the earthquake of June 20th. The major loss of life occurred, when an 8-storey concrete frame apartment building in Thessaloniki collapsed killing 37 people. Another 4 people were killed elsewhere by falling bricks and an additional 6 were reported to have died from heart attacks.

Aftershock researches registered 66159 buildings. Of these, 3170 (4.8%) were found dangerous, 13918 (21%) had to be repaired before they could be reoccupied and 49071 (74.2%) were found to be safe (A.U.TH and Y.A.Σ.B.E), as it is shown in Table 4.18.

Table 4.18 Observed damages in Thessaloniki

Damage state	Number of buildings	Percentage (%)	Colour
Very heavy	3170	4.8	
Moderate	13918	21.0	
None and slight	49071	74.2	
Total	66159	100.0	

4.6.3 Comparison between calculated and observed vulnerability

Comparing the three analyses (59-64-66) above, the analysis that could approach the observed damages from the 1978 Thessaloniki earthquake, is the one with the selection of the GMPE of Boore & Atkinson (2008), the demand spectrum of IBC and employed method of CSM.

Table 4.19 gathers the necessary data for comparison.

Table 4.19 Damages generated in ELER VS Observed damages

Results from ELER				VS	Observed damages %
	DS	Discrete percentage %	Total %		
>Heavy	Complete	0.25	3.4		4.8
	Extensive	3.18			
Moderate	Moderate	26.71	26.7		21.0
<Slight	Slight	29.53	69.9	74.2	
	None	40.34			
Total			100.0	100.0	

As it can be seen in Figure 4.38, the results obtained from analytical method are consistent with the real/observed one, thus the main goal of this scenario C, testing ELER in the region of Central Macedonia, is achieved.

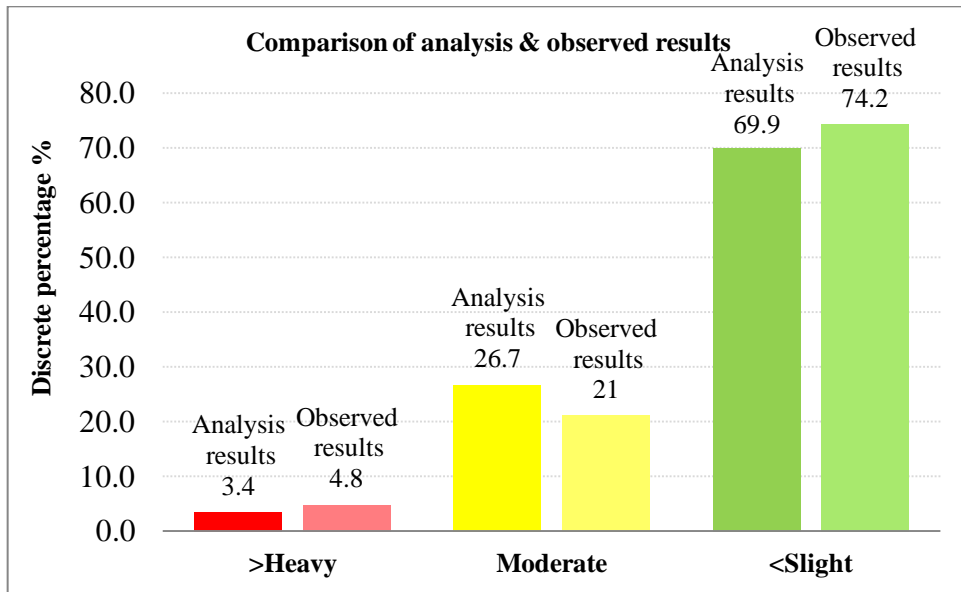


Figure 4.38 Bar chart with results obtained from observed data and analysis 59

4.6.4 Casualties

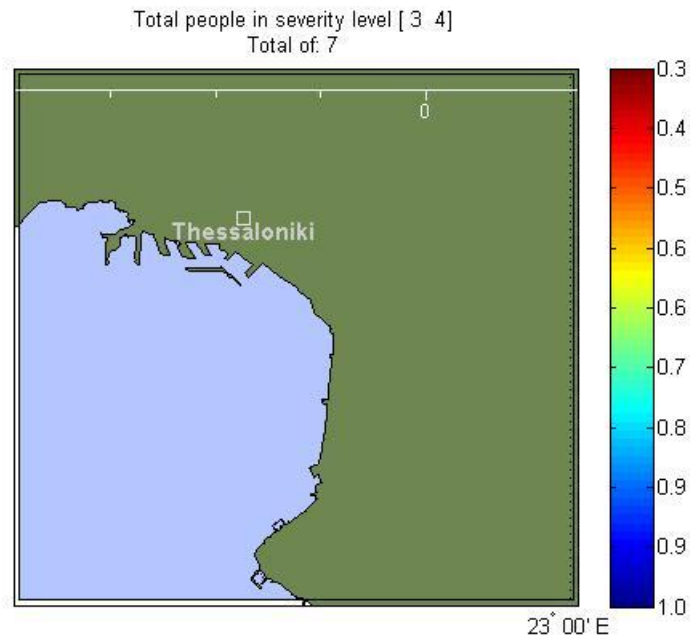


Figure 4.39 Human losses from the studied scenario calculated by HAZUS methodology

4.7 Building damages and casualties from Scenario D

4.7.1 Building damages (analysis results)

In this scenario, Anthemountas Fault is examined to check how hazardous could be as an active fault near to Thessaloniki. Likewise, hazard results obtained from Scenario D, are used to estimate loss assessment for Thessaloniki. Three different parameters were examined, like in scenario c:

1. Ground Motion Prediction Equations (GMPE's):

- Boore & Atkinson (2008)-----Analysis 67*
- Campbell & Bozorgnia (2008) ----Analysis 69
- Akkar & Bommer (2007) -----Analysis 71

**Analysis vol. denotes just the priority of the results done by the author in his personal database*

2. Demand spectrums

3. Approaches for the computation of the demand spectrum and the performance point

The results from the analysis 67 are presented in the Table 4.20.

Table 4.20 Damage estimation results for Thessaloniki (Scenario D) using the GMPE by Boore and Atkinson (2008)

Analysis-67		LEVEL 2							LEVEL 2								
SEISMIC HAZARD		IBC-International building code							EC8								
Event Data	Anthemountas	Demand Spectrum	Thess_2							Demand Spectrum	Thess_2						
Source type	Anthemountas fault	Classification	Thess rounding							Classification	Thess rounding						
Site correction	directly at surface	Building DB	6.5							Building DB	6.5						
Va30	Va30_Thess	Magnitude	Va30_Thess							Magnitude	Va30_Thess						
GMPE	Boore & Atkinson 08	Va30	-							Va30	-						
median	0	PGA	-							PGA	-						
PGA	-	Sa0.2	-							Sa0.2	-						
Sa0.2	-	Sa1.0	-							Sa1.0	-						
Sa1.0	-	Method	CSM-Capacity Spectrum Method	percentage (%)	CM-Coefficient method	percentage (%)	Average	Average perc (%)	Method	CSM-Capacity Spectrum Method	percentage (%)	CM-Coefficient method	percentage (%)	Average	Average perc (%)		
Comments		Complete	560	2.02	319	1.2	440	1.6	Complete	1580	5.70	521	1.9	1051	3.8		
phantom grid 1km, interpolation grid 0.0045°, map extent 0.6/0.7		Extensive	1801	6.50	2321	8.4	2061	7.4	Extensive	4048	14.60	2980	10.7	3514	12.7		
		Moderate	8380	30.22	10271	37.0	9326	33.6	Moderate	11071	39.93	11583	41.8	11327	40.9		
		Slight	7836	28.26	7545	27.2	7691	27.7	Slight	5986	21.59	7022	25.3	6504	23.5		
		None	9151	33.00	7272	26.2	8212	29.6	None	5043	18.19	5622	20.3	5333	19.2		
		Total	27728	100.00	27728	100.0	27728	100.0	Total	27728	100.00	27728	100.0	27728	100.0		

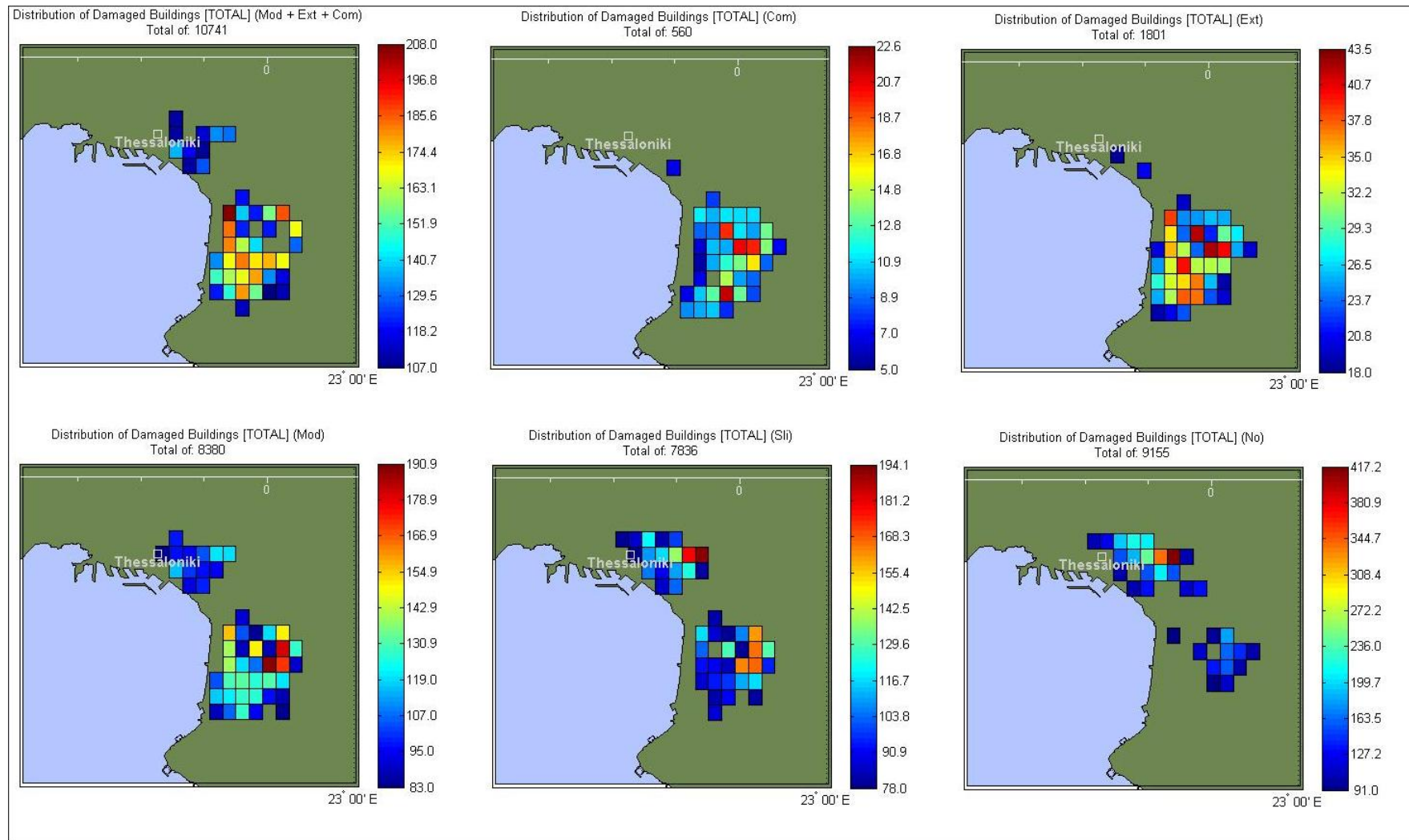


Figure 4.40 The distribution of damage buildings in Thessaloniki resulting from Analysis 67, IBC demand spectrum and CSM as selected method-Level 2 Analysis

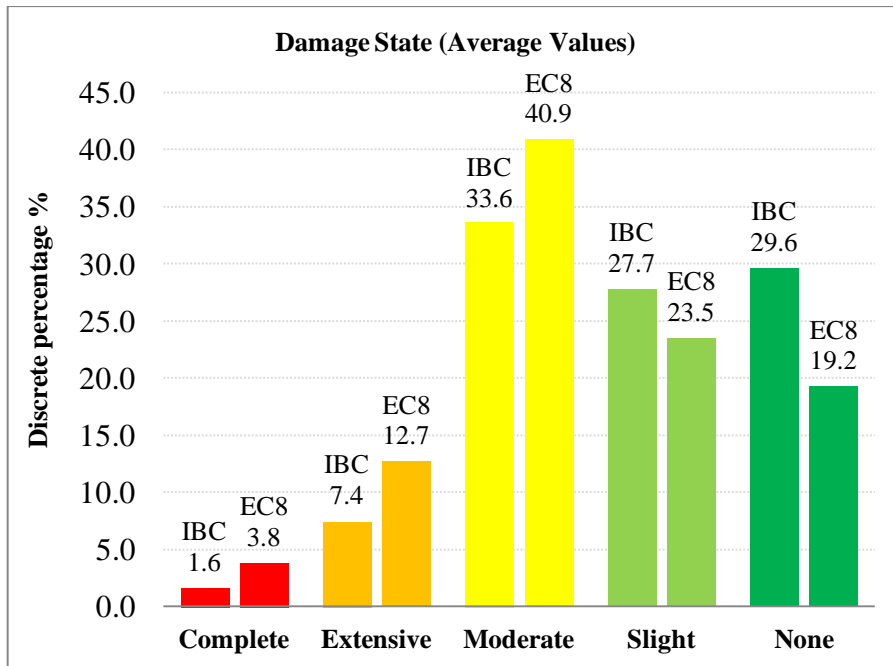


Figure 4.41 Discrete damage probabilities under Analysis 67 (Scenario D)

Evaluating the findings from scenario C and D, it can be understood that scenario D is more hazardous for Thessaloniki (Figure 4.42). Although magnitude in both scenarios is the same, the results are quite different. This is because of the focal depth and the fault length that in case of Anthemountas is larger than Gerakarou fault.

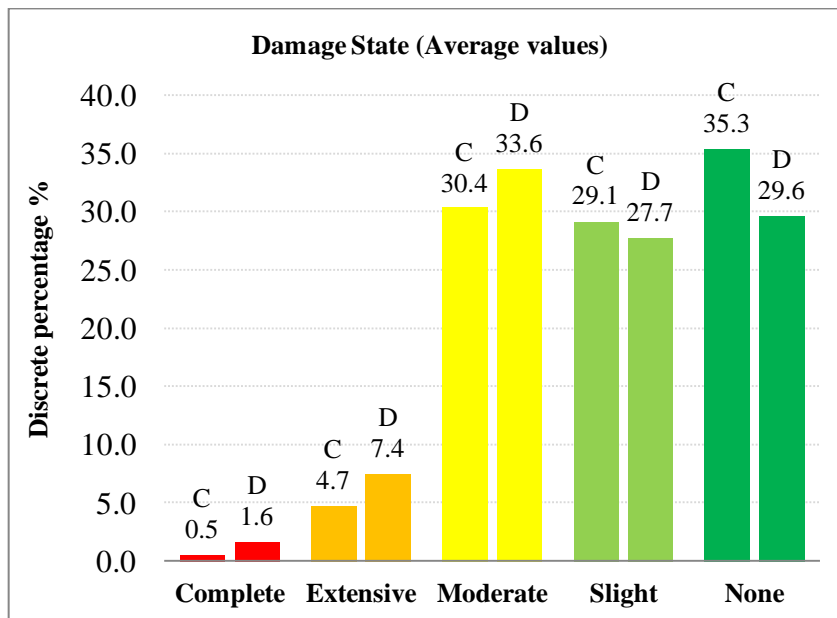


Figure 4.42 Discrete damage probabilities under Analysis 59 (scenario C) and 67 (scenario D)

Following the same concept, but changing the GMPE to Campbell & Bozorgnia (2008), the results are given in Table 4.21.

Table 4.21 Damage estimation results for Thessaloniki (Scenario D) using the GMPE by Campbell & Bozorgnia (2008)

Analysis-69		LEVEL 2							LEVEL 2								
SEISMIC HAZARD		IBC-International building code							EC8								
Event Data	Anthemountas	Demand Spectrum	Thess_2							Demand Spectrum	Thess_2						
Source type	Anthemountas fault	Classification	Thess rounding							Classification	Thess rounding						
Site correction	directly at surface	Building DB	6.5							Building DB	6.5						
Vs30	Vs30_Thess	Magnitude	Vs30_Thess							Magnitude	Vs30_Thess						
GMPE	Campbell & Bozorgnia 08	Vs30	-							Vs30	-						
median	0	PGA	-							PGA	-						
PGA	-	Sa0.2	-							Sa0.2	-						
Sa0.2	-	Sa1.0	-							Sa1.0	-						
Sa1.0	-	Method	CSM-Capacity Spectrum Method	percentage (%)	CM-Coefficient method	percentage (%)	Average	Average perc (%)	Method	CSM-Capacity Spectrum Method	percentage (%)	CM-Coefficient method	percentage (%)	Average	Average perc (%)		
Comments		Complete	1363	4.92	758	2.7	1061	3.8	Complete	2139	7.71	714	2.6	1427	5.1		
phantom grid 1km, interpolation grid 0.0045', map extent 0.6/0.7		Extensive	3226	11.63	3894	14.0	3560	12.8	Extensive	4855	17.51	3622	13.1	4239	15.3		
		Moderate	10262	37.01	11982	43.2	11122	40.1	Moderate	11329	40.86	12155	43.8	11742	42.3		
		Slight	6830	24.63	6508	23.5	6669	24.1	Slight	5342	19.27	6543	23.6	5943	21.4		
		None	6047	21.81	4586	16.5	5317	19.2	None	4063	14.65	4694	16.9	4379	15.8		
		Total	27728	100.00	27728	100.0	27728	100.0	Total	27728	100.00	27728	100.0	27728	100.0		

Figure 4.43 shows the comparative difference using the two demand spectrums IBC and EC8. Damages at each level are very close. Figure 4.44 summarizes in one single bar chart the damages using different GMPE's. It is obvious that the Campbell & Bozorgnia (2008) overestimates the number of unusable buildings (complete + extensive + moderate).

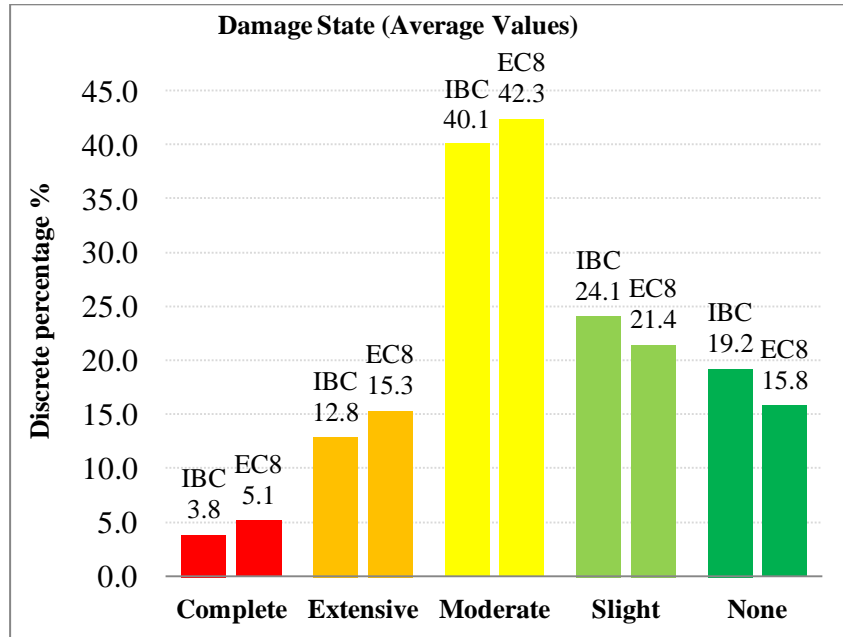


Figure 4.43 Discrete damage probabilities under Analysis 69

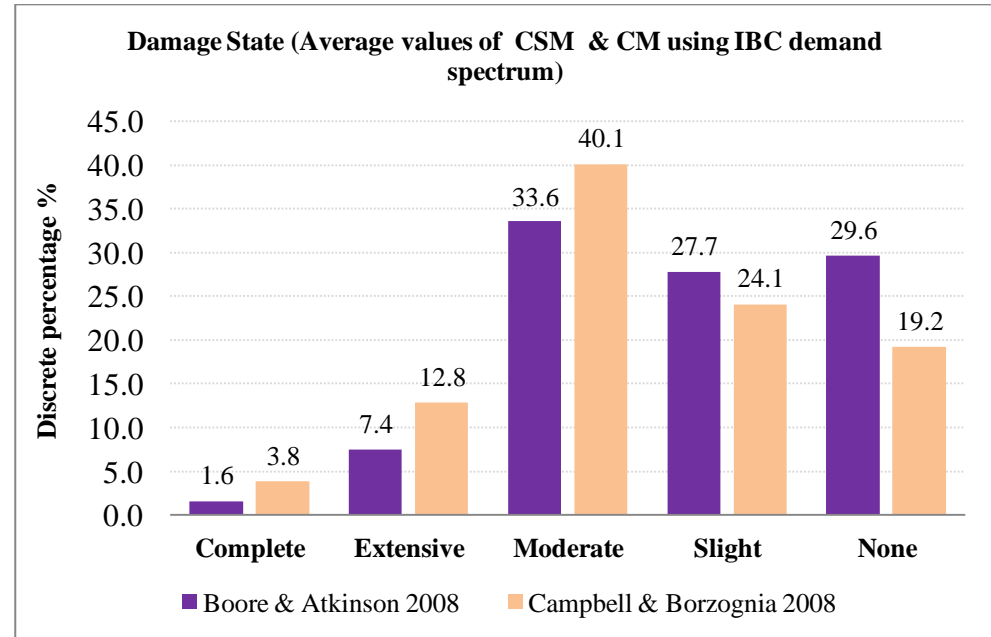


Figure 4.44 Comparison of damages between the selected GMPE

Table 4.22 Damage estimation results for Thessaloniki (Scenario D) using the GMPE's by Akkar & Bommer (2007)

Analysis-71		LEVEL 2						
SEISMIC HAZARD		LEVEL 2						
Event Data	Anthemountas	Demand Spectrum	EC8					
Source type	Anthemountas fault	Classification	Thess_2					
Site correction	directly at surface	Building DB	Thess rounding					
Vs30	Vs30_Thess	Magnitude	6.5					
GMPE	Akkar & Bommer 07	Vs30	Vs30_Thess					
median	0	PGA	-					
PGA	-	Sa0.2	-					
Sa0.2	-	Sa1.0	-					
Sa1.0	-	Method	CSM-Capacity Spectrum Method	percentage (%)	CM-Coefficient method	percentage (%)	Average	Average perc (%)
<u>Comments</u>		Complete	2890	10.42	977	3.5	1934	7.0
phantom grid 1km, interpolation grid 0.0045°, map extent 0.6/0.7		Extensive	5737	20.69	4353	15.7	5045	18.2
		Moderate	11383	41.05	12626	45.5	12005	43.3
		Slight	4611	16.63	5976	21.5	5294	19.1
		None	3110	11.22	3799	13.7	3455	12.5
		Total	27731	100.01	27731	100.0	27731	100.0

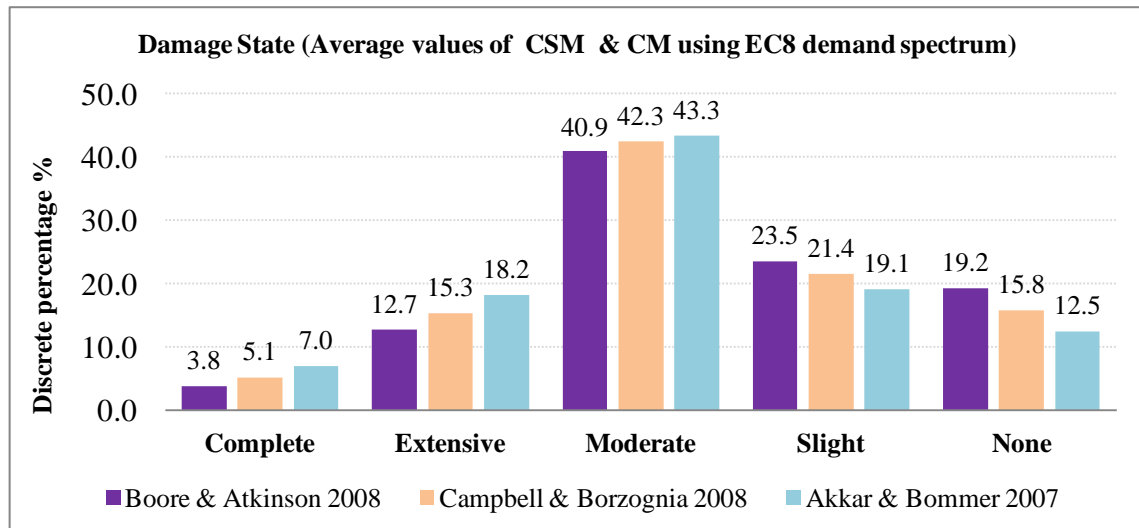


Figure 4.45 Damage results obtained from the ground motion of the three selected GMPE's

4.7.2 Casualties

Figure 4.46 illustrates the severity level of human losses. The number of expected casualties is expected to be about 61 people for the earthquake scenario caused by Anthemountas Fault.

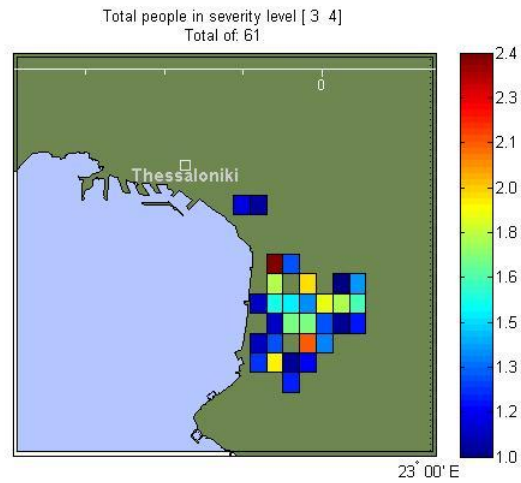


Figure 4.46 Human losses for the analysis 67 calculated by Hazus Methodology

5. Conclusion

To sum up, the motivation for the case of Thessaloniki is to demonstrate earthquake risk for the selected region with a user-defined earthquake scenario. Thus, assessment results demonstrate building damage, help to minimize the risks for the selected region, and offer the best reinforcement options for the buildings.

While this risk assessment relies on the best available data and methodologies, uncertainties are inherent in any loss-estimation methodology and arise in part from incomplete scientific knowledge concerning natural hazards and their effects on the built environment. Uncertainties also result from the following:

- Incomplete or dated inventory, demographic, or economic parameter data
- The unique nature, geographic extent, and severity of each hazard
- Fragility curves

These factors can result in a range of uncertainties in loss estimates. Therefore, potential exposure and loss estimates are approximate.

Consequently, both damage and human losses maps can be used to inform the local authorities and the civil protection services and help them to prepare the regional response, because they show where the effects of the earthquake are more likely to be stronger. Good planning does not stop the earthquake from happening. But knowing which places are more at risk can help to prevent serious infrastructure damages and human tragedies.

6. References

- Akkar, S., Bommer, J. J., (2007a), "Empirical prediction equations for peak ground velocity derived from strong-motion records from Europe and Middle East", *Bulletin of the Seismological Society of America*, 97(2), pp 511-530.
- Akkar, S., Bommer, J. J., (2007b), "Prediction of elastic displacement response spectra in Europe and Middle East", *earthquake engineering and Structural Dynamics*, 36(10), pp1275-1301.
- Ambraseys N., and Bommer J., (1995), "Attenuation relations for use in Europe: an overview", *Proc. 5th SECED Conference*, pp. 67-74, Chester
- Armijo, R., Meyer, B., Navarro, S., King, G. and Barka, A., (2002), "Asymmetric slip partitioning in the Sea of Marmara pull-apart: a clue to propagation processes of the North Anatolian Fault", *Terranova*, 14, 80-86.
- ASCE/SEI 41-06, (2007), "Seismic Rehabilitation of Existing Buildings", American Association of Civil Engineers, ASCE Standard No. ASCE/SEI 41-06.
- ATC 13, (1987), "Earthquake damage evaluation data for California", Applied Technology Council, Redwood City, California.
- ATC 25, (1991), "Seismic Vulnerability and Impact of Disruption of Lifelines in the Conterminous United States", Redwood City, California, Applied Technology Council Report; 440 pp.
- ATC 40, (1996), "Seismic Evaluation and Retrofit of Concrete Buildings", Applied Technology Council, Redwood city, California.
- Boore, D. M. and Atkinson, G. M., (2008), "Ground-Motion Prediction Equations for the Average Horizontal Component of PGA, PGV, and 5%-Damped PSA at Spectral Periods between 0.01 s and 10.0 s", *Earthquake Spectra*, Vol.24, No 1, pp 99-138.
- Bulut, F., Bohnoff, M., William, L., Aktar, M., Gresen, G., (2009), "Microseismicity at the North Anatolian fault in the Sea of Marmara offshore Istanbul, NW Turkey", USGS Staff- Published Research, paper 393, available at <http://digitalcommons.unl.edu/usgsstaffpub/393>.
- Campbell, K. W. and Bozorgnia, Y., (2007), "Campbell-Bozorgnia NGA Ground Motion Relations for the Geometric Mean Horizontal Component of Peak and Spectral Ground Motion Parameters", University of California, PEER 2007/02, Berkeley, USA, May.
- Carver, D., and Bollinger, G. A., (1981), "Aftershocks of the June 20, 1978 Greece earthquake: a multimode faulting sequence", *Tectonophysics*, 73, pp 343-363.
- Cheu, D.H., (1995), "Northridge Earthquake – January 17, 1994: The Hospital Response", Universal City, CA: FEMA. 17 January 1995:1-15, Northridge Earthquake: One Year Later.
- Coburn A. and Spence R., (1992), "Earthquake Protection", John Wiley & Sons Ltd., Chichester, England.
- Demircioglu, M. B., Erdik, M., Hancilar, U., Harmandar, E., Kamer, Y., Sesetyan, K., Tuzun, C., Yenidogan, C., and Zulfikar, A. C., (2010), "Technical Manual and Users Guide – Earthquake Loss Estimation Routine ELER-v3.0", Bogazici University, Department of Earthquake Engineering, Istanbul, pp. 133.
- Dowrick, D.J., (1992), "Attenuation of Modified Mercalli Intensity in New Zealand earthquakes", *Earthquake Engineering and Structural Dynamics*, Vol. 21, pp. 181-196.
- Durkin M. E. and Thiel C. C., (1993), "Towards a Comprehensive Regional Earthquake Casualty Modeling Process", *Proc. of National Earthquake Conference Vol I*, Central U.S. Earthquake Consortium, pp. 557-566.
- "Earthquake Risk Assessment for Istanbul Metropolitan Area: executive summary", URL: <http://webarchive.iiasa.ac.at/Research/RMS/dpri2002/Papers/erdik2.pdf>, September 15, 2012.
- Erdik, M., Cagnan, Z., Zulfikar, C., Sesetyan, K., Demircioglu, M.B., Durukal, E., Kariptas, C., (2008), "Development of Rapid Earthquake Loss Assessment Mehtodologies for Euro-Med Region" The 14th World Conference on Earthquake Enginnering, Beijing, China, October 17-18.

- Erdik, M., “Modelling of Earthquake Risk”, 1st International Istanbul Insurance Conference”, available at http://www.sigortatder.org.tr/eski/sunum/M_Erdik_std.pdf .
- Erdik, M., Demircioglu, M., Sesetyan, K., Durukal, E. and Siyahi, B., (2004), “Earthquake hazard in Marmara Region, Turkey”, 13th World Conference on Earthquake Engineering, Vancouver, B.C., Canada, August 1-6, paper No 270.
- Erdik, M., “Earthquake Risk, Earthquake Rapid Response System, and Early Warning System in Istanbul”, Macalester International, Vol. 15, available at http://digitalcommons.macalester.edu/cgi/viewcontent.cgi?article=1394&context=macintl&sei-redir=1&referer=http%3A%2F%2Fwww.google.gr%2Furl%3Fsa%3Dt%26rct%3Dj%26q%3Dearthquake%2520risk%252C%2520earthquake%2520rapid%2520response%2520system%252C%2520and%2520early%2520warning%2520system%2520in%2520istanbul%26source%3Dweb%26cd%3D2%26ved%3D0CDIQFjAB%26url%3Dhttp%253A%252F%252Fdigitalcommons.macalester.edu%252Fcgi%252Fviewcontent.cgi%253Farticle%253D1394%2526content%253Dmacintl%26ei%3DbZOeULT1G4bm4QSVmoHADw%26usg%3DAFQjCNEbNi3BA6asROcO_v3Zis8Qbjdzg%26cad%3Drja#search=%22earthquake%20risk%2C%20earthquake%20rapid%20response%20system%2C%20early%20warning%20system%20istanbul%22 .
- Erduran, E., Crempien, J., Lang, D.H., Lindholm, C.D. and Molina, S., (2010), “Sensitivity of Earthquake Risk Models to Uncertainties in Hazard, Exposure and Vulnerability Models”, 14th ECEE, Ohrid, FYROM, August 30-September 3.
- Eurocode 8 (2003), “Design of Structures for Earthquake Resistance”, Draft No. 6, European Committee for Standardization , Brussels.
- “Event report, Kocaeli, Turkey Earthquake”, URL: http://www.rms.com/publications/turkey_event.pdf, September 18, 2012.
- Fahjan, Y., “Earthquake Loss Estimation and Risk Assessment methodology from Concept to Real Applications”, URL: http://www.msc-sahc.org/upload/docs/01_yasin_fahjan_%20presentation.pdf , September 30, 2012.
- Fajfar P., (2000), “A non linear analysis method for performance-based seismic design”, Earthquake Spectra, 16, 3, pp. 573-591.
- FEMA (1999), “HAZUS99 user and technical manuals”, Federal Emergency Management Agency Report: HAZUS 1999, Washington D.C., USA.
- FEMA (2003), “HAZUS-MH Technical Manual”, Federal Emergency Management Agency, Washington D.C., USA.
- FEMA 222A (1994), “NEHRP recommended provisions for the development of seismic regulations or new buildings”, 1994 edition, Part 1 – provisions, Federal Emergency Management Agency, 290.
- FEMA 440, (2005), “Improvement of nonlinear static seismic analysis procedures”. Federal Emergency Management Agency (FEMA) Report no.440, Applied Technology Council, Washington D.C., USA.
- FEMA 356 (2000), “NEHRP Guidelines for the seismic rehabilitation of buildings”. Federal Emergency Management Agency, Washington D. C., USA.
- “Izmit, Turkey Earthquake of August 17, 1999 (M7.4): An EQE Briefing”, URL: http://www.absconsulting.com/resources/Catastrophe_Reports/izmit-Turkey-1999.pdf, September 18, 2012.
- Gasperini, L., Polonia, A., Bortoluzzi, G., Henry, P., Le Pichon, X., Tryon, M., Cagatay, N. And Geli, L., (2011), “1999 Izmit Earthquake Surface Rupture”, Tectonics, Vol. 30, TC1010, DOI: 10.1029/2010TC002726.
- Giovinazzi S., (2005), “Vulnerability assessment and the damage scenario in seismic risk analysis”, PhD Thesis, Department of Civil Engineering of the Technical University Carolo-Wilhelmina at Braunschweig and Department of Civil Engineering, University of Florence, Italy.
- Giovinazzi S. and Lagomarsino S. (2004), “A Macroseismic Model for the vulnerability assessment of buildings”, 13th World Conference on Earthquake Engineering, Vancouver, Canada.
- Gülkan, P. and Kalkan, E., (2002), “Attenuation modeling of recent earthquakes in Turkey,” Journal of Seismology, 6(3), 397-409.

- Gülkan, P., Koçyiğit, A., Yüçemen, M. S., Doyuran, V., Başöz, N., (1993), “En son verilere göre hazırlanan Türkiye deprem bölgeleri haritası,” Orta Doğu Teknik Üniversitesi, Deprem Mühendisliği Araştırma Merkezi, Rapor No. 93-01. (in-Turkish)
- Hancilar, U., Tuzun, C., Yenidogan, C. and Erdik, M., (2010), “ELER software - a new tool for urban earthquake loss assessment”, *Nat. Hazards Earth Syst. Sci.*, 10, pp. 2677-2696.
- IBC (2006), “International Building Code”, International Code Council, USA.
- Kaklamanos, J., Boore, D. M., Thompson, E. M. and Campbell, K. W., (2010), (revised 2011), “Implementation of the Next generation Attenuation (NGA) Ground-Motion Prediction Equations in Fortran and R: U.S. Geological Survey Open-File Report 2010-1296”, 43 p.(v1.1), revised December 2, 2011), available at <http://pubs.usgs.gov/of/2010/1296/>.
- Kalkan, E., Gülkan, P., Yilmaz Ozturk, N. and Celebi, M., (2008), “Seismic Hazard in the Istanbul Metropolitan Area: a preliminary re-evaluation”, *Journal of Earthquake Engineering*, pp 1-12.
- Kalkan, E. and Gülkan, P., (2004a), “Empirical attenuation equations for vertical ground motion in Turkey”, *Earthquake Spectra*, 20(3), 853-882.
- Kalkan, E. and Gülkan, P., (2004b), “Site-dependent spectra derived from ground motion records in Turkey”, *Earthquake Spectra*, 20(4), 1111-1138.
- Kappos, A. J., Panagopoulos, G., Panagiotopoulos, C. and Penelis G., (2006), “A hybrid method for the vulnerability assessment of R/C and URM buildings”, *Bull Earthquake Eng*, DOI: 10.1007/s10518-006-9023-0.
- Karakostas, V., (1988), “Relation of seismic activity with geological and geo-morphological elements of the wider Aegean area”, PhD Thesis, Aristotle University of Thessaloniki, pp. 243.
- Karaman, H., Sahin, M., Elnashai, A. S. and Pineda, O., (2010), “Loss Assessment Study for the Zeytinburnu District of Istanbul using Maeviz-Istanbul (HAZTURK)”, *Journal of Earthquake Engineering*, DOI: 10.1080/13632460802014030.
- KOERI (Department of Earthquake Engineering), (2002), “Earthquake Risk Assessment for Istanbul Metropolitan Area”, Report prepared for American Red Cross and Turkish Red Crescent, Bogazici University, Istanbul, Turkey.
- Kythreoti, S., Pilakoutas, K., “Earthquake Risk Assessment Case Study: Cyprus”, URL: <http://webarchive.iiasa.ac.at/Research/RMP/july2000/Papers/stella.col.1107.pdf>, September 11, 2012.
- Le Pichon, X., Sengor, A.M.C., Demirbag, E., Rangin, C., Imren, C., Armijo, R., Gorur, N., Cagatay, N., Mercier de Lepinay, B., Meyer, B., Saatçilar, R. and Tok, B., (2001), “The active main Marmara fault,” *Earth and Planetary Science Letters*, 192, 595-616
- McClusky, S., S. Balassanian, A. Barka, C. Demir, S. Ergintav, I. Georgiev, O. Gurkan, M. Hamburger, K. Hurst, H. Kahle, K. Kastens, G. Kekelidze, R. King, V. Kotzev, O. Lenk, S. Mahmoud, A. Mishin, M. Nadariya, A. Ouzounis, D. Paradissis, Y. Peter, M. Prilepin, R. Reilinger, I. Sanli, H. Seeger, A. Tealeb, N. Toksöz and G. Veis, (2000), “Global Positioning System constraints on the plate kinematics and dynamics in the eastern Mediterranean and Caucasus”, *J. Geophys. Res.*, 105, 5695-5719.
- Mai, P.M., Spudich, P., and Boatwright J., (2005), “Hypocenter locations in finite-source rupture models”, *Bull. Seism. Soc. Am.* 95(3), pp 965-980.
- Manighetti, I., Campillo, M., Sammis, C., Mai, P.M., and King G., (2005), “Evidence for self-similar, triangular slip distributions on earthquakes: Implications for earthquake and fault mechanics”, *J. Geophys. Res.* 110.
- MATLAB® (R2008b), the MathWorks, Inc.
- Mercier, J.L., Mouyaris, N., Simeakis, C., Roundoyannis, T., and Anghelidhis, C., (1983), “Structural analysis of recent and active faults and regional state of stress in the epicentral area of the 1978 Thessaloniki earthquakes (Northern Greece)”, *Tectonics*, 2(6), pp. 577-600.

- Mert, A., Alcik, H., Erdik, M., Gul, M., Ozel, O. and Fahjan, Y. (2004), "Istanbul Earthquake Rapid Response and the Early Warning System", 13th World Conference on Earthquake Engineering, Vancouver, B.C., Canada, August 1-6, paper No 272.
- Mountrakis, D., Kiliyas, A., Pavlides, S., Sotiriadis, L., Psilovikos, A., Astara, Th., Vavliakis, E., Koufos, G., Dimopoulos, G., Soulios, G., Christaras, V., Skordilis, M., Tranos, M., Spyropoulos, N., Patras, D., Syrides, G., Lambrinos, N., and Laggalis, T., (1996a), "Neotectonic map of Greece, Langadhas sheet, 1:100,000", Earthquake Planning and Protection Organization and European Centre on Prevention and Forecasting of Earthquakes.
- Nachtigall, J., (2008), "Earthquake Information Systems using Wireless Mesh Networks", Magisterarbeit, Geographisches Institut, Humboldt Universitat zu Berlin, Berlin.
- Papazachos, B., Mountrakis, D., Psilovikos, A., and Leventakis, G., (1979), "Surface fault traces and fault plane solutions of the May-June 1978 major shocks in the Thessaloniki area, Greece", *Tectonophysics*, 53, pp 171-183.
- Parsons, T., S. Toda, R.S. Stein, A. Barka and J.H. Dieterich, (2000), "Heightened odds of large earthquakes near Istanbul: An interaction-based probability calculation", *Science*, 288, pp 661-665.
- Pitilakis, K., Anastasiadis, A., Kakderi, K., Alexoudi, M. and Argyroudis, S., (2010), "The role of soil and site conditions in the vulnerability and risk assessment of lifelines and infrastructures. The case of Thessaloniki (Greece)", 5th International Conference on Recent Advances in Geotechnical Earthquake Engineering and Soil Dynamics and Symposium in Honor of Professor I.M. Idriss, San Diego, California, May 24-29.
- Pitilakis, K., "Systemic Seismic Vulnerability and Risk Analysis for Building, Lifeline Networks and Infrastructures Safety Gain", URL: http://www.vce.at/SYNER-G/pdf/deliverables/D3.1_Syner-G_RC_final.pdf, October 5, 2012.
- Psycharis, I., (1978), "The Salonica (Thessaloniki) Earthquake of June 20, 1978", Earthquake Engineering Research Laboratory EERL 78-03, California Institute of Technology, USA.
- Pulido, N., Ojeda, A., Atakan, K., Kubo, T., (2004), "Strong ground motion estimation in the Sea of Marmara region (turkey) based on a scenario earthquake", Elsevier, DOI: 10.1016/j.tecto.2004.07.023, available at <http://web.itu.edu.tr/~taymaz/docs/NPulido-et-al.pdf>.
- RISK-UE 2004, "The European Risk-UE Project: An Advanced Approach to Earthquake Risk Scenarios", (2001-2004), www.risk-ue.net.
- Rossetto, T., Elnashai, A., (2003), "Derivation of vulnerability functions for European-type RC structures based on Observational Data", *Engineering Structures* 25 (2003) 1241-1263, DOI:10.1016/S0141-0296(03)00060-9.
- Roumelioti, Z., Theodulidis, N., and Kiratzi, A., (2007), "The 20 June 1978 Thessaloniki (Northern Greece) earthquake revisited: Slip distribution and forward modeling of geodetic and seismological observations", 4th Int. Earthq. Eng., June 25-28, Proceedings, paper No.1594.
- Scasserra, G., Stewart J. P., Bazzurro, P., Lanzo, G. And Mollaiolli, F., (2009), "A comparison of NGA Ground- motion Prediction Equations to Italian Data", *Bulletin of the Seismological Society of America*, DOI: 10.1785/0120080133.
- Somerville, P., Irikura, K., Graves, R., Sawada, S., Wald, D., Abrahamson, N., Iwasaki, Y., Kagawa, Smith, N., and Kowada A., (1999), "Characterizing crustal earthquake slip models for the prediction of strong ground motion", *Seism. Res. Let.* 70, pp 59-80.
- Soufleris, C., and Stewart, G., (1981), "A source study of the Thessaloniki (northern Greece) 1978 earthquake sequence", *Geophys. J. R. Astr. Soc.*, 67, pp 343-358.
- Straub, C., H.-G., Kahle and C. Schindler, (1997), "GPS and geologic estimates of the tectonic activity in the Marmara Sea region, NW Anatolia", *J. Geophys. Res.*, 102, 27587-27601.
- Taymaz, T., Tan, O. and Yolsal, S., "Active tectonics of Turkey and Surroundings and Seismic Risk in the Marmara Sea Region", URL: http://web.itu.edu.tr/~taymaz/docs/Taymaz_IWAM04_S3-09.pdf, September 17, 2012.
- TUIK (Turkiye Istatistik Kurumu, Turkish Statistical Institute), <http://www.tuik.gov.tr/Start.do>.
- Ulusay, R. Tuncay, E., Sonmez, H. and Gokceoglu, C., (2004), "An attenuation relationship based on Turkish strong motion data and iso-acceleration map of Turkey", *Engineering Geology*, 74(3-4), pp 265-291.

- Ulutas, E., Ozer, M. F., (2010), “Empirical Attenuation Relationship of Peak Ground Acceleration for Eastern Marmara Region in Turkey”, the Arabian Journal for Science and Engineering, Volume 35, Number 1A, pp 187-203.
- Wald, D. J., Worden B. C. Quitoriano, V. and Pankow, K. L., (2004), “ShakeMap Manual: Users Guide, Technical Manual and Software Guide”.
- Zervoroulou, A., Chatzipetros, A., Tsiokos, L., Syrides, G. and Pavlides, S., (2007), “Non-Seismic Surface Faulting: The Peraia Fault Case Study (Thessaloniki, N. Greece)”, 4th International Conference on Earthquake Engineering, Thessaloniki, Greece, paper No. 1610.
- Αβραμίδης, Ι., Αραβαντινός, Δ., Καλογήρου, Ν., Μουσιόπουλος, Ν., Πενέλης, Γ. και Στυλιανίδης, Κ., (2008), “30 χρόνια μετά το σεισμό της Θεσσαλονίκης-Μνήμες και Προοπτική”, Πολυτεχνική Σχολή Α.Π.Θ., Θεσσαλονίκη, Μάιος.
- Ζερβοπούλου, Α., Παυλίδης, Σ., (2008), “Νεοτεκτονικά Ρήγματα Πολεοδομικού Συγκροτήματος Θεσσαλονίκης”, 3^ο Πανελλήνιο Συνέδριο Αντισεισμικής Μηχανικής & Τεχνικής Σεισμολογίας, Αθήνα, 5-7 Νοέμβριος, Άρθρο 1865.
- Κάππος, Α., Στυλιανίδης, Κ., Σέξτος, Α., Κουρής, Λ., Παναγόπουλος, Γ., Παπανικολάου, Β., Παναγιωτόπουλος, Χ. και Γκουτζίκας, Ε., (2009), “Σενάρια σεισμικής διακινδύνευσης του κτιριακού αποθέματος της πόλης των Γρεβενών”, 16^ο Συνέδριο Σκυροδέματος, Πάφος, Κύπρος, 21-23 Οκτωβρίου.
- Κάππος Α., Πενέλης Γ., Σέξτος Α. (2008-2009), “Σημειώσεις για το μάθημα ΑΣΤΕ04: Αντισεισμικός Σχεδιασμός Κατασκευών από Σκυρόδεμα”, Τμήμα Πολιτικών Μηχανικών, Α.Π.Θ., Θεσσαλονίκη.
- Καραμήτρου, Α., Κυρατζή, Α. και Ρουμελιώτη, Ζ., (2008), “Στοχαστική προσομοίωση της ισχυρής σεισμικής κίνησης από ενεργές τεκτονικές δομές κοντά στην πόλη της Θεσσαλονίκης”, 3^ο Πανελλήνιο Συνέδριο Αντισεισμικής Μηχανικής & Τεχνικής Σεισμολογίας, Αθήνα, 5-7 Νοέμβριος, Άρθρο 2082.
- Πενέλης Γ., “Σεισμός της Θεσσαλονίκης 1978: Καμπή στην αντισεισμική προστασία της χώρας”
- Πιτλάκης, Κ., “Γεωτεχνική Σεισμική Μηχανική”, Θεσσαλονίκη, Εκδόσεις ΖΗΤΗ, 2010.